NOTCH1 Acts as a Tumor Suppressor That Induces Early Differentiation in Head and Neck Cancer

Chenfei Huang[1, 2,#] Shhyam Moorthy[3, 4,#] Qiuli Li[3, 5,#] Kazi Mokim. Ahmed[1], Kalil Saab[1], Defeng Deng[1, 6], Jiping Wang[3], Xiayu Rao[7], Jiexin Zhang[7], Yuanxin Xi[7], Jing Wang[7], Zhiyi Liu[3, 8], Noriaki Tanaka[3, 9], David A. Wheeler[10, 11], Eve Shibrot[10], Rami Saade[12], Curtis R. Pickering[3, 13], Tong-Xin Xie[3], Adel K. El-Naggar[14], Abdullah A. Osman[3], Kunal Rai[15], Patrick A. Zweidler-McKay[16], John V. Heymach[17], Lauren A. Byers[17], Faye M. Johnson[17, 18], Vlad C. Sandulache[1, 19, 20], Jeffrey N. Myers[3], Pedram Yadollahi[1],**, Mitchell J. Frederick[1],*

#Contributed equally
*First Co-corresponding author: Mitchell J. Frederick, Baylor College of Medicine, BLDG RM NA 520, 6501 Fannin St, Houston TX 77030-2703, mitchell.frederick@bcm.edu, 713-798-1963
** Second Co-corresponding author Pedram Yadollahi,, Baylor College of Medicine, BLDG RM NA 503, 6501 Fannin St, Houston TX 77030-2703, pedram.yadollahi@bcm.edu, 713-798-4512

[1]Bobby R. Alford Department of Otolaryngology-Head and Neck Surgery, Baylor College of Medicine, Houston, Texas. [2]Celularity Inc., Florham Park, New Jersey. [3]Department of Head and Neck Surgery, University of Texas M.D. Anderson Cancer Center, Houston, Texas. [4]Merck, Rahway, New Jersey. [5]Department of Head and Neck, Sun Yat-sen University Cancer Center, Guangzhou, China. [6]Department of Integrative Medicine, University of Texas M.D. Anderson Cancer Center, Houston, Texas. [7]Department of Bioinformatics and Computational Biology, University of Texas M.D. Anderson Cancer Center, Houston, Texas. [8]LC Sciences, Houston, Texas. [9]Department of Oral and Maxillofacial Surgery, Osaka University School of Dentistry, Suita City, Osaka. [10]Human Genome Sequencing Center, Baylor College of Medicine, Houston, Texas. [11]Department of Computational Biology, St. Jude Children's Research Hospital, Memphis, Tennessee. [12]Department of Otolaryngology, Lebanese American University, Beirut. [13]Department of Surgery-Otolaryngology, Yale School of Medicine, New Haven, Connecticut. [14]Department of Pathology, University of Texas M.D. Anderson Cancer Center, Houston, Texas. [15]Department of Genomic Medicine and MDACC Epigenomics Therapy Initiative, University of Texas M.D. Anderson Cancer Center, Houston, Texas. [16]Department of Pediatric Leukemia and Lymphoma, University of Texas M.D. Anderson Cancer Center, Houston, Texas. [17]Department of Thoracic/Head & Neck Medical Oncology, University of Texas M.D. Anderson Cancer Center, Houston, Texas. [18]The University of Texas Graduate School of Biomedical Sciences, Houston, Texas. [19]ENT Section, Operative Care Line, Michael E. DeBakey Veterans Affairs Medical Center, Houston, Texas. [20]Center for Translational Research on Inflammatory Diseases, Michael E. DeBakey Veterans Affairs Medical Center, Houston, Texas.

ABSTRACT

Inactivating *NOTCH1* mutations in head and neck squamous cell carcinoma (HNSCC) were described over a decade ago, suggesting a tumor-suppressor function—unlike its oncogenic role in other tumors. Today, much debate persists regarding a putative oncogenic role in HNSCC as well, with reports that NOTCH1 signaling drives tumor growth and a cancer-stem-cell (CSC) phenotype. In this work, comprehensive experiments unequivocally demonstrate that *NOTCH1* is a tumor suppressor in HNSCC regardless of mutation or activation status and that it reduces CSC frequency. We developed a signature of NOTCH1 activation showing the pathway is associated with very early differentiation, an altered tumor microenvironment, and better prognosis. Clarifying whether *NOTCH1* occasionally functions as an oncogenic driver in HNSCC is crucial to prognosis and personalized therapy. The results presented unify the field, reconcile conflicting data, and provide critical insights into the biological and clinical significance of *NOTCH1*, with broader implications in other squamous carcinomas with *NOTCH1* mutations.

KEYWORDS: oncogenes & tumor suppressors/oncogenes & tumor suppressors, head, neck & oral cancers/head, neck & oral cancers, tumor microenvironment/tumor microenvironment, stem cell biology/cancer stem cells

INTRODUCTION

The genomic landscape of head and neck squamous cell carcinoma (HNSCC) is predominated by tumor suppressors (1-4), posing challenges for the development of molecular targeted therapies. We identified frequent inactivating *NOTCH1* mutations in HNSCC (1, 3) and aggressive cutaneous SCC (cSCC) (5), indicating a potential tumor suppressive role. Subsequent investigations have confirmed similar mutation patterns in HNSCC (4, 6, 7), cSCC (8), and SCCs of the lung (LUSC) (9) and esophagus (ESCC) (10) through The Cancer Genome Atlas (TCGA) and independent studies, solidifying *NOTCH1* as one of the most commonly mutated genes across various SCCs. The presence of mutations in extracellular ligand binding domains and truncating mutations throughout the *NOTCH1* gene in SCCs aligns with its proposed tumor suppressor function (11), supported by earlier mouse studies demonstrating increased skin tumors upon conditional *NOTCH1* knockout (12). Conversely, *NOTCH1* is an oncogenic driver in T cell acute lymphoblastic leukemia (T-ALL), where activating missense mutations cluster in the heterodimerization (HD) domain and truncating mutations occur in the C-terminal PEST sequence, leading to increased *NOTCH1* activation (11, 13). This oncogenic role has also been reported in adenoid cystic carcinomas originating from the salivary gland (14), highlighting NOTCH1's context-specific dual role in cancer biology.

Although NOTCH1 plays opposing roles in cancers from different tissues, multiple studies suggest a dual function within HNSCC of the same histology, including an oncogenic role (7, 15-19). Activating mutations in the HD and Abruptex regions have been reported in Asian HNSCC cohorts (20, 21), although subsequent cloning of an Abruptex mutation later revealed that it was inactivating (22). Additionally, NOTCH1 RNA and protein overexpression has been correlated with poor prognosis (15, 17, 18, 23), and pharmacological inhibition or gene knockdown has linked NOTCH1 activation to proliferation (16, 19, 23), tumor growth (18, 24), spheroid formation (19, 24, 25), and resistance to chemotherapy (25). In contrast, we demonstrated that ectopic expression of activated intracellular NOTCH1 (ICN1) expression inhibits proliferation and tumor growth in NOTCH1-mutant HNSCC lines (2), supported by a report that nuclear cleaved NOTCH1 by IHC correlated with better patient survival (26).

Clarifying whether the NOTCH1 pathway occasionally functions as an oncogenic driver in HNSCC is crucial not only for academic discourse but also for the prognosis and personalized therapy of SCC patients with either wild-type (WT) or mutated *NOTCH1*. While NOTCH1 inhibition has been proposed for HNSCC tumors where the pathway is deemed oncogenic, we reported that HNSCC cell lines harboring inactivating *NOTCH1* mutations are highly sensitive to PI3K inhibitors (27-29), underscoring the complex interplay of signaling pathways in SCC. Here, we present a systematic and comprehensive analysis demonstrating that *NOTCH1* functions as a tumor suppressor in HNSCC regardless of mutation or activation status, despite its potential to induce pseudo-stem cell-like properties *in vitro.* We further demonstrate that restoration or activation of NOTCH1 signaling induces a program of very early differentiation—also manifested in human HNSCC primary tumors— that reshapes the tumor microenvironment and may influence which tumor dependencies can be clinically targeted successfully. Our findings challenge prevailing models that consider the de-differentiated state of squamous cell carcinomas to be irreversible due to genetic mutations, offering deeper insights into the mechanisms of tumor plasticity.

METHODS:

Cell lines, plasmids, and reagents.

The established HNSCC cell lines used in experiments were obtained from MD Anderson and are listed in Supplementary Table S1. Cells were passaged in growth media containing 10% FBS plus additives, validated by STR profiling, and profiled for somatic mutations as previously described (30). Full-length WT human *NOTCH1* receptor (NFL1) cDNA was obtained from OriGene (Rockville, MD), the ICN1 retroviral construct encoding activated human *NOTCH1* from Dr. Patrick Zweidler-McKay, and the cDNA encoding human cleaved *NOTCH1* detectable by commercial cl-NOTCH1 antibodies was subcloned through reverse transcriptase PCR using RNA derived from *NOTCH1* WT FaDu cells. Details regarding

these constructs, shRNAs targeting *AXL* and *α-CATULIN* and CRISPR vectors, and siRNA reagents targeting *HES/HEY* family members are provided in supplementary methods. Catalogue numbers for antibodies obtained from Cell Signaling Technologies (Danvers, MA) and Santa Cruz (Santa Cruz, CA) are provided in supplementary methods as well.

NOTCH Activation, Clonogenic Assays, Western Blots, Reverse Phase Protein Arrays.

For NOTCH activation experiments, tissue culture wells were pre-coated with immobilized recombinant JAG1 fused to an FC fragment or control IgG FC protein as described in supplementary methods. Proteins lysates were harvested, resolved by SDS-PAGE electrophoresis, electro-transferred to PVDF membranes, and probed with specific antibodies using standard methods as previously described. Antibodies to activated cleaved NOTCH1 (cl-NOTCH1), total NOTCH1, total NOTCH2, AXL, FLAG tag, were from Cell Signaling; whereas antibodies to α-CATULIN LAMC2, ITGA3, ITGA5 were from Santa Cruz and anti-Hes5 was from Abcam. For clonogenic assays, 1000 cells were seeded into replicate 6-well plates either uncoated or pretreated with Jag1 or control FC, grown for 7-10 days, fixed and stained with 0.5% crystal violet, and the number of colonies with greater than 60 cells were counted with Image J software (3). RPPAs were used to quantitate levels of 157 different protein/phosphoproteins using lysates prepared from a panel of HNSCC cell lines and validated antibodies according to methods we previously published. Pearson correlations with cl-NOTCH1 protein were calculated using JMP v19 (SAS, Cary, NC) and P-values were adjusted with a Benjamini-Hochberg (B-H) correction (FDR = 0.1, significance cutoff).

Differentially Expressed Gene (DEG) Analysis and RNA-seq.

After growing cells on plates coated with either JAG1 or FC control protein (in biologic triplicate) for 5 days, extracted RNA was processed by the MD Anderson Sequencing and Microarray Core Facility and individually quantitated following hybridization to Affymetrix HuGene 2.0 ST arrays. RNA expression after iICN1 induction in PJ34-iICN1 cells was determined by RNA-seq using replicate samples incubated with or without 1000 ng/ml DOX for 36 h. Detailed bioinformatics analyses, including DEG identification, consensus hierarchical clustering, and comparison to TCGA RNA-seq data from 423 HNSCC patients are described in supplementary methods. Human TCGA data were obtained from the BROAD firehose portal. Human OCSCC validation data and clinical information were obtained from the GEO public repository (GSE41116) and accompanying publication (PMID 23619168).

Quantitative Real Time PCR (qPCR)

RNA (2-5 μg) was converted to cDNA using a SuperScript First Strand synthesis Kit (Life Technologies) and 100 ng of cDNA was added to quadruplicate reactions containing FAM-MGB TaqMan PCR primers

(supplementary methods) and amplified in a c1000 Bio-Rad Thermal Cycler. Expression of targets was normalized to GAPDH by the ΔCT method using CFX Manager 3.1 software (BioRad).

Staining for β-galactosidase

Cells were fixed and stained with a β-Galactosidase Kit (Cell Signaling), according to supplied instructions and 5 random 10x objective fields were observed to count the number of positive and negative staining cells. For quantitating spheres, 25 random fields were counted.

Mouse Tumor models and Cancer Stem Cell Frequencies

Tongue orthotopic and subcutaneous flank tumor models were established in male nude mice (10 per group) using shRNA-expressing or iICN1-inducible cell lines, with DOX administered by oral gavage where indicated (see supplementary methods for details). Cancer stem cell frequencies in untreated and DOX-treated FaDu-iICN1 populations were estimated by limiting dilution using the ELDA software tool (31) at https://bioinf.wehi.edu.au/software/elda/. Male mice were used as this reflects the gender prevalence of HNSCC (75% male, 25% female); sex was not considered a biological variable as the genes tested are not linked to hormonal pathways and results were expected to be similar in female mice. All mouse studies were conducted in strict accordance with approved IACUC protocols (AN-7317, AN-7321).

Additional Statistical Analyses:

The log 2 transformation was used for all count data and the logit transformation for all percentage data before statistical testing. GraphPad Prism or JMP13 statistical software was used for most analyses. Two-sided t-tests were employed for comparisons involving only two groups ($P < 0.05$ threshold for two group), whereas experiments with multiple groups were analyzed using analysis of variance (ANOVA, $P < 0.05$ significance cutoff). For the latter, a post-hoc Tukey test was applied for pairwise comparisons, or Dunnett's test was used when comparing groups against a control treatment ($P < 0.05$ significance cutoff). Single sample gene set enrichment scores (ssGSEA) were calculated through the BROAD Institute's Gene Pattern public server at https://www.genepattern.org/ using published lists specific to individual cell types that we vetted through cross-correlation of gene expression across >.9,000 solid tumor samples from the TCGA. Gene ontology (GO) enrichment was performed through the GO website portal at https://geneontology.org/, which utilizes a hypergeometric/Fisher's exact test and corrects P values for multiple testing using a B-H correction (FDR < 0.1 as the significance cutoff). Survival data were analyzed through a Cox proportional hazards model (JMP 19), treating NOTCH and NRF2 score groups as binary nominal variables with a P-value threshold of < 0.05 for the likelihood ratio tests. The relationship between tumor immunological status

and the continuous variables NOTCH and NRF2 scores was analyzed with a nominal logistic fit model (JMP 19) using a P-value cutoff of 0.05 for Wald chi-square tests (parameter estimates) and likelihood ratio tests (effects). Optimal cutpoint selection to dichotomize continuous variables for survival analysis was done with an in-house Python script that used a data-driven approach to search over all observed values to maximize the log-rank test statistics. Colony counts (square root–transformed) were analyzed using a cell means model, fitting all cell line × treatment combinations as a single factor in a one-way ANOVA. Planned contrasts tested the simple effect of JAG versus FC within each cell line and the interaction between treatment and cell line genotype (each knockout versus parental), with Bonferroni correction applied to the interaction contrasts.

RESULTS

NOTCH1 Restoration Inhibits Growth in Two-Dimensional Cultures and Alters Morphology of Head and Neck Squamous Cell Carcinoma (HNSCC) Cell Lines Harboring Inactivating *NOTCH1* Mutations

To understand the consequences of NOTCH1 signaling in HNSCC lines harboring *NOTCH1* inactivating mutations (Table S1), we re-expressed WT full-length *NOTCH1* (NFL1) receptors using a bicistronic retroviral vector harboring an IRES-EGFP tag. This allowed purification and testing of NFL1 expressing cells while avoiding artifacts of long-term selection. Following NFL1 overexpression, cells were continuously cultured (1-10 days) on plates pre-coated with either recombinant NOTCH1-ligand Jagged1 fused to an FC-receptor (JAG1) or immobilized control FC protein. We detected cleaved/activated intracellular NOTCH1 (cl-NOTCH1) protein only in *NOTCH1* mutants infected with NFL1 and not empty vector control virus (MigR1), which increased substantially after just 16 h of growth on JAG1 compared to FC control protein (Fig. S1A) and confirmed that endogenous *NOTCH1* mutations were indeed inactivating. NFL1 overexpression alone, without external JAG1, modestly decreased colony formation in both UMSCC47 and UMSCC22A (Fig. S1B and S1C) over a 10-day period. However, when grown in the presence of immobilized JAG1 ligand, NFL1 expression led to a significant reduction in colony formation in four different *NOTCH1*-mutant cell lines when compared to growth on control FC protein (Fig. S1B and S1C).

Reduced colony growth in NOTCH1-mutant UMSCC22A expressing WT NFL1 that were exposed to JAG1 was accompanied by the onset of profound morphological changes after 3 to 5 days, which included a vast reduction in cell size and compact growth as loosely attached spheroids (Fig. S1D). A fraction of NOTCH1-mutant HN4 and HN31 cells expressing NFL1 became spindle-shaped after 3 to 5 days growth on JAG1 and positive for the senescent marker beta-galactosidase (β-Gal) (Fig. S2A and S2B). Likewise,

the loosely formed spheroids produced by NOTCH1-mutant UMSCC22A cells that express NFL1 and were grown on JAG1 showed considerable β-Gal staining (Fig. S2A) Collectively, reactivating NOTCH1 signaling in mutant tumors profoundly inhibited cell growth in two-dimensional cultures and led to altered morphology and senescence.

HNSCC Cell Lines Harboring Wild Type *NOTCH1* Show Similar Patterns of Growth Inhibition and Altered Morphology Following NOTCH1 Activation.

Next, we examined the morphological and proliferation phenotypes associated with NOTCH1 pathway activation in four randomly selected HNSCC cell lines expressing endogenous WT *NOTCH1* receptors (Table S1). Expression of full-length transmembrane NOTCH1 (Tm-NOTCH1) receptor proteins at various levels was confirmed by Western blotting (Fig. 1A). Levels of cl-NOTCH1 protein were examined in three of the cell lines grown on control FC protein and found to be barely detectable but increased following a brief 16 h exposure to JAG1 (Fig. 1A). Extended cultivation of *NOTCH1* WT tumors on immobilized JAG1 inhibited colony formation (Fig. 1B) in four cell lines tested (PJ34, 183, CAL27, and UMSCC1), particularly in 3 of 4 cell lines where JAG1-induced NOTCH1 activation was confirmed (e.g. Fig. 1A), consistent with growth inhibition observed in *NOTCH1* mutants. In the fourth NOTCH1 WT cell line, UMSCC1, JAG1 induced mild but significant reduction in colony formation (Fig. 1B). Remarkably, growth of 183 and PJ34 cell lines on JAG1 (but not control FC protein) led to the very same morphological transformation found earlier in UMSCC22A, characterized by substantial cell shrinkage and the formation of loosely attached compacted tumor spheroids (Fig. 1C). These spheroids also displayed positive staining for β-Gal (Fig. 1D).

The growth inhibition and associated morphological changes induced by JAG1 exposure in PJ34 were effectively reversed by expressing a dominant negative form of Mastermind-like 1 (Fig. 1E and F), known to inhibit NOTCH family signaling. Intrigued, we aimed to dissect the individual phenotypic contributions of NOTCH1 and NOTCH2 signaling in PJ34, since both receptors can be triggered by their shared ligand JAG1. Through CRISPR knockout (KO) experiments targeting *NOTCH1, NOTCH2*, or both genes (Supplementary Fig. S3A), we observed that knockout of either NOTCH gene only partially rescued PJ34 from the growth inhibition induced by JAG1 (Supplementary Fig. S3B). However, double knockout of both genes (N1N2KO) completely prevented JAG1-mediated growth inhibition (Supplementary Fig. S3B) and prevented morphological formation of tumor spheroids (Supplementary Fig. S3E). Re-expression of NFL1 alone in N1N2KO cells was sufficient to restore JAG1-induced NOTCH1 activation (Supplementary Fig. S3C), growth inhibition (Supplementary Fig. S3D), and morphological changes (Supplementary Fig. S3E).

NOTCH1 Activation Does not Drive Proliferation in HNSCC Tumors with High Endogenous NOTCH1 Signaling.

Because previous studies linked NOTCH1 signaling to proliferation and cancer stem cell like behavior in HNSCC cell lines, we investigated the function of NOTCH1 signaling in tumors with high endogenous levels of activated cl-NOTCH1 initially identified by reverse phase protein arrays (RPPA). Levels of cl-NOTCH1 along with 155 other proteins/phosphoproteins, including total NOTCH1 were measured across 53 different HNSCC cell lines with known *NOTCH1* and *NOTCH2* mutational status (Table S1). As predicted, RPPA levels of cl-NOTCH1 were significantly lower in cell lines harboring *NOTCH1* mutations (P =0.03, Fig. S4A). Western blotting (Supplementary Fig. S4B and S4C) confirmed relatively high levels of baseline cl-NOTCH1 protein in six cell lines (FaDu, SCC61, SCC15, PCI24, MDA1986LN, and MDA686LN) identified by RPPA, compared to two of the *NOTCH1* WT cell lines, PJ34 and CAL27, utilized earlier and found to undergo JAG1-mediated growth inhibition (e.g. Fig. 1B, and Fig. S4B). To evaluate the necessity of NOTCH1 signaling in these cells with high cl-NOTCH1 levels, we inhibited the formation of cl-NOTCH1 using 250 or 500 nM of the gamma secretase inhibitor DBZ in all six cell lines (Fig. 2A and Supplementary Fig. S4D). The inhibition of NOTCH1 activation persisted 48 to 72 hours post-DBZ treatment and continuous exposure to DBZ (refreshed every 48 hours) failed to inhibit clonogenic growth in NOTCH1-wild type cells FADU, PCI24, SCC61, SCC15, or MDA686LN (Fig. 2B and 2C). On the contrary, there was even a slight increase in colony formation for two of the cell lines with DBZ. Although MDA1986LN failed to form colonies, its growth was unaffected by DBZ in standard proliferation assays (not shown).

Proteins Correlating with NOTCH1 activation in HNSCC cell lines.

The top protein correlating with cl-NOTCH1 levels among analytes analyzed by RRPA was total NOTCH1 (r = 0.679, AdjP = 3.50E-06, Table S2), followed by FBXW7 (r= 0.612) and EZH2 (r = 0.608). FBXW7 is known to degrade active cl-NOTCH1 in the nucleus and likely represents negative feedback, while EZH2 is a histone methyltransferase that represses gene expression. NRF2, which is a stress-induced transcriptional activator responsive to reactive oxygen species (ROS) was also positively correlated (r =0.449), as was KEAP1 (0.331) that negatively regulates NRF2, and NF-kB-p65 (r = 0.382) which also responds to ROS. Among significantly anti-correlated proteins were the receptor tyrosine kinase AXL (r = -0.457) that regulates survival and proliferation and fibronectin (r =-0.385) an extracellular matrix protein that can mediate binding of fibroblasts.

Persistent NOTCH1 signaling downregulates Proto-Oncogenes, Growth Factors, and Integrins While Increasing Expression of Early Differentiation Markers.

To elucidate the molecular mechanisms and understand phenotypes associated with *prolonged activated NOTCH1 signaling*, we examined alterations in gene expression in *NOTCH1*-WT HNSCC cell lines (PJ34 and 183) induced by growth on JAG1 ligand for five days. A two-way ANOVA identified genes downregulated (Table S3) and upregulated (Table S4) due to growth on JAG1 as a main effect (e.g., JAG treatment) and for the individual cell lines PJ34 and 183 grown on JAG1 in post hoc analyses. We focused on the top significant genes that showed at least a 1.4-fold change in both cell lines and found 50 genes upregulated and 70 downregulated because of JAG1 exposure. Gene Ontology (GO) enrichment analysis of these 120 altered genes identified pathways related to proliferation, differentiation, cell adhesion, cytokine production, response to oxygen containing compounds, and cytokine production (Supplementary Table S5 and S6, and Supplementary Fig. S5). Among the top genes downregulated by NOTCH activation were three pro-survival/proliferation genes, *α-CATULIN* (*CTNNAL1*), *AXL*, and Epiregulin (*EREG*). Notably, *α-CATULIN* exhibited the most significant reduction in magnitude among all genes (e.g., 24-fold in 183) following NOTCH activation. *AXL* ranked among the top five genes with the greatest reduction in both cell lines and was consistent with the earlier finding of an inverse correlation between AXL protein and cl-NOTCH1 by RRPA (Supplementary Table S2). Multiple genes regulating cellular adhesion, including *ITGA3* (integrin α3), *ITGA5* (integrin α5), *LAMC2* (Laminin gamma 2), and *LAMC1*, were downregulated in both cell lines after NOTCH activation (Supplementary Table S3). Keratins 4 and 13 emerged as the top two upregulated genes in 183 cells (7.9- and 3.6-fold, respectively) and among the top 15 upregulated genes in PJ34 (2.0- and 1.8-fold, respectively) following NOTCH activation (Supplementary Table S4). Additionally, putative tumor suppressors such as *EPHA4, TP53INP1, PDCD4, DSP,* and *TXNIP* were among top genes upregulated by NOTCH activation. The specific pattern of integrins downregulated and keratins upregulated (Fig. 3A) mirrors what happens to normal oral mucosa during very early differentiation as basal stem cells divide and migrate upwards to the suprabasal layer of squamous epithelium. Collectively, the genes commonly regulated in both PJ34 and 183 cells after growth on ligand suggest a loss of proliferation and loss of substrate adhesion consistent with very early squamous cell differentiation.

Validation of Genes and Proteins Regulated by NOTCH1 Activation.

Given strong links between AXL and α-CATULIN and HNSCC aggressiveness, we validated their decreased protein expression following NOTCH1 activation in both WT and mutant tumors using multiple approaches. First, we exogenously expressed activated cl-NOTCH1 using a retroviral construct encoding

intracellular *NOTCH1* (ICN1) widely used by others for functional studies (32); construct integrity was confirmed as described in supplementary methods (Supplementary Fig. S6A). Infection with ICN1 but not empty vector MigR1 induced morphological changes in UMSCC22A and *NOTCH1* WT 183 and PJ34 cells identical to that observed earlier for growth of these cell lines on JAG1 (Supplemental Fig. S6B, S6C, S6D). ICN1 expression caused substantial reduction in AXL and a-CATULIN proteins in *NOTCH1* WT PJ34 and 183 (Fig. 3B and Supplementary Fig. S6E) and *NOTCH1* mutant HN31 and UMSCC22A (Fig. 3B, and Supplementary Fig. S6A). Likewise, growth of PJ34, or *NOTCH1* mutant cells with restored NFL1 receptors (HN31, UMSCC22A, and UM47) on JAG1 ligand also suppressed AXL and a-CATULIN protein levels (Fig. 3C). Decreased LAMC2 and ITGA3 protein was also confirmed following ICN1 expression in PJ34 and HN31. Consistent with negative regulation by NOTCH1, increased AXL and α-CATULIN protein were found after pharmacological inhibition of NOTCH1 signaling with DBZ in the *NOTCH1* WT cell lines with normally high NOTCH1 activation (Supplementary Fig. S7).

NOTCH1 Regulates Many Genes Indirectly

To better understand the mechanisms and timing of NOTCH1 activation, we constructed a doxycycline (DOX)-inducible ICN1 (iICN1) retroviral construct encoding intracellular NOTCH1 from the known cleavage site, enabling precise control over activation levels and detection by cl-NOTCH1-specific antibodies. We combined this tool with NOTCH1 Chip-seq experiments to identify genes directly regulated. *NOTCH1/NOTCH2* double knockout PJ34 cells (e.g., Supplementary Fig. S3) were engineered to express the Tet3 regulator (PJ34Tet3 cells) along with iICN1 (PJ34-iICN1) so that NOTCH1 was activated in the presence of DOX. Dose response experiments determined that 500-1000 ng/ml DOX induced levels of cl-NOTCH1 protein equivalent to those found after incubating parental PJ34 (PJ34-P) on JAG1 (Fig. 3D). Within one week after iICN1 induction with DOX, PJ34-iICN underwent the same morphological transformation observed earlier when parental PJ34 were grown on JAG1, characterized by massive cell shrinkage and formation of loosely attached tumor spheroids (Fig. 3E). RNA-seq performed from samples isolated 20 hours after peak iICN1 expression identified 1223 genes downregulated and 666 genes upregulated by 1.25-fold or greater (FDR <0.1) specifically in PJ34-iICN1 treated with DOX but not in control PJ34Tet3 cells treated with DOX (Table S7). NOTCH1 Chip-seq experiments identified 357 unique genes in PJ34-iICN1 bound by NOTCH1 at one or more loci in their gene promoters or gene bodies after DOX induction (Table S8). Venn diagrams illustrating the overlap of genes regulated by iICN1, JAG, and bound by ICN1 appear in Fig. 3F and 3G, with intersecting genes listed in Supplementary Tables S9 and S10. *AXL, α-CATULIN, ITGA3, ITGA5, LAMC1, and LAMC2* were all significantly downregulated by both iICN1 and JAG1 in PJ34, but only *LAMC2* was bound by ICN1 (e.g., within the gene body) in Chip-Seq

experiments, suggesting the majority of observed changes linked to early differentiation were an indirect but early effect of NOTCH1 activation.

Genes from the HES (Hairy and Enhancer of Split) and Hey (Hairy/enhancer-of split with YRPW motif) family of transcriptional repressors are key canonical downstream targets of NOTCH1 signaling cascades that were also found to be elevated after ICN1 induction and identified through NOTCH1 Chip-seq. Specifically, HES2, HES4, HEY2, and HEYL were all bound by NOTCH1 in their promoter/gene body regions and significantly upregulated by 20h iICN1 induction (Supplementary Table S7 and S8) but showed lower fold changes with prolonged growth on JAG1 incubation (Supplementary Table S3 and S7). This likely reflects the cyclical nature of HES/HEY transcription following NOTCH1 activation. HES5, on the other hand, was bound by ICN1, and was strongly elevated after ICN1 induction or prolonged JAG1 exposure (Supplementary Table S3, S7 and S8). In contrast, the early differentiation markers *KRT13, KRT4*, and tumor suppressors *EPHA4, PDCD4,* and *TXNIP* ―all upregulated by prolonged JAG1 exposure― were not identified as direct NOTCH1 targets by Chip-seq nor were they strongly induced within 20 h of ICN1 expression (Supplementary Table S10), suggesting these are later events indirectly triggered through NOTCH1 signaling. Collectively the data support a model through which NOTCH1 activation triggers early, but indirect suppression of cell adhesion receptors involved in transitioning away from basement membrane attachment with subsequent upregulation of differentiation markers.

NOTCH1 Signaling Drives Anchorage Independent Growth but Fails to Increase Frequency of Cancer Stem Cells or Promote *In Vivo* Tumor Growth.

In vitro growth of tumor spheroids in three-dimensional culture systems employing low-serum media is frequently used to propagate and quantify cancer stem cells (CSCs). The loosely attached tumor spheroids that formed in both *NOTCH1* mutant and *NOTCH1* WT cell lines after growth on JAG1 or NOTCH1 signaling stained positive for the senescence marker β-gal when cultivated in media with regular serum concentrations. However, serum is known to cause differentiation of CSCs. Therefore, we engineered some additional cell lines to robustly examine if NOTCH1 signaling would increase anchorage independent growth, survival, or expression of CSC markers in the presence of diminished serum, using our DOX iICN1 vector system. *NOTCH1*-null/mutant UMSCC22A cells were engineered to express the Tet3 regulator and iICN1. For FaDu, we used CRISPR gene KO to first delete endogenous *NOTCH1*, since baseline cl-NOTCH1 levels are normally high, before introducing the Tet3 regulator and iICN1. Titration experiments indicated that physiological levels of cl-NOTCH1 and the characteristic morphology changes and spheroid formation were achieved at doses of 250-500 ng/ml in FaDu-iICN1 (Fig. S8A and S8B). Physiological levels of activated NOTCH1 were achieved at 200-300 ng/ml DOX in UMSCC22A-iICN1, although

morphology changes happened at an even lower dose (Supplementary Fig. S8C and S8D). At these doses of DOX, profound inhibition of growth in two-dimensional cultures accompanied expression of cl-NOTCH1 in both cell lines as well as PJ34-iICN1 (Supplementary Fig. S9A and S9B). In the absence of iICN1 infection, DOX failed to induce morphology changes or growth inhibition in any of the control Tet3G cells (Supplementary Fig. S9C). DOX-induced iICN1 expression significantly increased the number of tumor orospheres formed from FaDu and UMSCC22A (Supplementary Fig. S10A and S10B) in suspension cultures maintained with low serum, compared to control Tet3G cells or cultures lacking DOX.

Next, we examined whether increased tumor spheroid survival reflected increased anoikis resistance (i.e., cell death associated with detachment). Following 48 h pretreatment with or without DOX, iICN1 induction was significantly protective against anoikis in both FaDu and UMSCC22A compared to cells without DOX or control Tet3G cells (Supplementary Fig. S10C). Because anoikis resistance and spheroid growth are both characteristics of CSCs, we examined whether NOTCH1 activation would also increase CSC markers previously associated with HNSCC, including Aldefluor activity, CD133 expression, and SOX2 protein levels. A 48-h induction of ICN1 failed to increase CD44+bright/Aldefluor positive cells in both UMSCC22A and FaDu (Supplementary Fig. S11), or the percentage and mean fluorescence of CD133-expressing cells (Supplementary Fig. S12A and S12B). However, SOX2 gene expression increased an average of 1.4-fold in PJ34 and 183 cells grown on JAG1 and 1.3-fold in PJ34 after ICN1 induction (Supplementary Tables S4 and S7), though SOX2 was not bound by NOTCH1 in ChIP-seq (Supplementary Table S8), ruling out direct regulation. SOX2 protein was similarly elevated 2- to 4-fold after ICN1 induction in PJ34, FaDu, and UMSCC22A (Supplementary Fig. S12C).

Although stem cell markers and tumor spheroid formation can be surrogates for CSCs, the gold standard remains measuring the *in vivo* tumor initiating frequency in mice through limiting dilution assays. We reasoned that if NOTCH1 signaling were driving CSC behavior, it would most likely happen in *NOTCH1* WT tumors that endogenously express activated NOTCH1, like FaDu. Furthermore, for tumors to grow *in vivo*, stem cells must be allowed to re-enter a proliferative state resembling progenitors by turning NOTCH1 signaling off again. To avoid artifacts from non-physiological levels of NOTCH1 activation we conducted pilot studies to determine the *in vivo* DOX dose that would be equivalent to an *in vitro* dose of 400 ng/ml, which induced physiological levels of NOTCH1 signaling in FaDu-iICN1 (Supplementary Fig. S8A). Using a reporter cell line engineered to express luciferase from the same inducible promoter as iICN1 a dose of 1 mg DOX by oral gavage in mice led to equivalent fold induction of luciferase as 400 ng/ml DOX *in vitro* (Supplementary Fig. S13).

FaDu-iICN1 cells were then treated with 400 ng/ml DOX *in vitro* for 72h to activate NOTCH1 and potentially enrich for CSCs before inoculating increasing amounts of cells (100-100,000 cells range) subcutaneously into mouse flanks. This was followed by daily oral gavage with 1 mg DOX for an additional week to maintain NOTCH1 activation, followed by discontinuation of DOX for the remaining period to allow tumor cells to transition back to a proliferative state. As a control, matching numbers of untreated FaDu-iICN1 cells (e.g., no DOX) were inoculated into mice that never received DOX. Tumor cells treated with DOX grew much slower (Fig. 4A-D) and formed tumors later than tumor cells never treated with DOX at every inoculum dose (Fig. 4E-H). Eventually, tumors formed in 100% of animals for all groups except for the lowest inoculum of 100 cells, where only 40% of mice from the DOX group ever formed tumors by 100 days compared to 100% of mice that grew tumors within 40 days when no DOX was given. Statistical analysis estimated a tumor initiating frequency of 1/189 for DOX treated tumors compared to 1/1 for FaDu with no NOTCH1 induction (Table S11, $P = 0.00142$), indicating a drastic reduction in CSC frequency with NOTCH1 activation.

When NOTCH1 signaling was restored in a *NOTCH1* mutant background using UMSCC22A-iICN, it also profoundly inhibited tumor growth. UMSCC22A-iICN1 were implanted into flanks of nude mice, which were randomized to receive placebo or 1 mg DOX by oral gavage daily for 3 weeks to persistently induce iICN1. NOTCH 1 activation profoundly suppressed *in vivo* tumor growth (Supplementary Fig. S14A). After discontinuation of DOX, tumors eventually grew in some mice. Histological staining revealed a roughly 50% reduction in the presence of mouse fibroblasts within the DOX treated tumor group ($P<0.01$, Supplementary Fig. S14B).

Suppression of Oncogenic AXL and α-CATULIN Expression Contributes to NOTCH1-mediated Growth Inhibition.

NOTCH1 activation increased expression of multiple tumor suppressor genes and simultaneously reduced expression of AXL and α-CATULIN, two oncogenic proteins linked to tumor growth and aggressiveness in HNSCC. We functionally examined the impact of reduced *AXL* and *α-CATULIN* expression on tumor growth *in vitro* and *in vivo*, with bicistronic shRNA IRES EGFP constructs targeting these two genes. Phenotypes were measured shortly after purifying infected (e.g., EGFP+) cells. Specific knockdown of either AXL or α-CATULIN protein in both *NOTCH1*-mutant HN31 and *NOTCH1*-WT PJ34 was confirmed by Western blotting (Supplementary Fig. S15A and S15B) and found to significantly reduce colony formation in clonogenic assays ($P<0.006$, Supplementary Fig. S15C and S15D). Importantly, shRNA knockdown of either *AXL* or *α-CATULIN* severely diminished tumor growth of HN31 in an

orthoptic tongue tumor model (Supplementary Fig. S15E) and in a subcutaneous flank model using alternate shRNA sequences (Supplementary Fig. S15F), demonstrating the phenotype was robust.

We used PJ34-iICN1 and UMSCC22A-iICN1 to functionally examine whether preventing NOTCH1-induced increases in HES/HEY family members would prevent associated decreases in *AXL* and *α-CATULIN* gene expression. In both cell lines, prior knockdown of *HES1, HES2, HES4, HEY1,* or *HEY2* with siRNA shortly before ICN1 induction reduced their elevation stemming from NOTCH1 activation but did little to prevent associated reductions in *AXL* and *α-CATULIN* expression (determined by qPCR, Supplementary Fig. 16). Furthermore, combined simultaneous knockdown of some of the more strongly induced NOTCH1 targets, *HES5/HEY1/HEY2*, also failed to prevent NOTCH1-induced decreases in *AXL* and *α-CATULIN* expression in both PJ34 and UMSCC22A (Not shown).

A Gene Expression Signature identifies Primary HNSCC Tumors with Intact NOTCH1 Signaling and an Altered Tumor Microenvironment.

A robust *in vivo* gene expression signature of NOTCH1 activation was developed based on the top 120 differentially regulated genes identified *in vitro* after JAG1 stimulation (Supplementary Fig. S5) by examining their cross-correlation in primary tumors from The Cancer Genome Atlas (TCGA) oral squamous cell carcinoma (OSCC) cohort of 312 patients. After removing one gene for low expression, two-way hierarchical clustering of cross-correlation coefficients identified two primary gene clusters or modules (Supplementary Fig. S17A) from the TCGA data. Genes from each cluster showed a dominant but opposite pattern of JAG1 regulation *in vitro*, identifying up- and downregulated gene groups. After removal of several inconsistently regulated genes, 95 genes remained in the final signature (Supplementary Fig. S17B and Table S12). We applied the 95 gene signature to perform consensus hierarchical clustering on the TCGA OCSCC and TCGA laryngeal\hypopharyngeal SCC (LHSCC) cohorts individually. Consensus clustering metrics identified that the choice of two sample clusters was optimal for both TCGA cohorts (Supplementary Fig. S18). After two-way clustering (Fig. 5A and 5B), it was predicted that NOTCH1 signaling is off in sample cluster 1 but on in sample cluster 2 for both OCSCC and LHSCC cohorts, based on the direction of gene regulation from the 95-gene signature observed (Tables S13-14). The predicted NOTCH1 pathway states were compared to the *NOTCH1* mutational status of samples in both cohorts to validate the NOTCH1 signature. In both cases, sample cluster 2 was depleted for *NOTCH1* mutations but sample cluster 1 was enriched ($P = 0.015$ and $P = 0.013$, Fig. 5A and B), consistent with inactivating *NOTCH1* mutations preventing NOTCH1 pathway signaling. Consequently, the gene signature likely distinguished tumors based on their NOTCH1 pathway status, and the data suggests that NOTCH1 signaling is active in a subset of OCSCC and LHSCC tumors (e.g., sample cluster 2).

Next, we identified *all genes* differentially expressed by the subset of TCGA tumors predicted to have NOTCH1 activated in the OCSCC (Table S15) and LHSCC (Table S16) cohorts and compared them to genes found differentially regulated by JAG1 binding *in vitro*, including the subset of 95 genes defining the pathway signature. Venn diagrams depicting overlap of differentially expressed genes appear in Fig. 5 C and D. Among the commonly *upregulated* genes (Supplementary Table S17) were early differentiation markers ***KRT13, KRT14, and KRT15***; the immune checkpoint **VTCN1**; and several enzymes involved in the antioxidant response, including ***AKR1C3***, which neutralizes lipid peroxides, as well as ***GCLC, GSTA1***, and **GSTA4**, which are essential for glutathione synthesis and anti-oxidant response. Among commonly downregulated genes (Supplementary Table S18) were multiple integrins and cell adhesion molecules ***ITGA3, ITGA5, ITGB6, LAMC2, KIRREL1, CDH13,*** including ***COL17A1*** (collagen XVII) that mediates adhesion to basement membranes as a component of hemidesmosomes. The pro-oncogenic genes ***AXL*** and ***α-CATULIN*** were also commonly downregulated. So was ***WNT7A***, which contributes to HNSCC growth by stimulating β-catenin, as well as ***EREG*** and ***TGFA***, both EGFR ligands that promote HNSCC.

Single sample Gene Set Enrichment Analysis (ssGSEA) was used to determine associations between the tumor microenvironment and NOTCH1 signaling, using published lists (Table S19) specific for immune subtypes, endothelial cells, and a robust gene list we constructed for cancer associated fibroblasts (CAFs). Our CAF signature was derived by clustering cross-correlation coefficients for fibroblast associated genes across more than 9000 solid tumors from the TCGA. In the TCGA OCSCC cohort, tumors with a NOTCH1 activation signature had significantly reduced proportions of nearly every immune subset analyzed (Table S20), indicating they are immunologically "cold". Two-way hierarchical clustering with the immune subset ssGSEA scores demonstrated significant depletion of tumors with active NOTCH1 signaling among OCSCC "hot" tumors ($P<0.0001$, Fig. 6A). In LHSCC samples with NOTCH1 activation there was a similar trend of broad decrease in leukocytes subpopulations present when NOTCH1 signaling was on, although differences only reached statistical significance for T helper type 1 and mast cells (Table S21). Because we previously showed that a cold immune microenvironment was associated with elevated NRF2 gene signatures specifically in OCSCC but not LHSCC (33), we revisited the connection between NOTCH1 signaling and the antioxidant response inferred from some of the top genes commonly regulated by NOTCH1 (Fig. 5C) or proteins correlating with cl-NOTCH1 (Table S2). HNSCC TCGA tumors with NOTCH1 activation had NRF2 pathway scores (Fig. 6B) that were on average profoundly elevated regardless of disease subsite ($P<0.0001$). In contrast, NOTCH1 activation was associated with a significant reduction in the proportion of CAFs present, imputed from CAF ssGSEA scores in both OCSCC and LHSCC (Fig. 6C), which was supported by gross differences in fibroblast content visible in H&E images downloaded from the TCGA project (Supplementary Fig. S19).

NOTCH1 Signaling Correlates with Survival and *PIK3CA* Genomic Alterations

When NOTCH1 signaling status was treated as a dichotomous variable for OCSCC TCGA samples based on clustering, there was no significant association (Fig. 7A) with overall survival (OS). Because signaling pathways are rarely binary, we used the NOTCH1 gene signature to generate ssGSEA scores for samples and treated NOTCH1 signaling as a continuous variable, which demonstrated clear separation between sample clusters found previously (Fig. 7B). Optimal dichotomization identified a NOTCH1 ssGSEA threshold of -1554 that stratified OCSCC patients into two groups which differed significantly by survival with poor survival corresponding to lower levels of NOTCH1 signaling (P = 0.0061, Fig. 7C). The threshold identified seemed biologically meaningful as it corresponded to roughly the average value for samples from the NOTCH1-off clusters in both OCSCC and LHSCC (Fig. 7B), and it also separated the LHSCC samples into two groups that differed in survival in the same manner (P = 0.0.0045, Fig. 7D). Likewise, patients with NOTCH1 ssGSEA scores below this same threshold had significantly worse progression free survival in both disease subsites (Fig. 7E and F). Using an independent cohort of OCSCC tumors (N =43) previously characterized by our group (2) but profiled for gene expression using a microarray platform, we were able to validate that NOTCH pathway activation was associated with better survival (Supplementary Fig. S20). Patients whose tumors had low NOTCH scores had a median survival time that was roughly half of that for those with tumors having a high NOTCH score. No associations were found between lymph node stage, tumor stage, or smoking history in either disease subsite, although there was a significant decline in NOTCH signaling levels among poorly differentiated tumors found in OCSCC tumors (not shown).

The improved survival associated with higher NOTCH signaling in tumors conflicts with what would be predicted based on their higher levels of NRF2 signaling (e.g. Fig. 6B), which itself is associated with worse survival and a colder tumor immune microenvironment (33). To disentangle the relationships between NOTCH, NRF2, leukocyte infiltration, and survival, we plotted NRF2 versus NOTCH scores in TCGA OCSCC tumors, confirming a positive correlation (Supplementary Figure S21A). An overlay of the pathway thresholds defined 4 quadrants or risk groups (Supplementary Figure S21A). As predicted, tumors annotated by immunological status above the NRF2 threshold tended to be immunologically colder. Kaplan-Meier plots (Supplementary Figure S21B) revealed that patients whose tumors had high NRF2 and low NOTCH signaling (quadrant 1) had the worst median survival time (15.2 months). Patients whose tumors had low NRF2 and high NOTCH scores had the best prognosis with a median survival of 71.2 months, with patients in the remaining two quadrants showing an intermediate and similar survival phenotype. A Cox proportional hazards model fit of survival time demonstrated independent contributions of both NRF2 (P = 0.008) and NOTCH (P = 0.0206) pathway status with no significant interaction (Table

S22). Having either a low NOTCH score or high NRF2 score led to an increased chance of death, with hazard ratios (HR) = 1.24 and 1.3, respectively.

Next, we examined the relationship between these pathways and immunological status of OCSCC tumors in a nominal logistic regression model (Table S23). NRF2 was the dominant factor driving colder tumors ($P<0.0001$) with an odds ratio of 5.08 (per 1000 units of NRF2 score, $P <0.0001$), but NOTCH score did have a significant and smaller independent effect ($P<0.03$) with an odds ratio of 0.78 (per 1000 units of NOTCH score, $P <0.05$), signifying that lower NOTCH score (e.g. NOTCH off) was associated with hotter tumors.

We previously reported that HNSCC cell lines harboring *NOTCH1* loss of function mutations are exquisitely sensitive to PI3K inhibitors (27, 28), which was supported by a small clinical trial we conducted (29). Direct links between NOTCH1 signaling and PI3K inhibitor sensitivity proved context dependent, leading us to hypothesize that tumors evolving with *NOTCH1* mutations may have altered pathway dependencies, including PI3K. We analyzed the relationship between TCGA NOTCH1 sample clusters and found that the presence of PIK3CA genomic alterations (e.g., high level copy gains or mutations) was significantly enriched among OCSCC ($P = 0.024$) and LHSCC samples ($P = 0.0004$) belonging to the NOTCH-On clusters (Supplementary Fig. S22).

DISCUSSION

More than a decade has passed since our group and others first identified inactivating *NOTCH1* mutations as a driver of HNSCC (1, 3). Yet, the function and significance of NOTCH1 signaling in this cancer are still poorly understood. Adding to the complexity, WT *NOTCH1* has been reported as an oncogenic driver inducing CSC-like properties in some HNSCC cell lines (7, 26), with strong NOTCH1 signaling observed in subsets of primary tumors. Here, we clarify these conflicts and unify the field.

Regardless of *NOTCH1* mutational status or endogenous levels of signaling, the pathway activates a program of very early differentiation that involves downregulation of cell adhesion molecules, which normally tether cells to their basement membrane, accompanied by upregulation of keratin differentiation markers. These changes in adhesion accompanied by increased anoikis resistance, which is likely a vestige of squamous epithelial stratification, promotes growth of cells in a non-adherent spheroid state and likely explains reports that NOTCH1 signaling triggers HNSCC tumors to become more CSC like (19, 25). However, using an inducible cl-NOTCH1 expression system in *NOTCH1* WT FaDu clearly showed a substantial decrease in tumor initiating cells *in vivo* using the gold standard limiting dilution assay. Furthermore, we found that a NOTCH1 inhibitor DBZ, more potent and specific than DAPT frequently used in prior NOTCH studies (16, 23, 34), had no effect on *in vitro* growth of six different HNSCC tumor

lines specifically chosen for high basal cl-NOTCH1expression. Collectively, this refutes the idea that NOTCH1 actively drives cell proliferation in HNSCC. Interestingly, we find evidence of limited NOTCH1 signaling in HNSCC cell lines with high basal cl-NOTCH1 expression, given the strong anti-correlation with AXL protein—one of the genes robustly downregulated by NOTCH1 activation. That said, no obvious growth phenotypes distinguished cell lines with high NOTCH1 signaling but when the gene was knocked out in FaDu and cl-NOTCH1 re-expressed at physiological levels there was a dramatic morphologic transformation to tumor spheroid growth not otherwise observed for parental FaDu with equivalent NOTCH1 signaling. Expression of Fbxw7 protein, the known E3-ligase to degrade intracellular activated NOTCH1, strongly correlated with cl-NOTCH1 protein by RPPA in cell lines. Collectively, our data suggest that some HNSCC cell lines can tolerate NOTCH1 signaling *in vitro* and that growth in two-dimensional cultures may select for diminished downstream phenotypes.

By defining genes altered after physiological activation of NOTCH1 *in vitro*, we were able to construct an empirically derived gene expression signature of NOTCH1 activation that was validated in primary HNSCC tumors from two different disease sites, allowing stratification of patients' samples based on relative levels of NOTCH1 signaling. Wholesale downregulation of cell adhesion receptors, particularly integrins along with genes encoding extracellular matrix proteins such as laminins and COL17A1 were found to accompany NOTCH1 activation in both preclinical models and primary tumors, consistent with very early differentiation of tumors that mirrors transition from the basal to suprabasal layer in normal mucosa. Possibly, the shift in cell adhesion and extracellular matrix proteins could impact the tumor microenvironment and contribute to the diminished presence of CAFs. We found evidence of this in our preclinical model and in both disease subsites when NOTCH1 signaling was elevated. A surprising finding was the association between NOTCH1 activation and increased NRF2 pathway signaling, which has implications for chemoradioresistance, and is consistent with reports that NOTCH1 signaling increases chemotherapy resistance (25). Elevated NRF2 activity contributes to cisplatin resistance using preclinical models (35, 36) and elevated NRF2 activity is associated with an immunologically cold tumor immune microenvironment in multiple tobacco associated tumors (33), including OCSCC but not LHSCC. Consistent with this, we found NRF2 scores were significantly correlated with NOTCH scores. Both the NRF2 and NOTCH pathways independently associated with worse survival, defining four distinct risk groups in which patients whose tumors were NRF2 high/NOTCH low had the poorest outcomes of all groups. While both high NOTCH and NRF2 activation were significantly associated with immunologically cold tumors, the effects of NRF2 were considerably stronger.

Many genes altered by NOTCH1 were modulated within an early time frame but were not directly regulated by binding of intracellular NOTCH1 to their promoters or enhancers. Of these, *AXL* (37, 38) and *α-CATULIN* (39, 40) reportedly contribute to HNSCC tumor growth in preclinical models and are associated with clinical aggressiveness. We confirmed their pro-oncogenic function *in vitro* and in *vivo* through knockdown experiments and they contributed to some of the growth inhibition triggered by NOTCH 1 activation. However, the multiplicity of genes commonly regulated by NOTCH1 both *in vitro* and *in vivo* suggests cooperative gene expression programing with possibly redundant function. SOX2 was the one gene tied to CSC that we and others found upregulated by NOTCH1 activation (24, 41). However, IHC has shown that SOX2 (42) along with cl-NOTCH1 (7) is frequently present in the normal mucosal suprabasal layer and elevated SOX2 correlates with better HNSCC prognosis (42), consistent with our proposed model of very early differentiation.

If NOTCH1 signaling turns on a program of very early differentiation and is not associated with CSC maintenance, then we might expect tumors with higher NOTCH1 signaling to have a better prognosis. Consistent with what others reported for cleaved NOTCH1 staining (26), we found that subsets of tumors with higher NOTCH1 signaling scores had improved OS and PFS across disease subsites. Our preclinical models demonstrated that WT *NOTCH1* tumors retain plasticity and can undergo very early differentiation in response to NOTCH1 signaling. This is consistent with prior work proposing that *NOTCH1* LOF mutations drive carcinogenesis by preventing early stem cell differentiation and promoting accumulation of secondary mutations in an expanding pool of stem cells (43). Possibly, precancerous lesions arising with *NOTCH1* mutations avoid early differentiation and retain some pathway dependencies of stem cells that may include the PI3K pathway, which has been linked to survival and maintenance of CSCs (44). This could explain the sensitivity to PI3K inhibitors associated with *NOTCH1* mutations we reported in the absence of *PIK3CA* mutations (27). If early differentiation driven by NOTCH1 activation in WT tumors were accompanied by a shift away from the PI3K pathway, then perhaps these tumors rely more on genomic alterations in the *PIK3CA* gene to re-establish signaling. This is supported by our findings that mutations and high-level amplifications of the *PIK3CA* gene are more frequent in tumors with higher NOTCH1 signaling. Nevertheless, *NOTCH1* mutations sometimes do co-occur in HNSCC tumors harboring PIK3CA mutations (4). We have also seen this in a few established HNSCC cell lines (27), and it has been reported by others that *NOTCH1* deletion accelerates growth of genetically engineered mouse models (GEMMs) of HNSCC driven by activating *PIK3CA* mutations (45). While the trend towards mutual exclusivity may reflect steps in carcinogenesis, evidence from GEMM studies supports that loss of *NOTCH1* function can still be advantageous in HNSCC tumors driven by PIK3CA oncogenes.

A dual oncogenic/tumor suppressive function for *NOTCH1* has been reported in HPV-positive (HPV+) tumors in HNSCC GEMMs (46) driven by expression of HPV-derived E6/E7 oncogenes plus an activating KRAS mutation (KHR mice), where faster tumor growth occurred when KHR mice expressed activated ICN1 or lost *NOTCH1* gene. However, the authors noted that KHR tumors had impaired differentiation persisting with *NOTCH1* alterations, making extrapolation to our work difficult as this genomic background may obscure differentiation pathway changes. The same study showed that in HPV-negative GEMMs with mutated KRAS, homozygous *NOTCH1* loss accelerated tumor growth — supporting a tumor suppressor function, consistent with conditional *NOTCH1* knockout accelerating skin squamous cell carcinomas formation in mice (47). One *NOTCH1*-mutant line in our study (UMSCC47) is HPV+, and NOTCH1 restoration inhibited colony formation similarly to HPV-negative lines. NOTCH pathway scores showed a trend toward worse survival in HPV+ TCGA HNSCC patients (not shown), possibly because HPV oncogenes interfere with differentiation programs, reducing reliability of downstream target-based tumor separation. The paucity of *NOTCH1* mutations among HPV+ HNSCC tumors (4), suggests these cancers escape early differentiation through E6/E7 transformation rather than *NOTCH1* loss, with little evidence of activating *NOTCH1* mutations in HPV+ tumors.

How then do we reconcile our conclusions with multiple reports of NOTCH1 behaving like an oncogene in HNSCC? Many factors likely contribute, including overinterpretation of tumor spheroid properties in this context, frequent use of antibodies that detect inactive membranous/cytoplasmic NOTCH1 rather than active cleaved NOTCH1 for IHC studies, nonspecific pharmacological inhibitors to block NOTCH1 signaling, widely available constructs to overexpress activated NOTCH1 that cannot be validated with cleavage specific antibodies, and/or ambiguous use of antibodies recognizing C-terminal NOTCH1 peptides in lieu of those specific for activated NOTCH1. In summary, we find molecular evidence of NOTCH1 signaling in subsets of HNSCC tumors that has broad gene expression consequences impacting tumor biology, the tumor microenvironment and clinical behavior. However, most of the evidence unequivocally supports a tumor suppressor function for *NOTCH1,* regardless of mutational status or baseline NOTCH1 signaling, which triggers early differentiation accompanied by decreased cell attachment.

Declarations

Ethics approval and consent to participate

The research did involve any human subjects. All human data or cell lines used are publicly available and therefore no consent is required.
All animal experiments were performed in accordance with protocols and ethics approved by our Institutional Animal Care and Use Committee at Baylor College of Medicine and The University of Texas MD Anderson Cancer Center.

Consent for publication

Availability of data and materials

All human clinical specimen data used, including gene expression, are available from public databases. Raw harmonized TCGA RNA-seq data was downloaded from the University of Santa Cruz Xena browser at https://xenabrowser.net. TCGA genomic and clinical data was obtained from cbioportal website at https://www.cbioportal.org/. Normalized RNA microarray expression data from the MD Anderson validation was downloaded from the GEO database (GSE41116) and the data with converted gene symbols is available in the supplementary values tables. Normalized microarray and RNA-seq data from experiments for individual genes across replicate samples is available in the primary supplementary tables. Bulk RNA sequencing was performed for this study more than five years ago. The original raw sequencing files (FASTQ) are no longer available due to data archiving limitations at the time the experiments were conducted. Processed gene expression matrices and all data used for analysis are provided in the Supplementary Data.
All cell line models engineered will be made available upon request.

Competing interests

The authors declare no relevant competing financial interests and no financial conflicts that could have appeared to influence the work reported in this paper. VCS is a consultant for Femtovox Inc. This material is based upon work supported in part by the Department of Veterans Affairs, Veterans Health Administration, Office of Research and Development. The views expressed in this article are those of the authors and do not necessarily reflect the position or policy of the Department of Veterans Affairs or the United States government.

Funding to acknowledge: This work was supported by the National Institute of Dental and Craniofacial Research through RO1DE024179 (M.J.F.), the National Cancer Institute (NCI) through RO1CA235620 (M.J.F.), U54CA274321 (V.C.S, M.J.F, J.N.M, A.O.); I01BX006380 (V.C.S, M.J.F); U01DE025181 (M.J.F, J.N.M), and the Cancer Prevention Institute of Texas through RP200369 (M.J.F, F.J).

Author Contributions

All author contributions are listed at the end of article before References.

Acknowledgments

Not applicable.

LIST OF ADDITIONAL FILES

NOTCH_suppelmentary methods.docx:
NOTCH_Supplementary Tables S1 to S14.xlsx:
NOTCH_Supplementary Table S15.xlsx:
NOTCH_Supplementary Table S16.xlsx:
NOTCH_Supplementary Table S17 to S23.xlsx:

Authors Contributions: Detail each author's specific contributions using initials.

Chenfei Huang[1, 2,#] Shhyam Moorthy[3, 4,#] Qiuli Li[3, 5,#] Kazi Mokim. Ahmed[1], Kalil Saab[1], Defeng Deng[1, 6], Jiping Wang[3], Xiayu Rao[7], Jiexin Zhang[7], Yuanxin Xi[7], Jing Wang[7], Zhiyi Liu[3, 8], Noriaki Tanaka[3, 9], David A. Wheeler[10, 11], Eve Shibrot[10], Rami Saade[12], Curtis R. Pickering[3, 13], Tong-Xin Xie[3], Adel K. El-Naggar[14], Abdullah A. Osman[3], Kunal Rai[15], Patrick A. Zweidler-McKay[16], John V. Heymach[17], Lauren A. Byers[17], Faye M. Johnson[17, 18], Vlad C. Sandulache[1, 19, 20], Jeffrey N. Myers[3], Pedram Yadollahi[1],**, Mitchell J. Frederick[1],*

The co-first authors (C.H., S.M., Q.L.) contributed equally. Author order was determined by the senior author (M.J.F.) based on overall contribution to project completion: C.H. completed critical experimental gaps including in vivo studies; S.M. performed foundational experiments that enabled subsequent work; Q.L. generated all CRISPR knockout models and conducted validation experiments. Collectively their contributions were deemed equivalent in scientific contribution and importance.

C.H., Investigation,
S.M, Investigation
Q.L., Investigation
K.M.A, Investigation
K.S., Investigation
D.D., Investigation
J.W., Investigation
X.R., Formal analysis
J.Z., Formal analysis
Y.X., Formal analysis
J.W., Formal analysis
Z.L., Investigation
N.T., Investigation
D.A.W., Formal analysis
E.S., Formal analysis
R.S., Investigation
C.R.P., Writing-original draft
T.X., Investigation
A.K. E., Formal analysis
A.A.O., Investigation
K.R., Investigation
P.A.Z., Resources and Writing-original draft
J.V. H., Investigation
L.A.B., Investigation
F.M.J., Writing-original draft, Funding acquisition,
V.C.S, Investigation and Writing-original draft
J.N.M., Writing-original draft, Funding acquisition
P.Y. Investigation and Writing-original draft
M.J.F., Conceptualization, Data Curation, Formal analysis, Funding acquisition, Investigation, Methodology, Project administration, Supervision, Writing-original draft.

REFERENCES

1. Agrawal N, Frederick MJ, Pickering CR, Bettegowda C, Chang K, Li RJ, et al. Exome sequencing of head and neck squamous cell carcinoma reveals inactivating mutations in NOTCH1. *Science*. 2011;333(6046):1154-7.
2. Pickering CR, Zhang J, Yoo SY, Bengtsson L, Moorthy S, Neskey DM, et al. Integrative genomic characterization of oral squamous cell carcinoma identifies frequent somatic drivers. *Cancer Discov*. 2013;3(7):770-81.
3. Stransky N, Egloff AM, Tward AD, Kostic AD, Cibulskis K, Sivachenko A, et al. The mutational landscape of head and neck squamous cell carcinoma. *Science*. 2011;333(6046):1157-60.
4. Cancer Genome Atlas N. Comprehensive genomic characterization of head and neck squamous cell carcinomas. *Nature*. 2015;517(7536):576-82.
5. Pickering CR, Zhou JH, Lee JJ, Drummond JA, Peng SA, Saade RE, et al. Mutational landscape of aggressive cutaneous squamous cell carcinoma. *Clin Cancer Res*. 2014;20(24):6582-92.
6. Sun W, Gaykalova DA, Ochs MF, Mambo E, Arnaoutakis D, Liu Y, et al. Activation of the NOTCH pathway in head and neck cancer. *Cancer research*. 2014;74(4):1091-104.
7. Rettig EM, Chung CH, Bishop JA, Howard JD, Sharma R, Li RJ, et al. Cleaved NOTCH1 Expression Pattern in Head and Neck Squamous Cell Carcinoma Is Associated with NOTCH1 Mutation, HPV Status, and High-Risk Features. *Cancer prevention research*. 2015;8(4):287-95.
8. Wang NJ, Sanborn Z, Arnett KL, Bayston LJ, Liao W, Proby CM, et al. Loss-of-function mutations in Notch receptors in cutaneous and lung squamous cell carcinoma. *Proc Natl Acad Sci U S A*. 2011;108(43):17761-6.
9. Cancer Genome Atlas Research N. Comprehensive genomic characterization of squamous cell lung cancers. *Nature*. 2012;489(7417):519-25.
10. Sawada G, Niida A, Uchi R, Hirata H, Shimamura T, Suzuki Y, et al. Genomic Landscape of Esophageal Squamous Cell Carcinoma in a Japanese Population. *Gastroenterology*. 2016;150(5):1171-82.
11. Shah PA, Huang C, Li Q, Kazi SA, Byers LA, Wang J, et al. NOTCH1 Signaling in Head and Neck Squamous Cell Carcinoma. *Cells*. 2020;9(12).
12. Nicolas M, Wolfer A, Raj K, Kummer JA, Mill P, van Noort M, et al. Notch1 functions as a tumor suppressor in mouse skin. *Nature genetics*. 2003;33(3):416-21.
13. Weng AP, Ferrando AA, Lee W, Morris JPt, Silverman LB, Sanchez-Irizarry C, et al. Activating mutations of NOTCH1 in human T cell acute lymphoblastic leukemia. *Science*. 2004;306(5694):269-71.
14. Ferrarotto R, Mitani Y, Diao L, Guijarro I, Wang J, Zweidler-McKay P, et al. Activating NOTCH1 Mutations Define a Distinct Subgroup of Patients With Adenoid Cystic Carcinoma Who Have Poor Prognosis, Propensity to Bone and Liver Metastasis, and Potential Responsiveness to Notch1 Inhibitors. *J Clin Oncol*. 2017;35(3):352-60.
15. Mohammedsaleh ZM, Moawadh MS, Saleh FM, Jalal MM, Al-Otaibi AS, Saeedi NH, et al. Increased NOTCH1 expression is associated with low survival in moderate/ poor differentiated human oral squamous cell carcinoma patients. *J Cancer*. 2023;14(16):3023-7.
16. Schmidl B, Siegl M, Boxberg M, Stogbauer F, Jira D, Winter C, et al. NOTCH1 Intracellular Domain and the Tumor Microenvironment as Prognostic Markers in HNSCC. *Cancers (Basel)*. 2022;14(4).

17. de Freitas Filho SAJ, Coutinho-Camillo CM, Oliveira KK, Bettim BB, Pinto CAL, Kowalski LP, et al. Prognostic Implications of ALDH1 and Notch1 in Different Subtypes of Oral Cancer. *J Oncol*. 2021;2021:6663720.
18. Gan RH, Wei H, Xie J, Zheng DP, Luo EL, Huang XY, et al. Notch1 regulates tongue cancer cells proliferation, apoptosis and invasion. *Cell Cycle*. 2018;17(2):216-24.
19. Upadhyay P, Nair S, Kaur E, Aich J, Dani P, Sethunath V, et al. Notch pathway activation is essential for maintenance of stem-like cells in early tongue cancer. *Oncotarget*. 2016;7(31):50437-49.
20. Song X, Xia R, Li J, Long Z, Ren H, Chen W, et al. Common and complex Notch1 mutations in Chinese oral squamous cell carcinoma. *Clin Cancer Res*. 2014;20(3):701-10.
21. Liu YF, Chiang SL, Lin CY, Chang JG, Chung CM, Ko AM, et al. Somatic Mutations and Genetic Variants of NOTCH1 in Head and Neck Squamous Cell Carcinoma Occurrence and Development. *Sci Rep*. 2016;6:24014.
22. Zheng Y, Wang Z, Ding X, Zhang W, Li G, Liu L, et al. A novel Notch1 missense mutation (C1133Y) in the Abruptex domain exhibits enhanced proliferation and invasion in oral squamous cell carcinoma. *Cancer Cell International*. 2018;18:6.
23. Zhang Z, Zhou Z, Zhang M, Gross N, Gong L, Zhang S, et al. High Notch1 expression affects chemosensitivity of head and neck squamous cell carcinoma to paclitaxel and cisplatin treatment. *Biomed Pharmacother*. 2019;118:109306.
24. Lee SH, Do SI, Lee HJ, Kang HJ, Koo BS, and Lim YC. Notch1 signaling contributes to stemness in head and neck squamous cell carcinoma. *Lab Invest*. 2016;96(5):508-16.
25. Byun JY, Huang K, Lee JS, Huang W, Hu L, Zheng X, et al. Targeting HIF-1alpha/NOTCH1 pathway eliminates CD44(+) cancer stem-like cell phenotypes, malignancy, and resistance to therapy in head and neck squamous cell carcinoma. *Oncogene*. 2022;41(9):1352-63.
26. Grilli G, Hermida-Prado F, Alvarez-Fernandez M, Allonca E, Alvarez-Gonzalez M, Astudillo A, et al. Impact of notch signaling on the prognosis of patients with head and neck squamous cell carcinoma. *Oral Oncol*. 2020;110:105003.
27. Sambandam V, Frederick MJ, Shen L, Tong P, Rao X, Peng S, et al. PDK1 Mediates NOTCH1-Mutated Head and Neck Squamous Carcinoma Vulnerability to Therapeutic PI3K/mTOR Inhibition. *Clin Cancer Res*. 2019;25(11):3329-40.
28. Shah PA, Sambandam V, Fernandez AM, Zhao H, Mazumdar T, Shen L, et al. Sustained Aurora Kinase B Expression Confers Resistance to PI3K Inhibition in Head and Neck Squamous Cell Carcinoma. *Cancer research*. 2022;82(23):4444-56.
29. Johnson FM, Janku F, Gouda MA, Tran HT, Kawedia JD, Schmitz D, et al. Inhibition of the Phosphatidylinositol-3 Kinase Pathway Using Bimiralisib in Loss-of-Function NOTCH1-Mutant Head and Neck Cancer. *Oncologist*. 2022;27(12):1004-e926.
30. Zhao M, Sano D, Pickering CR, Jasser SA, Henderson YC, Clayman GL, et al. Assembly and initial characterization of a panel of 85 genomically validated cell lines from diverse head and neck tumor sites. *Clin Cancer Res*. 2011;17(23):7248-64.
31. Hu Y, and Smyth GK. ELDA: extreme limiting dilution analysis for comparing depleted and enriched populations in stem cell and other assays. *J Immunol Methods*. 2009;347(1-2):70-8.
32. Pui JC, Allman D, Xu L, DeRocco S, Karnell FG, Bakkour S, et al. Notch1 expression in early lymphopoiesis influences B versus T lineage determination. *Immunity*. 1999;11(3):299-308.
33. Ahmed KM, Veeramachaneni R, Deng D, Putluri N, Putluri V, Cardenas MF, et al. Glutathione peroxidase 2 is a metabolic driver of the tumor immune microenvironment and immune checkpoint inhibitor response. *J Immunother Cancer*. 2022;10(8).

34. Inamura N, Kimura T, Wang L, Yanagi H, Tsuda M, Tanino M, et al. Notch1 regulates invasion and metastasis of head and neck squamous cell carcinoma by inducing EMT through c-Myc. *Auris Nasus Larynx*. 2017;44(4):447-57.
35. Yu W, Chen Y, Putluri N, Osman A, Coarfa C, Putluri V, et al. Evolution of cisplatin resistance through coordinated metabolic reprogramming of the cellular reductive state. *Br J Cancer*. 2023;128(11):2013-24.
36. Osman AA, Arslan E, Bartels M, Michikawa C, Lindemann A, Tomczak K, et al. Dysregulation and Epigenetic Reprogramming of NRF2 Signaling Axis Promote Acquisition of Cisplatin Resistance and Metastasis in Head and Neck Squamous Cell Carcinoma. *Clin Cancer Res*. 2023;29(7):1344-59.
37. Brand TM, Iida M, Stein AP, Corrigan KL, Braverman CM, Coan JP, et al. AXL Is a Logical Molecular Target in Head and Neck Squamous Cell Carcinoma. *Clinical Cancer Research*. 2015;21(11):2601-12.
38. Hagege A, Saada-Bouzid E, Ambrosetti D, Rastoin O, Boyer J, He X, et al. Targeting of c-MET and AXL by cabozantinib is a potential therapeutic strategy for patients with head and neck cell carcinoma. *Cell Rep Med*. 2022;3(9):100659.
39. Zhang Z, Yang XF, Huang KQ, Ren L, Zhao S, Gou WF, et al. The upregulated alpha-catulin expression was involved in head-neck squamous cell carcinogenesis by promoting proliferation, migration, invasion, and epithelial to mesenchymal transition. *Tumour Biology*. 2016;37(2):1671-81.
40. Cao C, Chen Y, Masood R, Sinha UK, and Kobielak A. alpha-Catulin marks the invasion front of squamous cell carcinoma and is important for tumor cell metastasis. *Molecular Cancer Research: MCR*. 2012;10(7):892-903.
41. Kulsum S, Sudheendra HV, Pandian R, Ravindra DR, Siddappa G, R N, et al. Cancer stem cell mediated acquired chemoresistance in head and neck cancer can be abrogated by aldehyde dehydrogenase 1 A1 inhibition. *Mol Carcinog*. 2017;56(2):694-711.
42. Baumeister P, Hollmann A, Kitz J, Afthonidou A, Simon F, Shakhtour J, et al. High Expression of EpCAM and Sox2 is a Positive Prognosticator of Clinical Outcome for Head and Neck Carcinoma. *Sci Rep*. 2018;8(1):14582.
43. Alcolea MP, and Jones PH. Cell competition: winning out by losing notch. *Cell Cycle*. 2015;14(1):9-17.
44. Karami Fath M, Ebrahimi M, Nourbakhsh E, Zia Hazara A, Mirzaei A, Shafieyari S, et al. PI3K/Akt/mTOR signaling pathway in cancer stem cells. *Pathol Res Pract*. 2022;237:154010.
45. Michmerhuizen NL, Heenan C, Wang J, Leonard E, Bellile E, Loganathan SK, et al. Combined Pik3ca-H1047R and loss-of-function Notch1 alleles decrease survival time in a 4-nitroquinoline N-oxide-driven head and neck squamous cell carcinoma model. *Oral Oncol*. 2022;126:105770.
46. Zhong R, Bao R, Faber PW, Bindokas VP, Bechill J, Lingen MW, et al. Notch1 Activation or Loss Promotes HPV-Induced Oral Tumorigenesis. *Cancer research*. 2015;75(18):3958-69.
47. Demehri S, Turkoz A, and Kopan R. Epidermal Notch1 loss promotes skin tumorigenesis by impacting the stromal microenvironment. *Cancer Cell*. 2009;16(1):55-66.

MAIN FIGURES AND LEGENDS

Figure 1

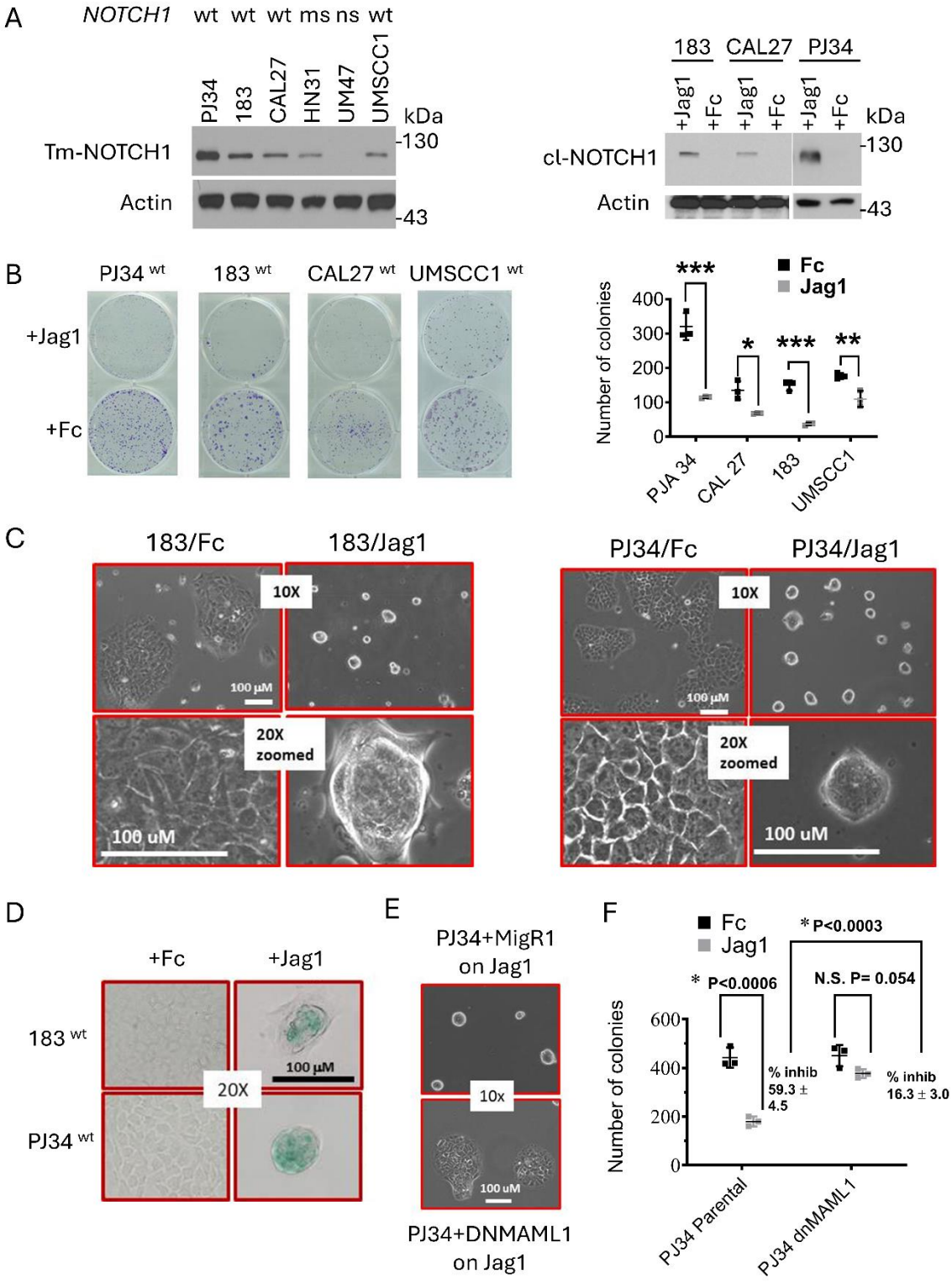

Figure 1. **NOTCH signaling alters cell morphology and inhibits growth in two-dimensional cultures.** **A.** Expression of full length transmembrane NOTCH1 (Tm-NOTCH1) in cells with WT *NOTCH1* (PJ34, 183, CAL27, and UMSCC1) and cleaved activated NOTCH1 (cl-NOTCH1) protein after 16 h growth on immobilized Notch1 ligand (JAG1) or FC control protein (FC). HN31 and UM47 harbor homozygous missense (ms) and nonsense (ns) *NOTCH1* mutations, respectively. **B.** Extended growth (e.g. 8-10 days) on JAG1 ligand significantly reduced colony formation compared to control FC protein in four *NOTCH1* WT cell lines. **C.** Growth on JAG1, but not control FC induces morphological transformation of cell lines with WT *NOTCH1* (183 and PJ34) observed by 5 days, characterized by reduced cell size and formation of loosely attached tumor spheroids. **D.** Tumor spheroids induced by growth on JAG1 express the senescence marker β-gal. **E.** Ectopic expression of dominant negative MAML1 (dnMAML1), which inhibits *NOTCH1* mediated transcriptional regulation, prevents JAG1-induced tumor spheroid formation and reverses inhibition of colon formation in PJ34 cells. **F.** Quantitation of colonies from parental PJ34 or PJ34 expressing dnMAML1 cultured on either control FC or JAG1 protein. Differences between FC and JAG1 treatment (simple contrasts) or comparison of JAG1-mediated inhibition in parental or cells expressing dnMAML1 (interaction contrasts) were determined with a cell means model. ****P<0.0001, *P<0.05

Figure 2

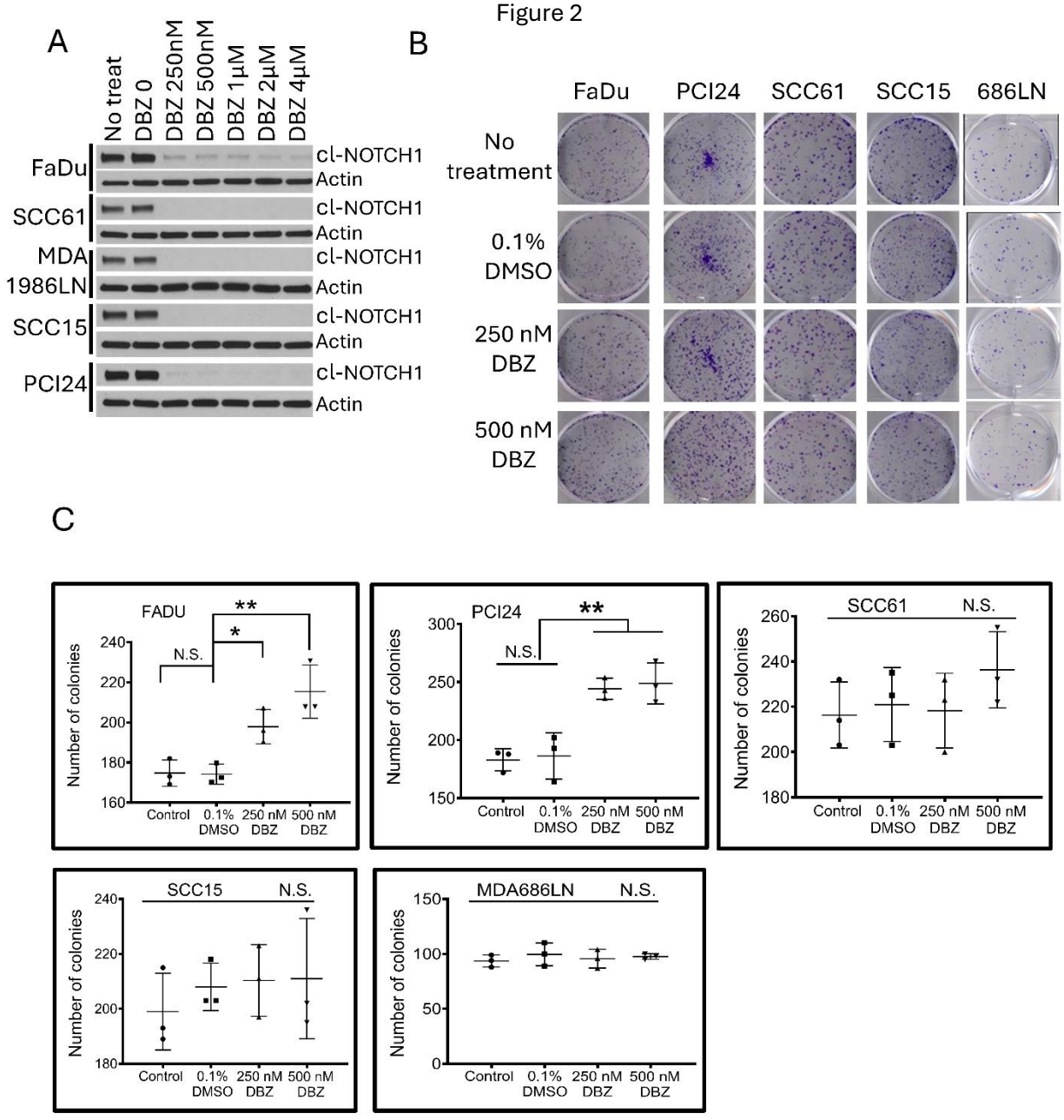
A
No treat
DBZ 0
DBZ 250nM
DBZ 500nM
DBZ 1µM
DBZ 2µM
DBZ 4µM
FaDu
SCC61
MDA 1986LN
SCC15
PCI24
cl-NOTCH1
Actin
B
FaDu
PCI24
SCC61
SCC15
686LN
No treatment
0.1% DMSO
250 nM DBZ
500 nM DBZ
C
FADU
PCI24
SCC61
SCC15
MDA686LN
N.S.
Number of colonies
Control
0.1% DMSO
250 nM DBZ
500 nM DBZ

Figure 2. NOTCH1 is not a driver of cell growth in multiple HNSCC cell lines with high endogenous NOTCH1 activation. A. Western blot validation of high basal levels of cl-NOTCH1protein in 5 untreated *NOTCH1* WT HNSCC cell lines (i.e., no treat) with different genomic backgrounds and persistent inhibition of NOTCH1 signaling after 72 h treatment with various doses of the NOTCH1 inhibitor DBZ. **B**. Staining of colony formation in the presence or absence of continuous treatment with DBZ inhibitor (replaced every 48 h) for the duration of culture. **C.** Quantitation of colony formation shows no decrease in growth after continued treatment with DBZ. For each cell line, comparisons between treatment groups were analyzed by an ANOVA and individual comparisons were made using a post-hoc Tukey test. * $P < 0.05$; ** $P < 0.01$

Figure 3

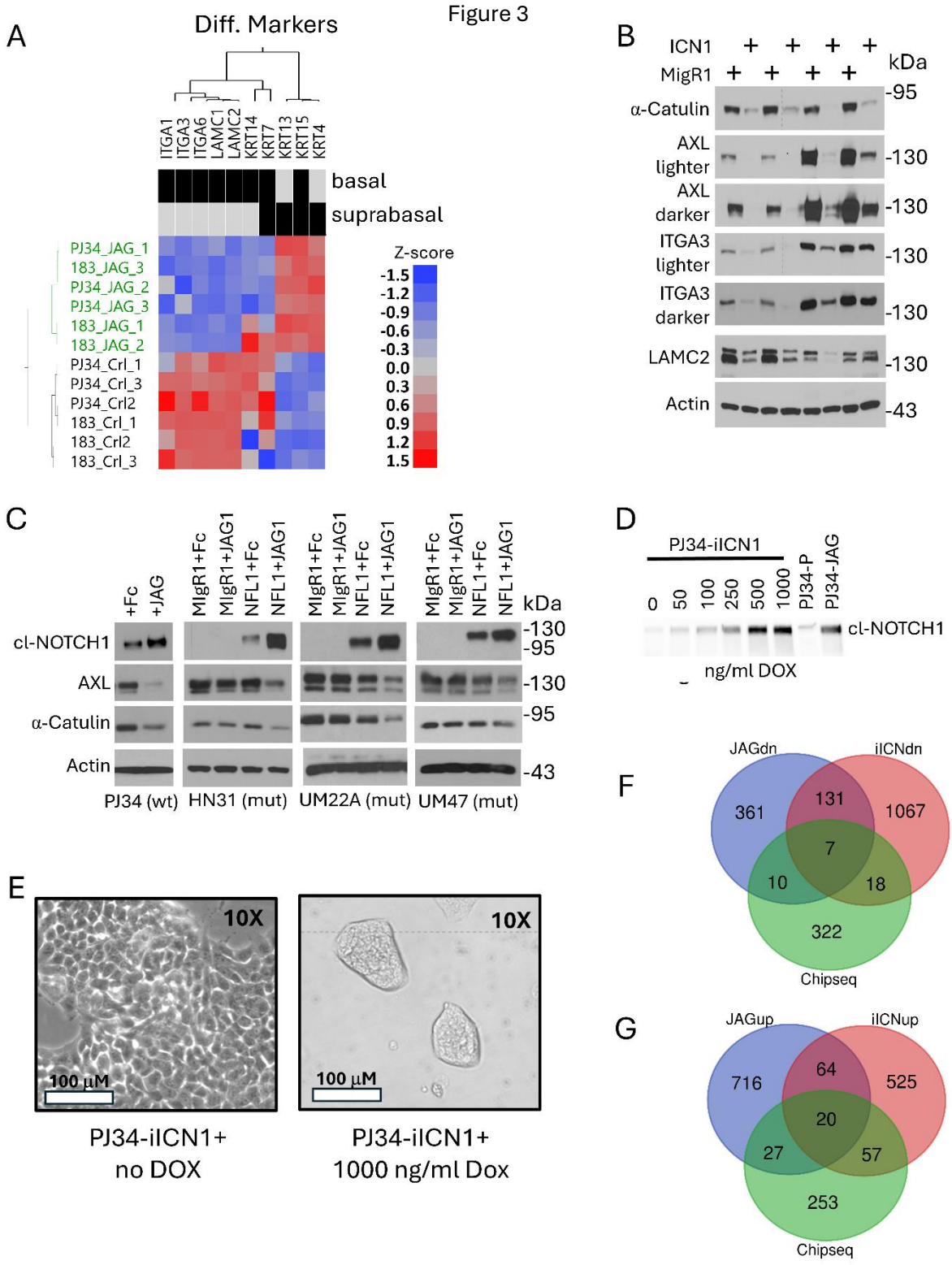
A
Diff. Markers
ITGA1
ITGA3
ITGA6
LAMC1
LAMC2
KRT14
KRT7
KRT13
KRT15
KRT4
basal
suprabasal
PJ34_JAG_1
183_JAG_3
PJ34_JAG_2
PJ34_JAG_3
183_JAG_1
183_JAG_2
PJ34_Crl_1
PJ34_Crl_3
PJ34_Crl2
183_Crl_1
183_Crl2
183_Crl_3
Z-score
-1.5
-1.2
-0.9
-0.6
-0.3
0.0
0.3
0.6
0.9
1.2
1.5
B
ICN1
MigR1
kDa
α-Catulin
-95
AXL lighter
AXL darker
-130
ITGA3 lighter
ITGA3 darker
LAMC2
Actin
-43
C
+Fc
+JAG
MIgR1+Fc
MIgR1+JAG1
NFL1+Fc
NFL1+JAG1
kDa
cl-NOTCH1
AXL
α-Catulin
Actin
-130
-95
-43
PJ34 (wt)
HN31 (mut)
UM22A (mut)
UM47 (mut)
D
PJ34-iICN1
0
50
100
250
500
1000
PJ34-P
PJ34-JAG
cl-NOTCH1
ng/ml DOX
E
10X
100 µM
PJ34-iICN1+
no DOX
PJ34-iICN1+
1000 ng/ml Dox
F
JAGdn
iICNdn
361
131
1067
7
10
18
322
Chipseq
G
JAGup
iICNup
716
64
525
20
27
57
253
Chipseq

Figure 3. The activation of NOTCH1 signaling through multiple experimental approaches consistently downregulates oncogenic drivers and modulates adhesion or other markers of early differentiation. A. Growth for 5 days on JAG1 significantly inhibited RNA expression of the basal cell marker genes ITGA1, ITGA3, ITGA6, LAMC1, and LAMC2 in two NOTCH1 WT cell lines PJ34 and 183, while stimulating expression of the suprabasal maker genes KRT4and KRT13. **B.** Ectopic expression of cDNA encoding cl-NOTCH1decreased expression of ITGA3, LAMC2, AXL, and α-CATULIN at 3 days and 5-days post infection in a NOTCH1 WT cell (PJ34) and in a NOTCH1-mutant cell (HN31). **C**. AXL and a-CATULIN protein levels decline in NOTCH1 WT (PJ34) tumor cells grown on JAG1 (3 days) and in 3 different *NOTCH1* mutant cell lines (HN31, UMSCC22A, UMSCC47) when expression of WT full length NOTCH1 receptors (NFL1) is restored (NFL1) and then grown on JAG1 ligand for 3 days. Cells were also infected with empty vector (MigR1) and/or grown on control FC protein. **D.** PJ34 with CRISPR-mediated *NOTCH1* KO were further engineered to express a DOX inducible cl-NOTCH cDNA (PJ34-iICN1)whose expression was titrated after 72 h treatment with different doses of DOX, to achieve protein levels equivalent to parental PJ34 stimulated with JAG1 for 16 hr. **E.** ICN1 induction with 1000 ng/ml DOX caused massive cell shrinkage and formation of loosely attached tumor spheroids. **F.** Venn diagram illustrates overlap of genes in PJ34 significantly upregulated (FDR <0.1, |Fold change| ≥ 1.25-fold) by growth on JAG1 or after 24 h iICN1 induction, and genes specifically bound in the promoter or gene body regions by iICN1 after Chip-seq experiments. **G.** Venn diagram illustrates overlap of genes in PJ34 significantly downregulated (FDR <0.1, |Fold change| ≥ 1.25-fold) by growth on JAG1 or after 24 h iICN1 induction, and genes specifically bound in the promoter or gene body regions by iICN1 after Chip-seq experiments.

Figure 4

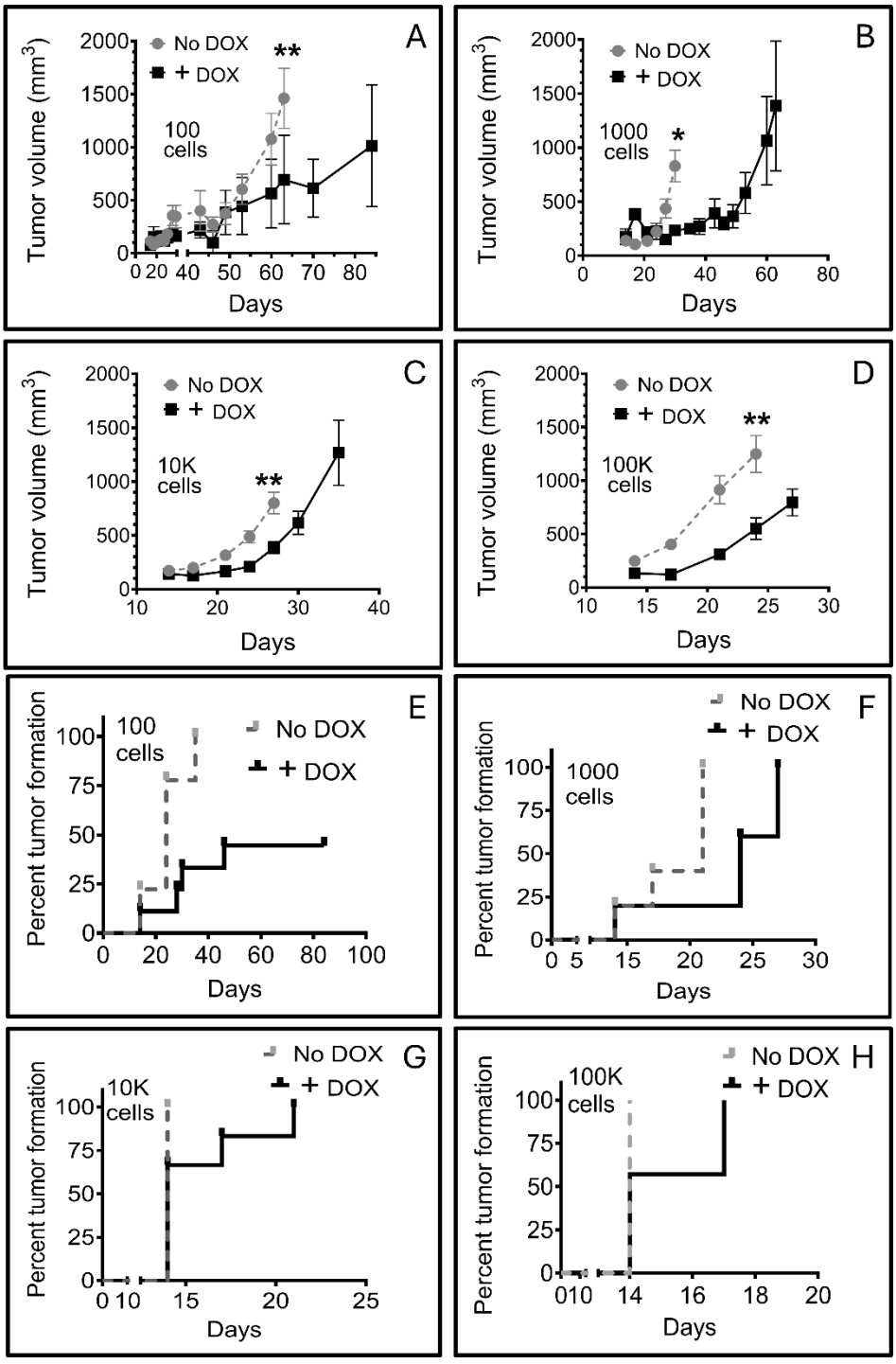
A
Tumor volume (mm3)
No DOX
+ DOX
100 cells
**
Days
B
1000 cells
*
C
10K cells
**
D
100K cells
**
E
Percent tumor formation
F
G
H

Figure 4. NOTCH1 activation reduces *in vivo* tumor growth and formation in NOTCH1 WT FaDu. After CRISPR-mediated *NOTCH1* KO, FaDu were engineered to express iICN1 and pretreated with or without 300 ng/ml DOX for 72 hours *in vitro* before injecting 100 cells (A), 1000 cells (B), 10,000 cells (C), or 100,000 cells (D) into flanks of mice. Equivalent numbers of untreated *NOTCH1* KO FaDu were also inoculated and grown in mice receiving no DOX. The DOX treated group received additional *in vivo* DOX (1 mg) for one week by oral gavage after implantation and tumor growth was plotted verses post-inoculation time. DOX-treated tumors (square) grew considerably slower than untreated controls (circles). Time to tumor formation in mice was plotted verses post-inoculation time for 100, 1000, 10,000, or 100,000 inoculated tumor cells (E-H) in the no Dox groups (grey dotted lines) or DOX treated groups (black solid lines). Differences in tumor volumes (A, B, C, D) were compared with a two-sided student's t-test. * $P < 0.05$; ** $P < 0.01$

Figure 5

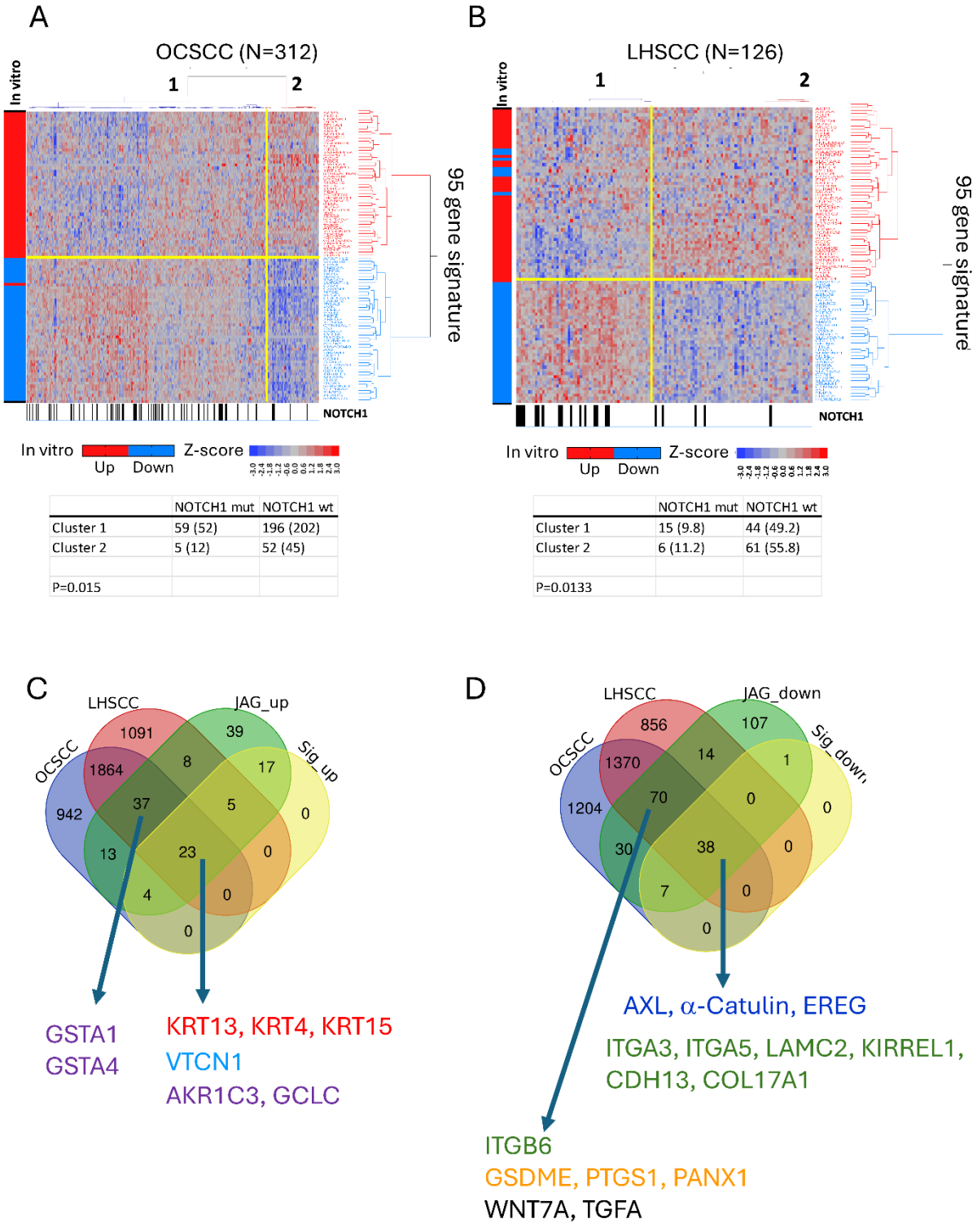

	NOTCH1 mut	NOTCH1 wt
Cluster 1	59 (52)	196 (202)
Cluster 2	5 (12)	52 (45)
P=0.015		

	NOTCH1 mut	NOTCH1 wt
Cluster 1	15 (9.8)	44 (49.2)
Cluster 2	6 (11.2)	61 (55.8)
P=0.0133		

Figure 5. Comparison of genes regulated by NOTCH1 *in vitro* and genes differentially expressed in primary HNSCC tumors with a NOTCH1 activation signature. A. Consensus hierarchical clustering of TCGA OCSCC primary tumors based on a 95-gene NOTCH1 activation signature identified a cluster of patient tumors (Cluster 2, N = 57) with an expression pattern indicative of active NOTCH1 signaling and another cluster (Cluster 1, N = 255) predicted to have loss of NOTCH1 signaling. Genes are annotated with vertical boxes according to whether they were upregulated (red) or downregulated (blue) by JAG1 *in vitro.* Samples with a *NOTCH1* mutation are annotated horizontally with a black box and association between *NOTCH1* mutation status and cluster for patients with sequencing information was analyzed by Chi-square analysis. **B.** Parallel clustering and analysis of TCGA LHSCC primary tumors using the same 95-gene NOTCH1 signature. **C.** Venn diagram illustrating overlap of genes upregulated (FDR<0.1, |FC|≥1.25) by NOTCH1 *in vitro* (JAG_up), the subset of upregulated genes part of the NOTCH1 signature (Sig_up), and genes upregulated (FDR<0.1, |FC|≥1.25) in Cluster 2 from OCSCC or LHSCC. **D.** Venn diagram illustrating overlap of genes downregulated (FDR<0.1, |FC|≥1.25) by NOTCH1 *in vitro* (JAG_down), the subset of downregulated genes part of the NOTCH1 signature (Sig_down), and genes downregulated (FDR<0.1, |FC|≥1.25) in Cluster 2 from OCSCC or LHSCC.

Figure 6

A

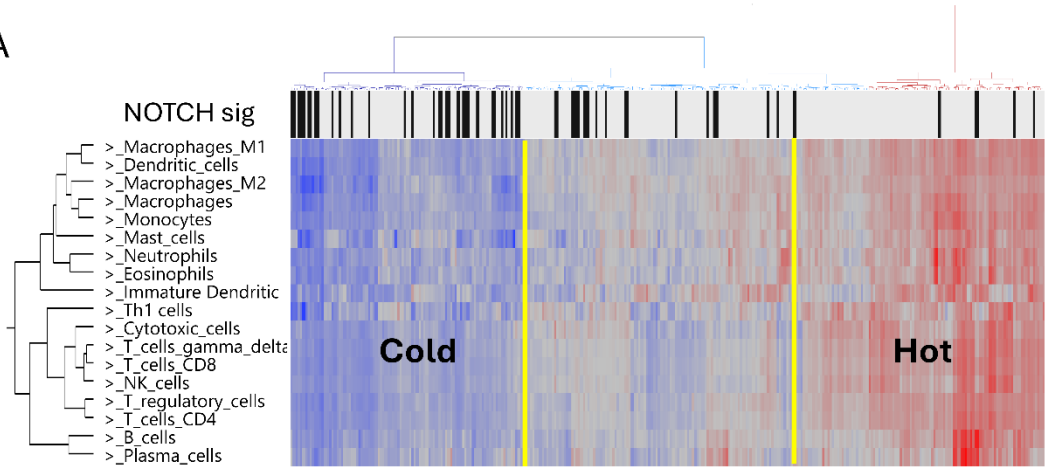

	NOTCH on	NOTCH off
Hot	5 (15.9)	68 (57.1)
Cold	32 (21.1)	65 (75.9)
p=0.000043		

B

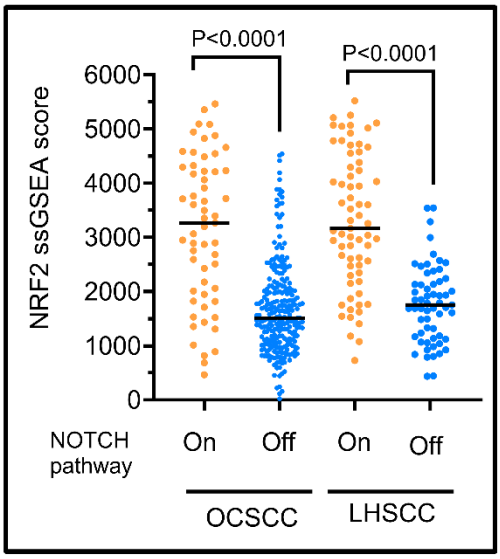

C

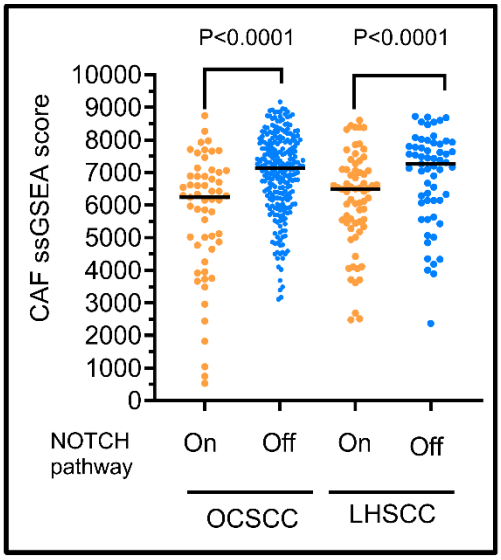

Figure 6. NOTCH1 activation in primary HNSCC is associated with changes to the tumor microenvironment. A. ssGSEA scores representing 18 different leukocyte subsets derived from TCGA OCSCC were used for hierarchical clustering to classify samples as immunologically cold (sample cluster 1) or hot (sample cluster 3) and the membership of samples from previous clustering based on the NOTCH1 gene signature is annotated with a black box for NOTCH1 signaling on or a grey box for NOTCH1 signaling off. Tumors with activated NOTCH1 are depleted from immunologically hot tumors and enriched in cold tumors by Chi-square analysis ($P<0.0001$). **B.** NRF2 pathway activation scores are significantly higher among OCSCC and LHSCC tumors when NOTCH is activated. **C.** CAF pathway scores are significantly higher in OCSCC and LHSCC tumors where NOTCH signaling is turned off. Differences in NRF2 pathway scores were analyzed with a two-sided student's t-test (C and D).

Figure 7

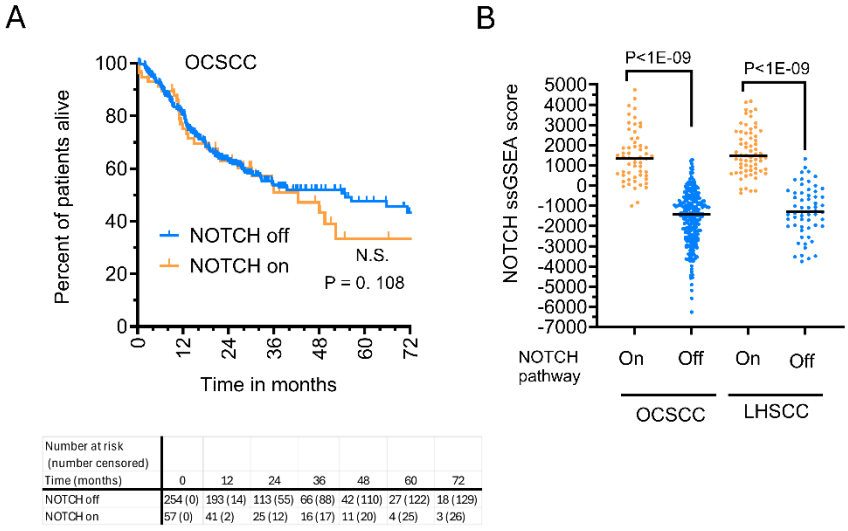

Number at risk (number censored)							
Time (months)	0	12	24	36	48	60	72
NOTCH off	254 (0)	193 (14)	113 (55)	66 (88)	42 (110)	27 (122)	18 (129)
NOTCH on	57 (0)	41 (2)	25 (12)	16 (17)	11 (20)	4 (25)	3 (26)

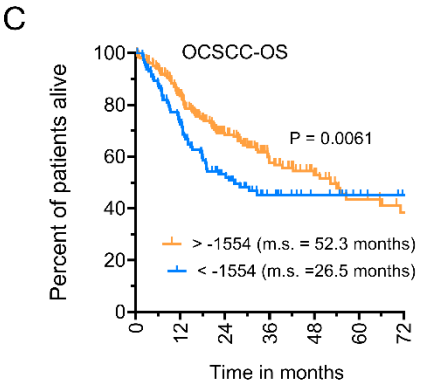

Number at risk (number censored)							
Time	0	12	24	36	48	60	72
NOTCH low	113 (0)	77 (7)	44 (20)	25 (33)	17 (41)	11 (47)	7 (51)
NOTCH high	198 (0)	157 (9)	94 (47)	57 (72)	36 (89)	20 (100)	14 (104)

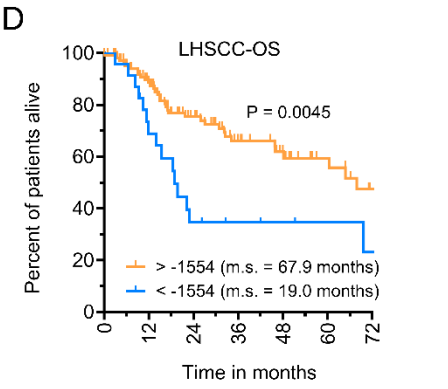

Number at risk (number censored)							
Time	0	12	24	36	48	60	72
NOTCH low	23 (0)	15 (1)	7 (2)	5 (4)	4 (5)	3 (6)	2 (6)
NOTCH high	103 (0)	81 (11)	54 (27)	38 (37)	27 (46)	16 (56)	9 (60)

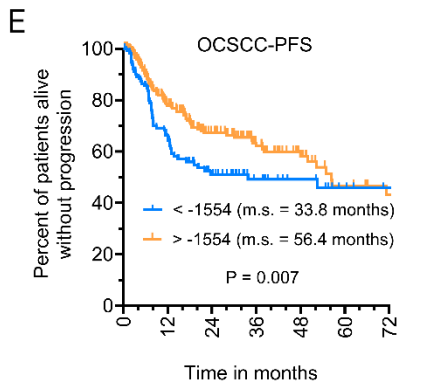

Number at risk (number censored)							
Time	0	12	24	36	48	60	72
NOTCH low	113 (0)	66 (11)	40 (23)	23 (39)	16 (46)	10 (51)	7 (54)
NOTCH high	198 (0)	137 (20)	87 (54)	54 (82)	34 (99)	18 (110)	13 (114)

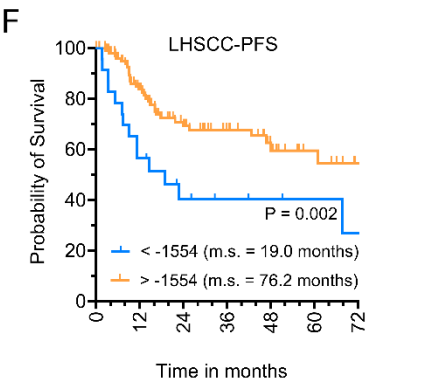

Number at risk (number censored)							
Time	0	12	24	36	48	60	72
NOTCH low	23 (0)	12 (1)	7 (3)	5 (5)	4 (6)	3 (7)	2 (7)
NOTCH high	103 (0)	74 (14)	46 (32)	34 (42)	22 (52)	12 (61)	5 (67)

Figure 7. Higher levels of NOTCH1 activation correlate with better survival in OCSCC and LHSCC TCGA cohorts. A. No difference in OS among TCGA OCSCC patients when NOTCH1 activation is treated as a categorical variable based on clusters with the NOTCH gene signature. **B**. Validation that ssGSEA scores derived from the NOTCH1 gene signature provide a continuous value measurement that faithfully replicates sample clustering. **C.** OCSCC samples with higher ssGSEA scores (e.g., NOTCH1 signaling) above a threshold (-1554) determined by optimal cutpoint selection have significantly improved OS. **D.** LHSCC samples with higher ssGSEA scores above the same threshold (-1554) have significantly improved OS, validating the threshold. **E.** OCSCC patients with higher NOTCH1 signaling have improved PFS. **F.** LHSCC patients with higher NOTCH1 signaling have improved PFS. At-risk tables underneath Kaplan-Meier curves indicate the number of patients still at risk or censored at the indicated time intervals. P values for survival curves were determined with a log rank test.

SUPPLEMENTARY FIGURE LEGENDS

Supplementary Figure 1

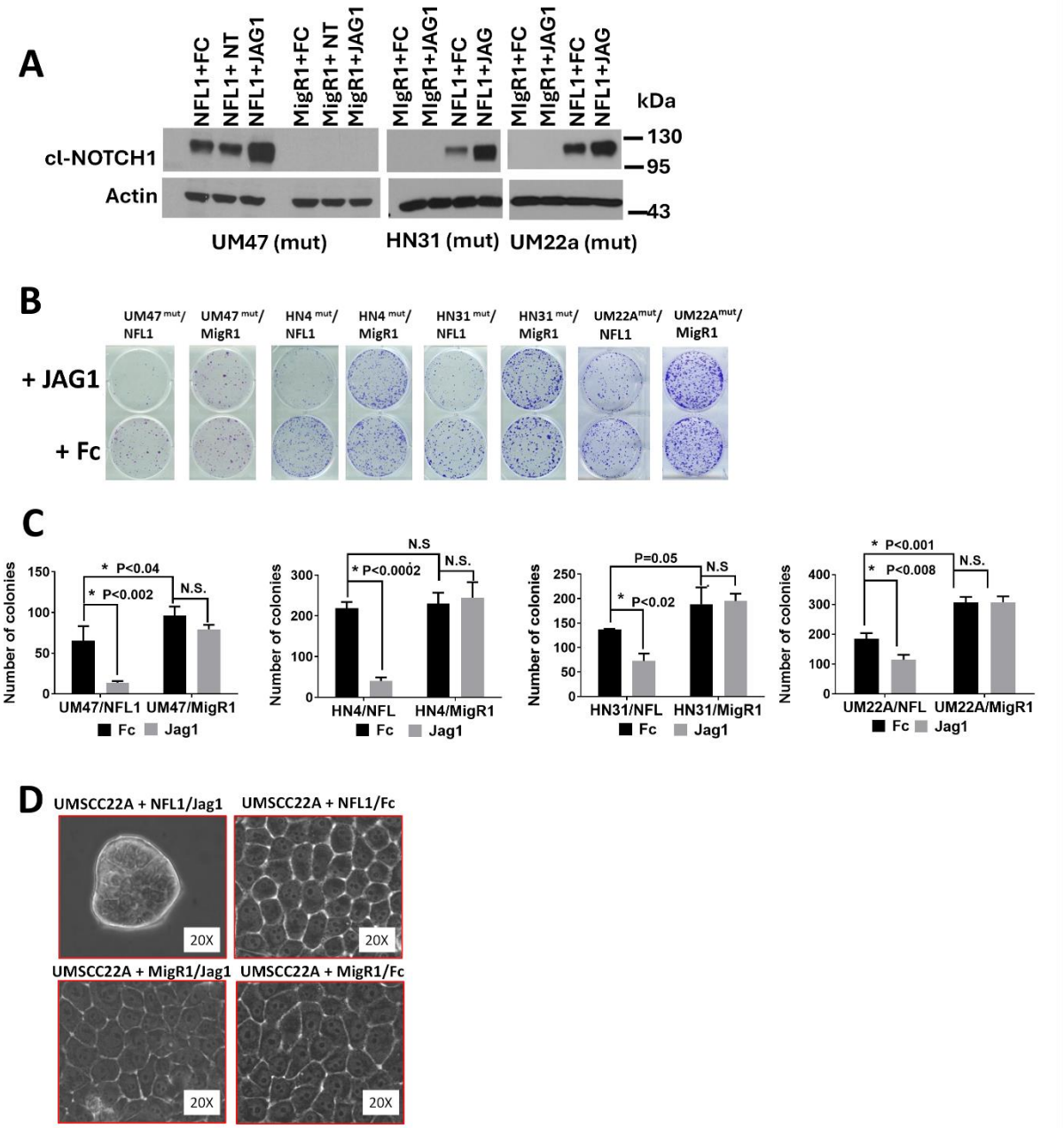

Supplementary Figure 1. **Restoration of NOTCH1 signaling inhibits *in vitro* growth and alters morphology in *NOTCH1* mutant HNSCC tumors. A**. Ectopic expression of WT full-length NOTCH1 receptors (NFL1) leads to activation and cleavage of NOTCH1 (cl-NOTCH1) protein in 3 different NOTCH1-mutant HNSCC cell lines that increases upon 16 h stimulation with immobilized JAG1 ligand, compared to control FC protein. **B**. Continued growth on immobilized JAG1 for 8-10 days inhibits colony formation in *NOTCH1*-mutant cell lines with restored NFL1. **C**. Quantitation of NFL1-mediated growth inhibition of colonies. **D.** Restoration of NFL1 signaling in UMSCC-22A led to dramatic reduction in cell size and formation of loosely attached tumor spheroids after 5 days only in the presence of JAG1. UM47 = UMSCC47, UM22A = UMSCC22A. Differences in colony number between treatments for each cell line were analyzed by an ANOVA, with P-values for individual comparisons determined with a post-hoc Tukey test.

Supplementary Figure 2

A

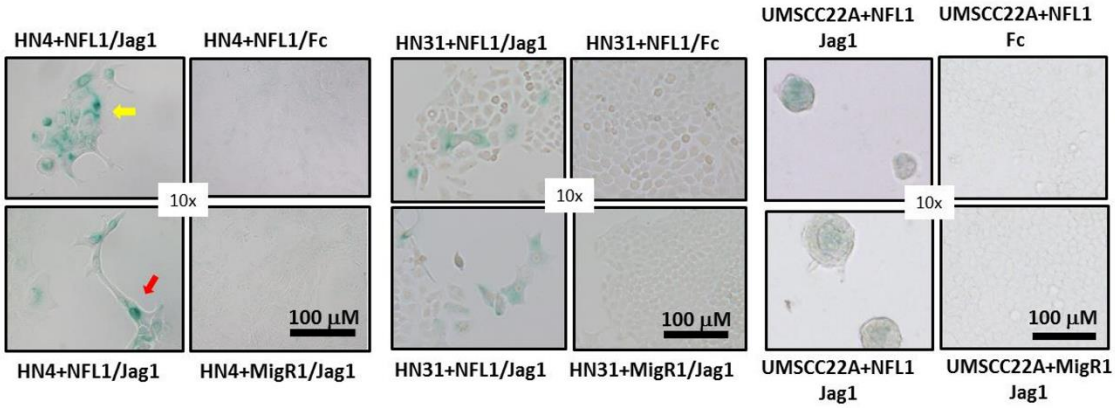

B

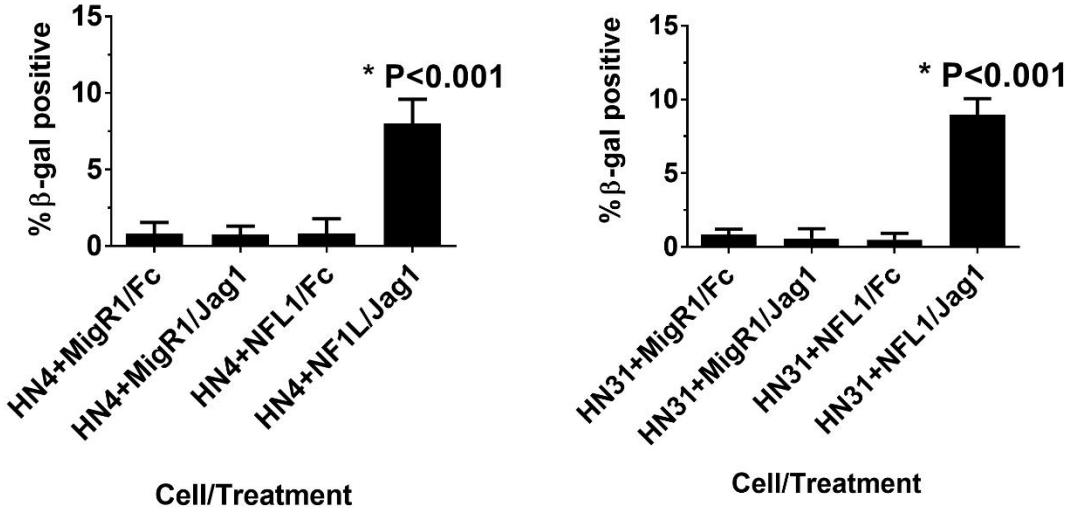

Supplementary Figure 2. **Restoration of NOTCH1 signaling induces senescence in NOTCH1 mutant tumor cell lines**. **A.** Photomicrographs of *NOTCH1*-mutant HNSCC cell lines infected with NFL1 or empty MigR1 grown on either JAG1 or FC control protein and stained for β-gal after 5 to 7 days culture. **B.** Quantitation shows significant elevation of β-gal staining in the presence of NFL1 expression and growth on JAG1 ligand. Differences in percentage of β-gal staining among treatments for each cell line were analyzed by an ANOVA, with P-values for individual comparisons determined using a post-hoc Tukey test. Treatments with no P-value showing were not significantly different from each other but were all significantly different from cells infected with NFL and plated on JAG1 ligand.

Supplementary Figure 3

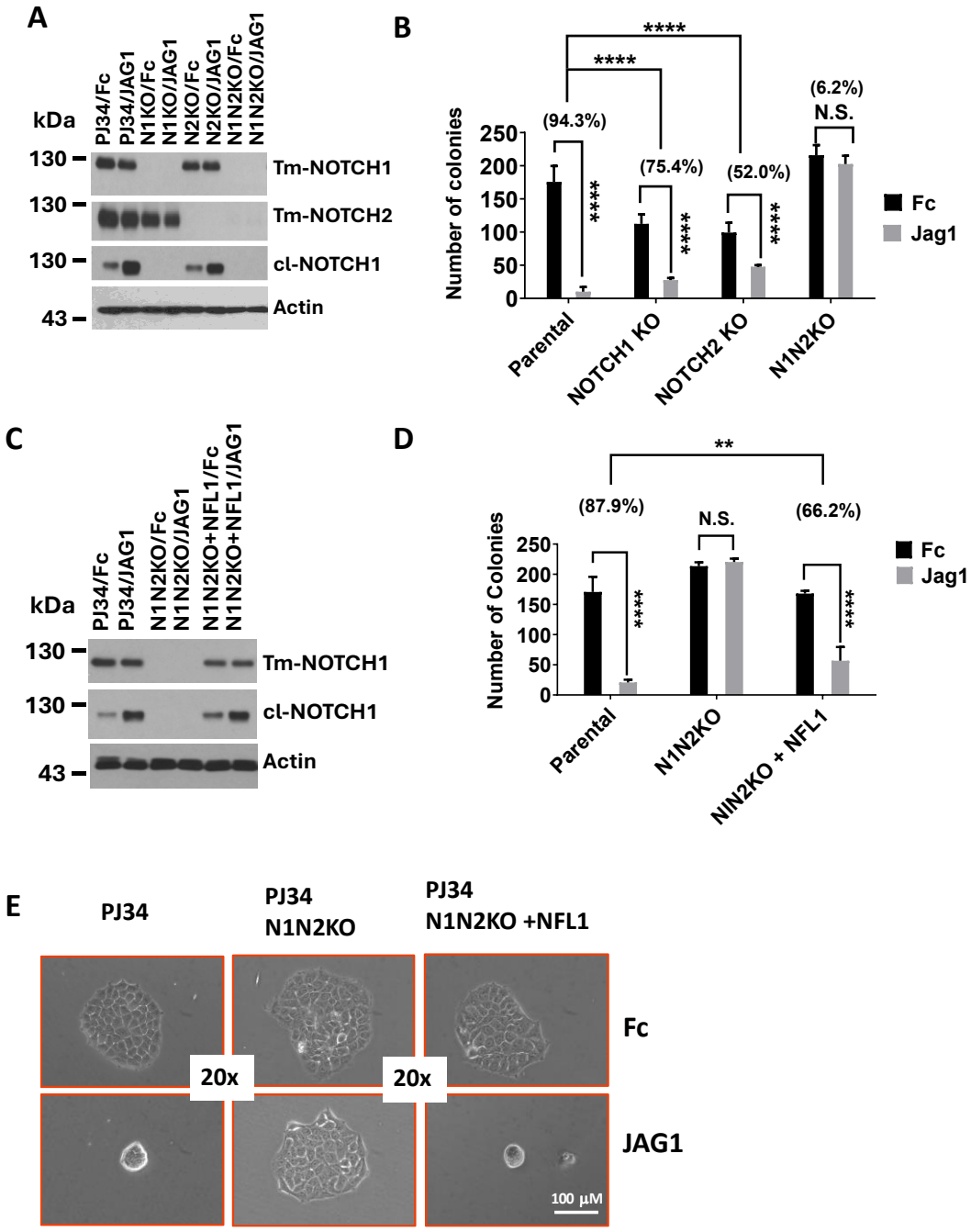

Supplementary Figure 3. **Both NOTCH1 and NOTCH2 signaling contribute to JAG1-induced growth inhibition but NOTCH1 signaling is sufficient. A.** CRISPR KO of either *NOTCH1* (NIKO), NOTCH2 (N2KO) or double KO (N1N2 KO) in PJ34 were validated by western blotting for total NOTCH1 and NOTCH2. Appearance of cl-NOTCH1 was absent in N1KO or N1N2KO after stimulation with JAG1 for 16 h. **B.** N1KO or N2KO partially blocked JAG1-induced inhibition of colony formation compared to that observed in parental cells ($P < 0.0001$) , while double N1K2 KO completely prevented growth inhibition. **C.** Infection with ectopic NFL1 cDNA restored NOTCH1 signaling in N1N2 KO cells. **D.** Re-Expression of NFL1 in PJ34 after N1N2KO partially restored JAG1-mediated inhibition of colony growth. **E.** Loss of both *NOTCH1* and *NOTCH2* (N1N2KO*)* in PJ34 protected cells from JAG1-induced morphology changes while re-expression of NFL1 restored spheroid formation caused by growth on JAG1. Changes in colony growth after growth on JAG1 ligand for each cell line compared to growth on FC control protein, or the differences in JAG1-induced effects between cell lines were analyzed with a cell means model using simple and interaction contrasts. ****$P < 0.0001$, **$P < 0.01$.

Supplementary Figure 4

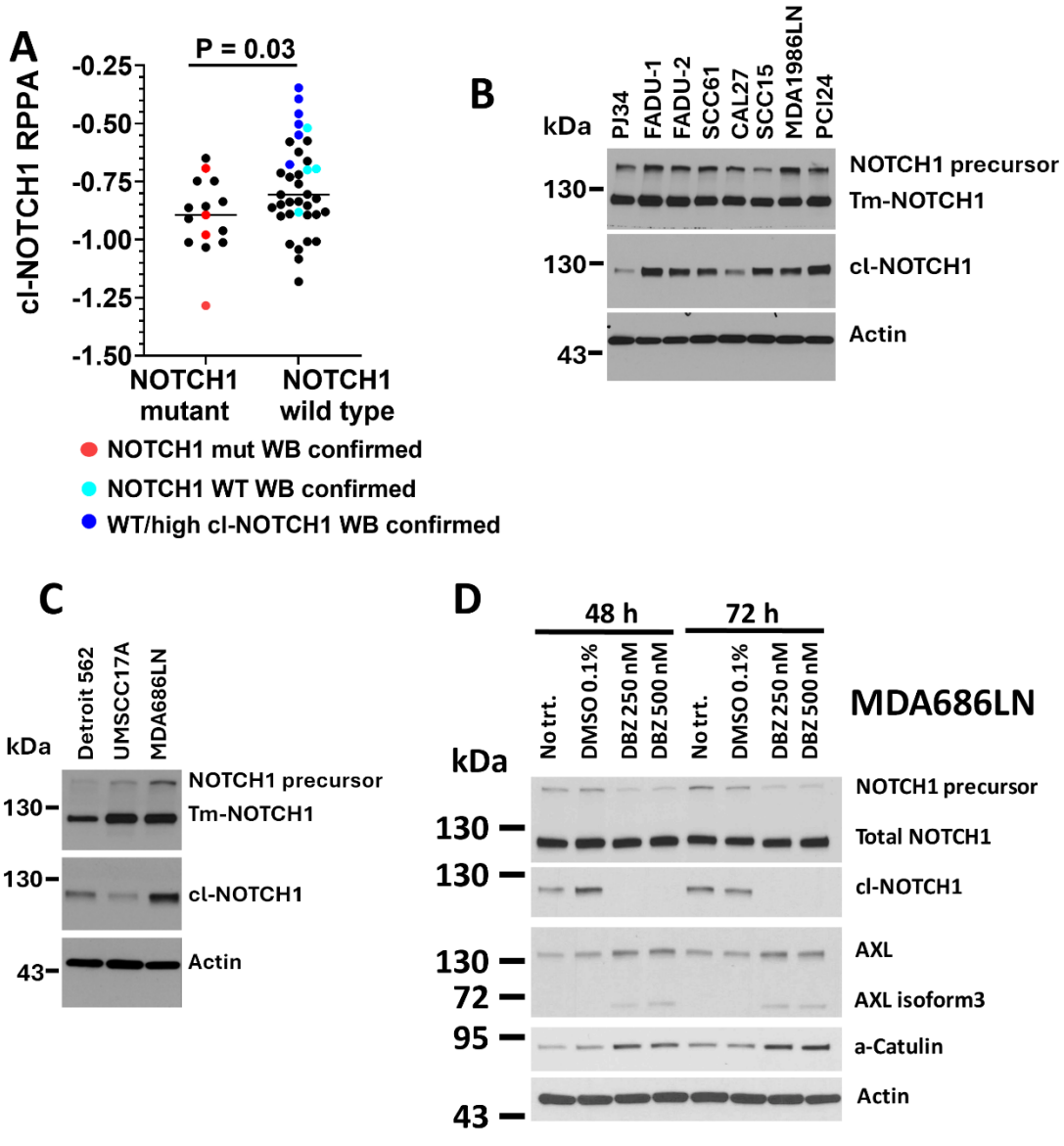

Supplementary Figure 4. RPPA identifies *NOTCH1* WT cell lines with elevated baseline cl-NOTCH1expression which was inversely correlated with protein expression of AXL and a-CATULIN. **A.** Normalized RPPA values of cl-NOTCH1 protein measured from *NOTCH1* mutant and *NOTCH1* WT HNSCC cell lines. Cell lines where cl-NOTCH1 protein was validated by western blots (WB) are indicated by colored symbols, with red dots for NOTCH1 mutants (HN31, UMSCC22A, UMSCC47, and HN4), light blue dots for NOTCH1 WT cells with low to moderate baseline cl-NOTCH (PJ34, 183, CAL27, and UMSCC1), and dark blue dots corresponding to *NOTCH1* WT cells with high basal cl-NOTCH1 (FaDu, PCI24, SCC61, SCC15, and MDA1986LN). **B.** Western blot confirmation of high cl-NOTCH1 protein in subsets of WT cell lines, compared to PJ34 with low baseline activation. C. Confirmation of high baseline NOTCH1 activation in MDA686LN. **D**. DBZ inhibited cl-NOTCH1 protein and increased levels of both AXL and α-CATULIN protein. Differences in average cl-NOTCH1 measured by RPPA between *NOTCH1* mutant and wild type cell lines were analyzed with a two-sided student's t-test (A).

Supplementary Figure 5

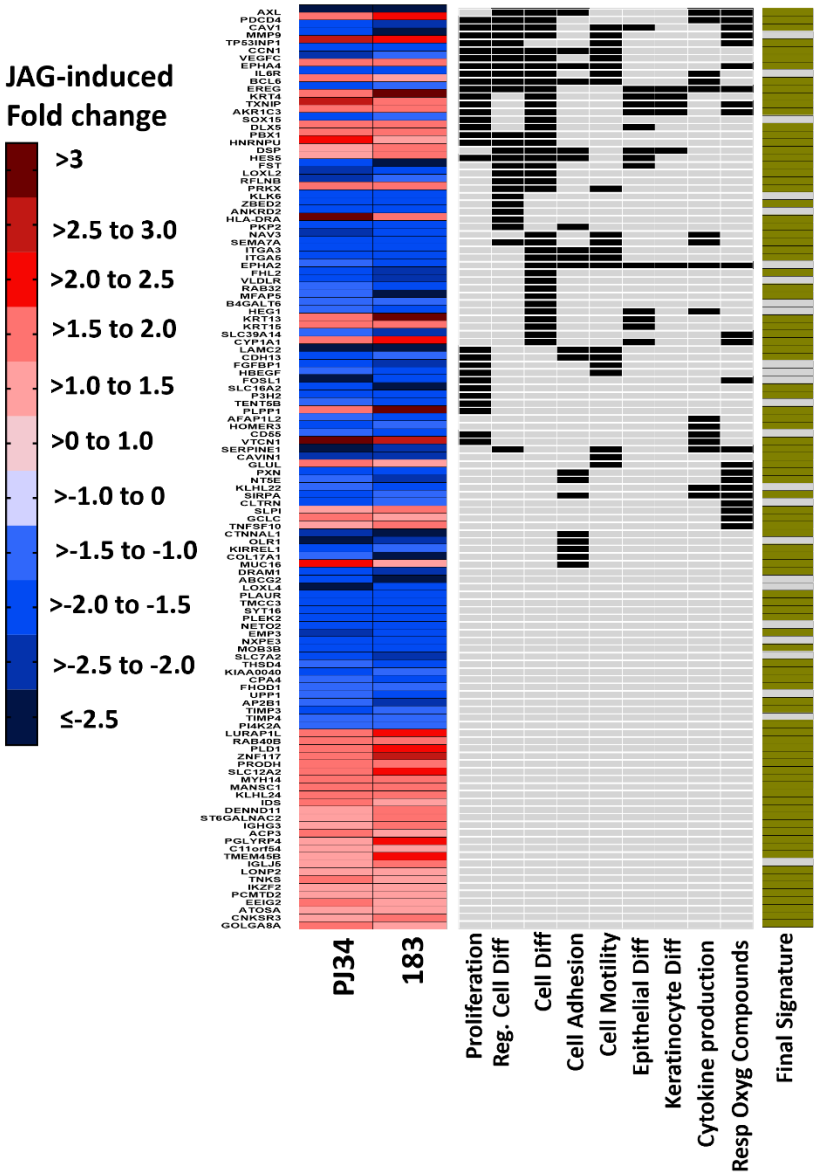

Supplementary Figure 5. NOTCH1 regulates genes involved in proliferation, differentiation, attachment, motility, and response to oxygen containing compounds. The top 120 significant genes (i.e., minimum of 1.4-fold change, **FDR <0.1**) from *NOTCH1* WT PJ34 and 183 cells regulated in common by growth on JAG1 and their biological pathways. The fold change in each cell line after growth for 5 days on JAG1 is annotated vertically as a color gradient with red boxes representing increases, and blue boxes representing decreases. Membership in select GO pathways that were enriched in the gene set is annotated with black boxes, and gold boxes indicate genes that were included in the final NOTCH1 gene activation signature discussed in the text.

Supplementary Figure 6

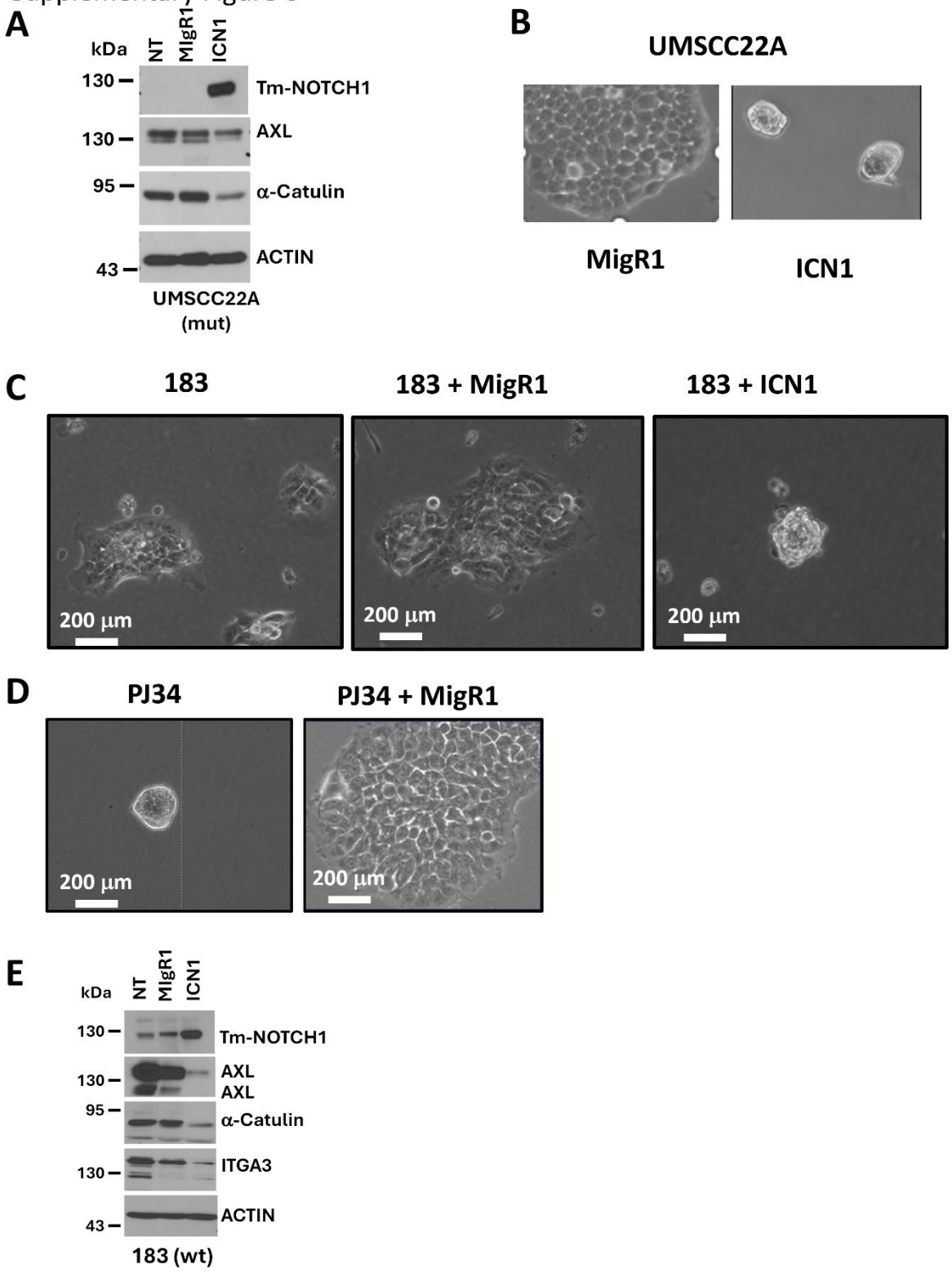

Supplementary Figure 6. **Ectopic expression of ICN1 mimics changes induced by JAG1 stimulation**. **A.** Infection with ICN1 but not empty vector (MigR1) strongly inhibited protein expression of AXL and α-CATULIN. Widely used ICN1 cDNA product which begins several amino acids downstream of the native cleavage site is recognized by antibodies to the C-terminal region of NOTCH1 but not antibodies specific to the cleavage site. **B.** Expression of ICN1 in *NOTCH1* mutant UMSCC22A produced the same morphological changes observed earlier upon expression of NFL1 and growth on JAG1. **C.** Expression of ICN1 in *NOTCH1* WT 183 produced the same morphological changes observed earlier with growth on JAG1. **D.** Expression of ICN1 but not MigR1 control in *NOTCH1* WT PJ34 produced the same morphological changes observed earlier with growth on JAG1. E. ICN1 expression triggered decreased protein expression of AXL, α-CATULIN, and ITGA3 in 183 cells.

Supplementary Figure 7

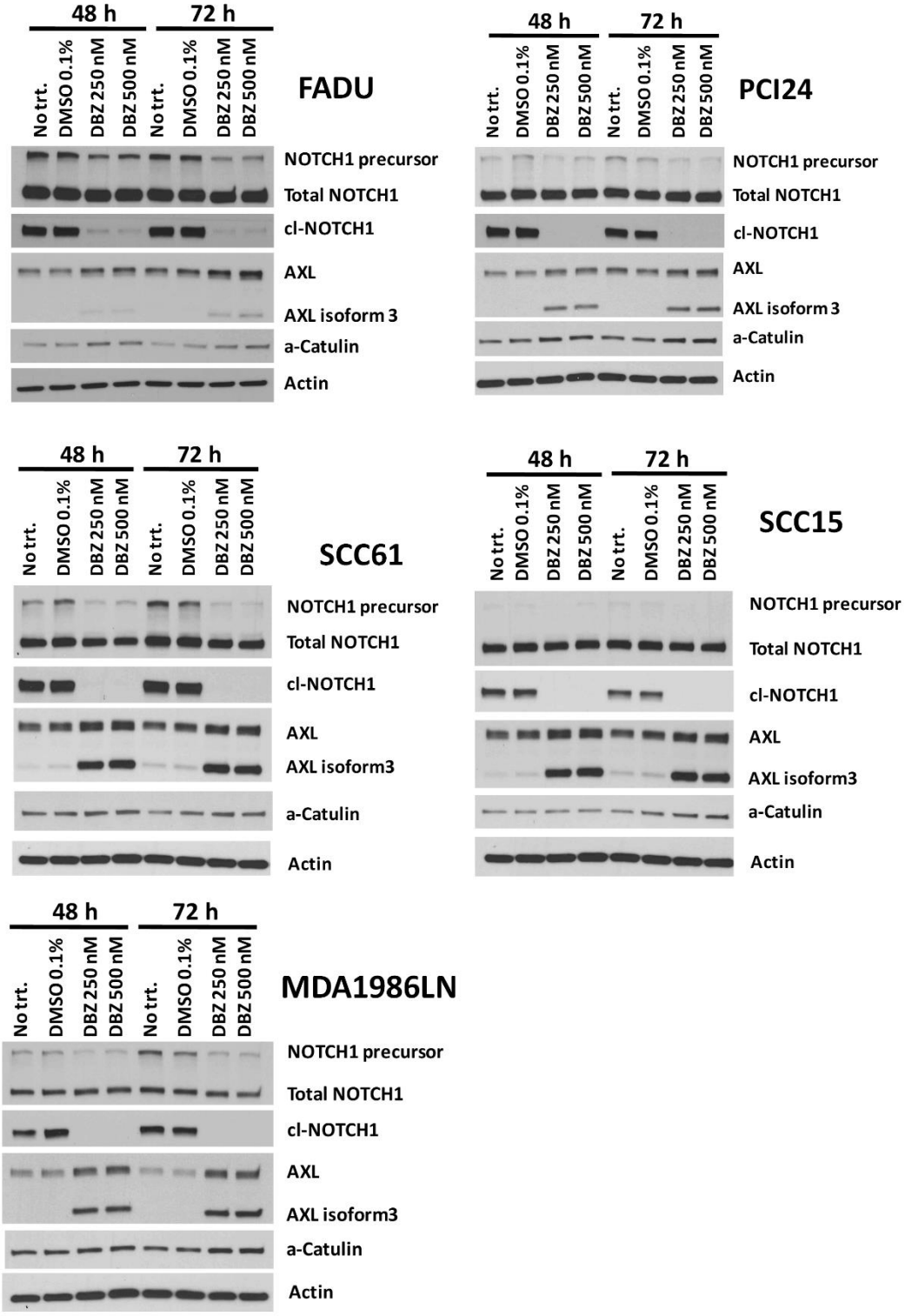

Supplementary Figure 7.**Evidence of NOTCH1 signaling that suppresses AXL and α-CATULIN expression in a subset of NOTCH1 wt HNSCC tumor cell lines.** Protein levels of both AXL and α-CATULIN increase when activated cl-NOTCH1 formation is blocked with the NOTCH inhibitor DBZ in five different *NOTCH1* WT cell lines with high endogenous NOTCH1 activity.

Supplementary Figure 8

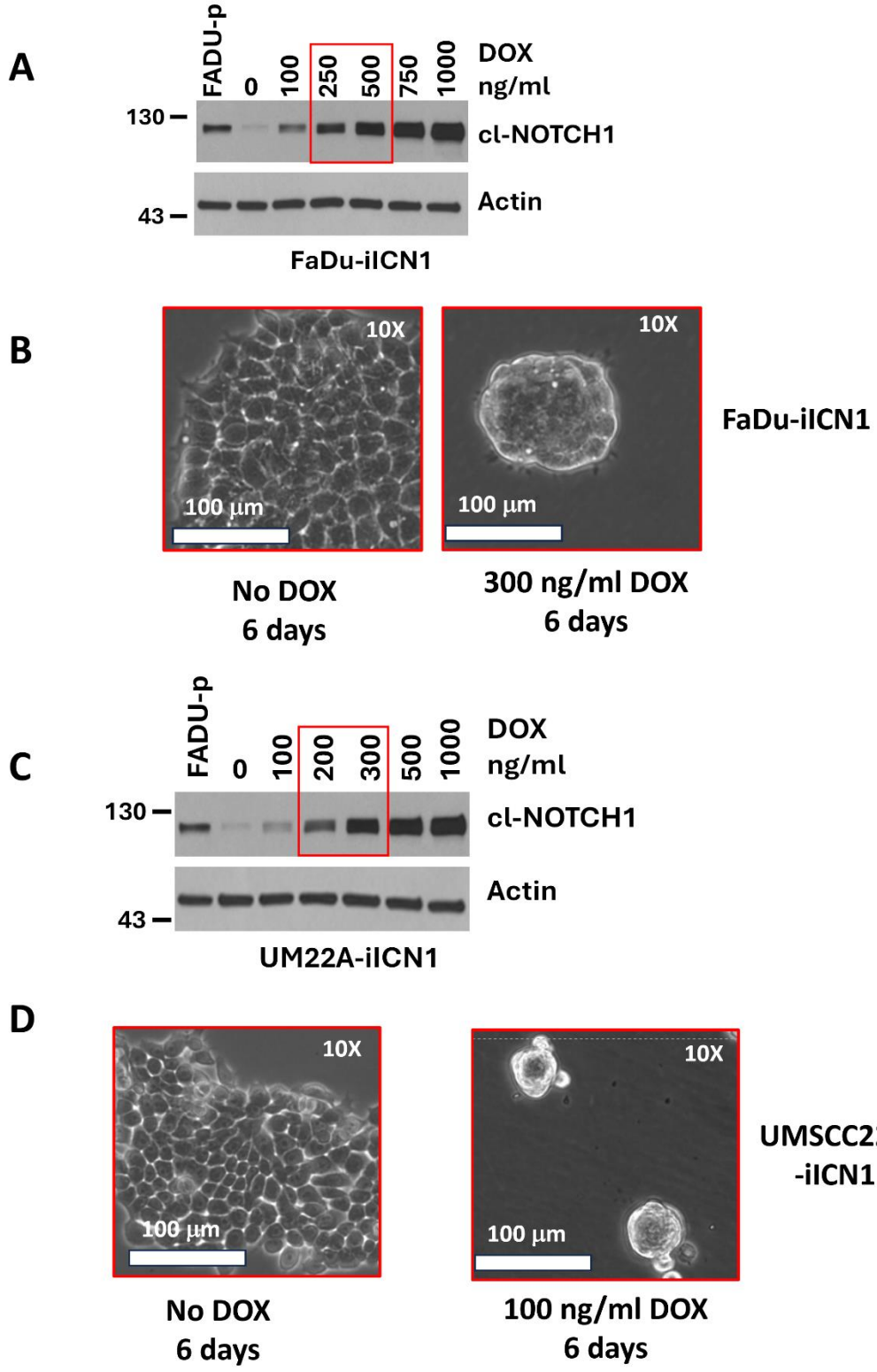

Supplementary Figure 8. Physiological levels of iICN1 trigger morphology changes in *NOTCH1* WT and mutant tumor cell lines. A. Titration demonstrates that treating FADU NIKO cells engineered to express iICN1 (FaDu-iICN1) with 250ng-500 ng/ml DOX for 36 h induces protein levels of iICN1 equivalent to parental FaDu (FADU-p) **B**. As little as 300 ng/ml DOX for 6 days causes tumor spheroid formation in FaDu-iICN1. **C.** cl-NOTCH1 protein levels in UMSCC22A-iICN1 treated with 200-300 ng/ml DOX for 36 h are similar to basal levels in parental FaDu. **D.** Tumor spheroid formation in UMSCC22A-iICN1 cells after 6 days treatment with 100 ng/ml DOX.

Supplementary Figure 9

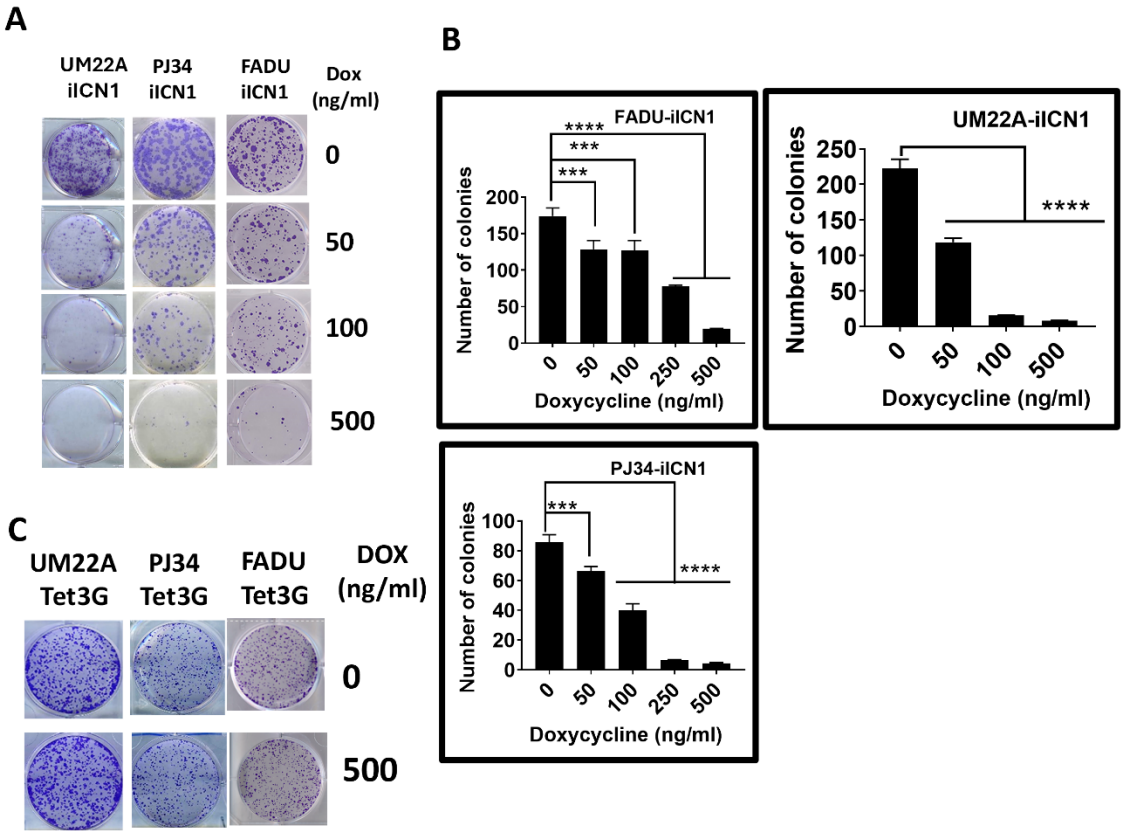

Supplementary Figure 9. Dose response inhibition of colony formation by iICN1 in NOTCH1 mutant and WT cell lines. A. Crystal violet stain of colonies after increasing doses of DOX. **B**. Quantitation of colony inhibition after treating cells with increasing DOX doses. **C.** Treatment of control Tet3G expressing cell lines, lacking an iICN1 construct, with 1000 μg/ml DOX did not inhibit colony growth. Differences in colony number between treatments for each cell line were analyzed with an ANOVA followed by a post-hoc Tukey test to determine P-values for specific comparisons. *** $P < 0.001$, **** $P < 0.0001$.

Supplementary Figure 10

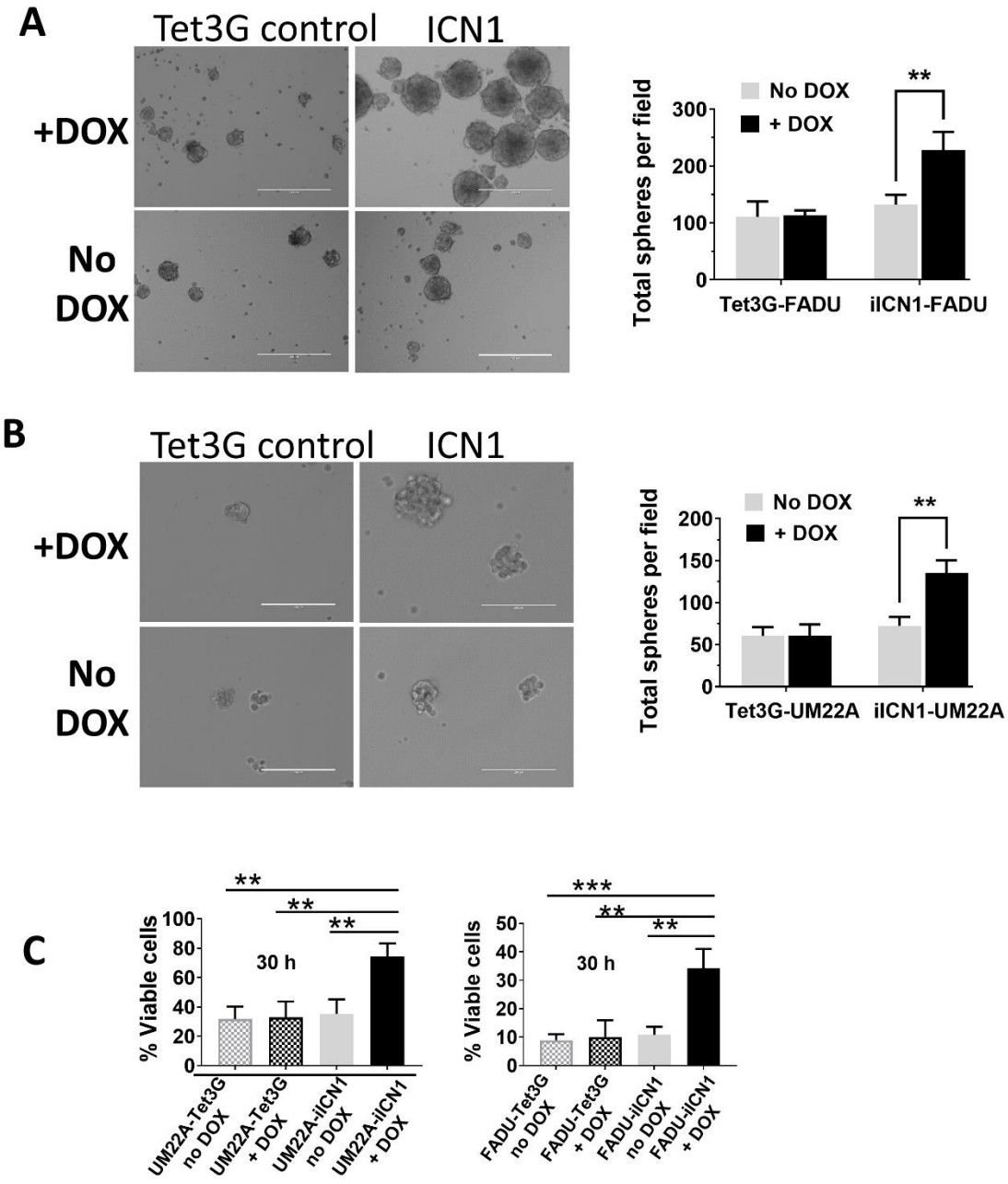

Supplementary Figure 10. NOTCH1 activation increases tumor spheroid growth and anoikis resistance. A. Addition of 1000 mg/ml DOX increases the number of orospheres derived from FaDu-iICN1 in non-adherent low serum concentrations for 1 week. **B**. Increased orosphere numbers after growing UMSCC22A-iICN1 in 300 mg/ml DOX non-adherent low serum cultures for 1 week. **C.** DOX was added to attached UMSCC22A-iCN1 at 300 mg/ml, FaDU-iICN1 at 1000 mg/ml, or control Tet3G cells for 48 h before single cell suspensions were prepared in low serum containing media and rotated in non-adherent tubes inside a humidified 37 ^{0}C cell incubator for an additional 30 hours, in continued presence or absence of DOX. Viability of replicate cultures was examined with an automated cell counter. Differences in spheroid count in cell lines before and after DOX treatment (A and B) were determined with a two-sided student's t-test, and treatments lacking P-values were not significantly different from each other ($P > 0.05$). Differences in the percentage of viable cells expressing the control plasmid Tet3G in the presence or absence of DOX or in iICN1 infected cells minus DOX were all compared to iICN1 infected cells plus Dox with an ANOVA followed by a Dunnett's multi-comparison test (C). ** $P < 0.01$, *** $P < 0.001$.

Supplementary Figure 11

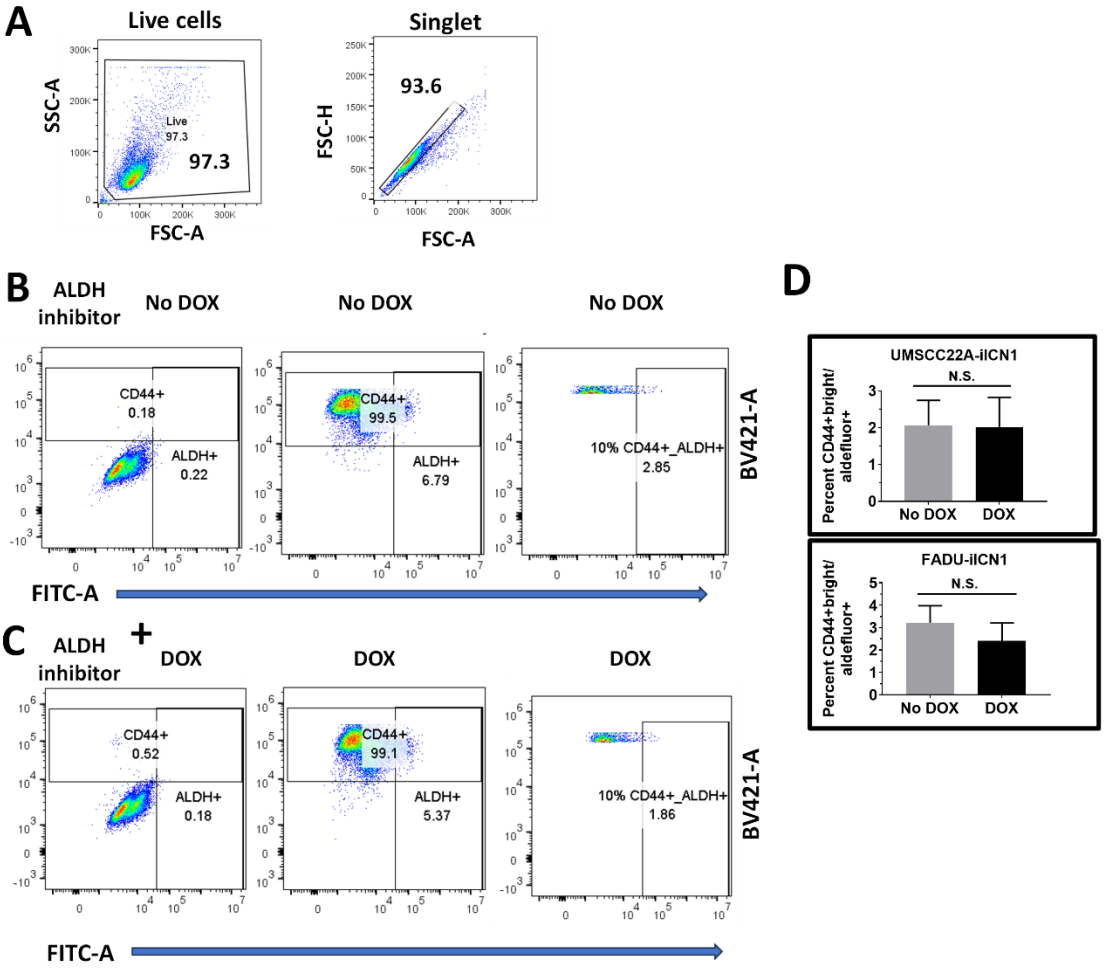

Supplementary Figure 11. **Activation of NOTCH1 does not increase the percentage of CD44+bright ALDEFLUOR-positive cells in NOTCH1 mutant or WT tumor lines. A.** Flow cytometry gating strategy to identify live single cells. **B.** Representative gating of UMSCC22A-iICN1 cells in absence of Dox. The sample is split and one tube treated with a BV-421 conjugated isotype control antibody and the aldehyde dehydrogenase inhibitor (DEAB) before adding fluorescein conjugated substrate to set the background gates (left panel). The second tube is incubated with BV421-A conjugated anti-CD44 and Aldefluor substrate without *DEAB* to gate on the CD44+/Aldefulor+ population (middle panel) and a single fixed threshold is set for the top 10% brightest CD44+ (e.g., CD44+ bright), which is uniformly applied to all remaining UMSCC22A-iICN1 samples. The CD44+ bright population is further analyzed for the percentage of Aldefluor+ cells (right panel). **C.** A UMSCC22A-iICN1 sample pretreated with 200 ng/ml DOX for 48 h to induce ICN1 before staining is gated in the same fashion, except Aldefluor gating is set with a sample specific tube treated with DEAB (left panel) and CD44+bright cells are analyzed in a companion tube without DEAB for percentage of Aldefulor+ using the previously set CD44+ threshold (right panel). D. The total percentage of CD44+bright/Aldefluor+ cells does not increase after iICN1 induction in either UMSCC22A-iICN1 or FaDu-iICN1. No significant differences were found in the percentage of CD44+bright/Aldefluor+ cells following a two-sided student's t-test.

Supplementary Figure 12

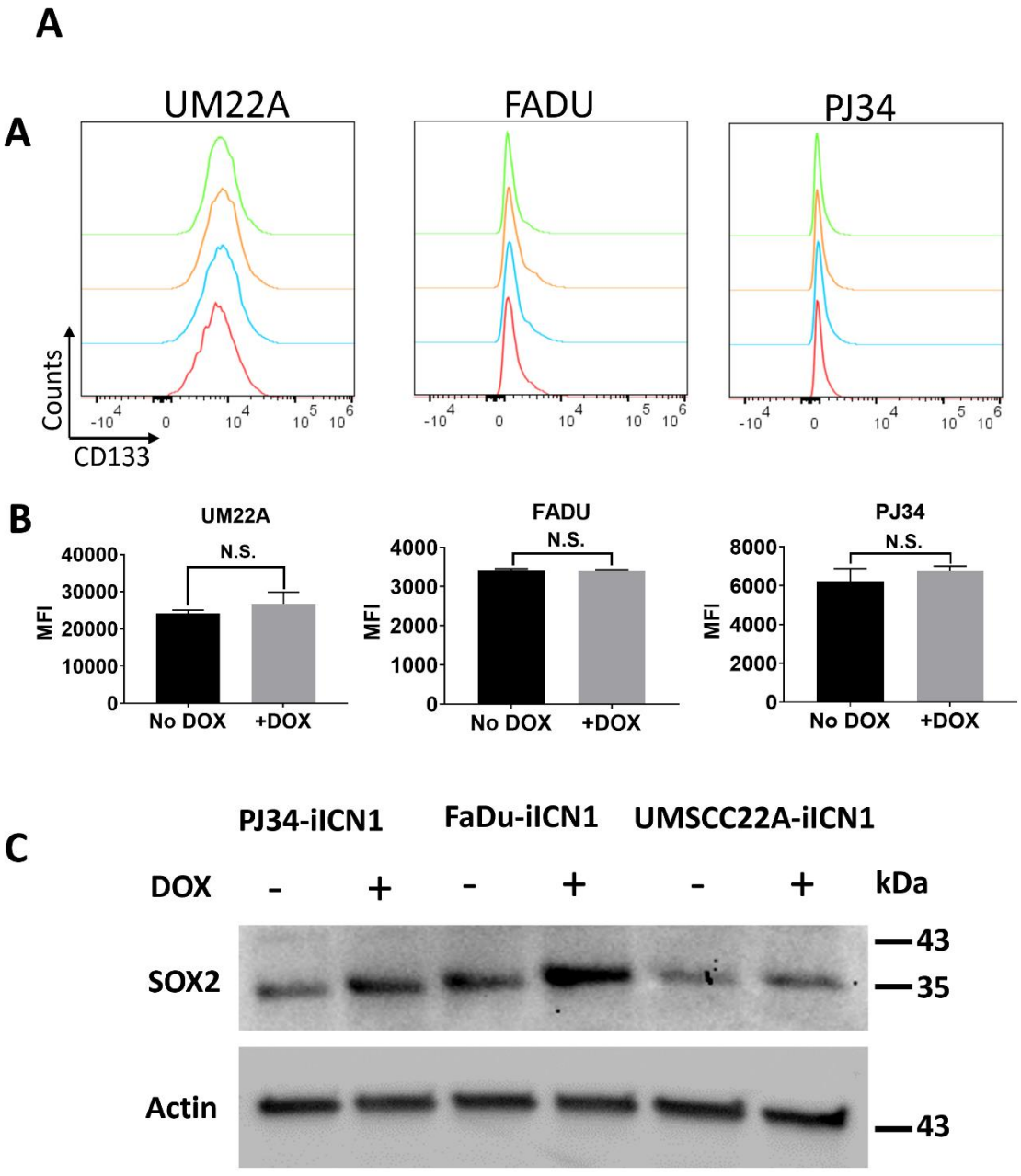

Supplementary Figure 12. Activation of NOTCH1 fails to increase surface CD133+ but increases expression of SOX2 in *NOTCH1* mutant (UMSCC22A-iICN1), or *NOTCH1* WT cell lines (FaDu-iICN1 and PJ34-iICN1). A. Cells were incubated for 48 h with or without DOX at 200 ng/ml (UMSCC22A), 300 ng/ml (FaDu), or 1000 ng/ml (PJ34) before staining with antibody to surface CD133 by flow cytometry. Fluorescent intensity histograms are shown for control biological replicates without DOX (red and light blue traces) or after DOX treatment (green and orange traces). **B.** Statistical comparison of CD133 mean fluorescence intensity (MFI). No significant differences were found in the mean intensities following a two-sided student's t-test. **C.** Western blot analysis of SOX2 protein expression in similarly treated cells.

Supplementary Figure 13

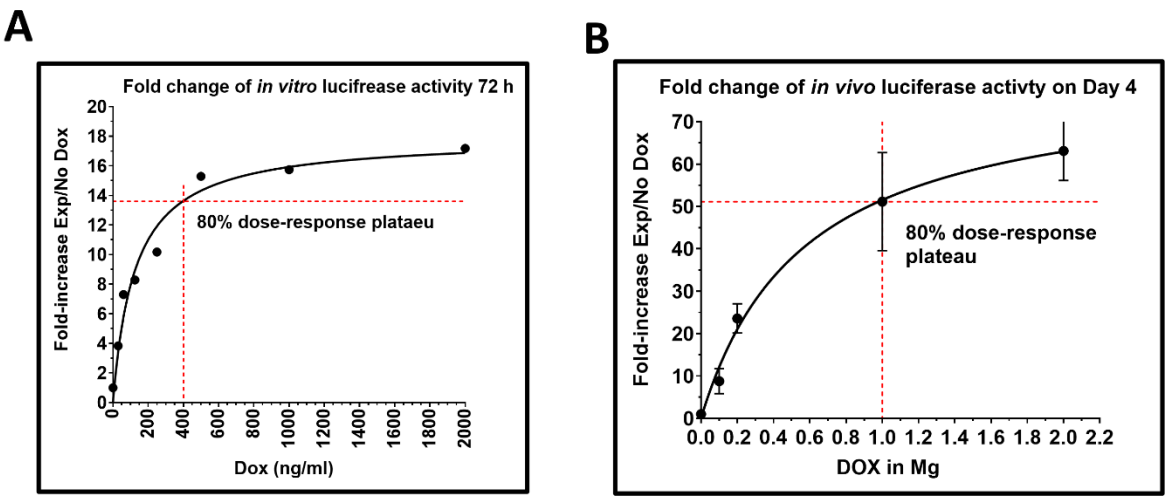

Supplementary Figure 13. ***In vitro* and *in vivo* dose response of the inducible DOX promoter**. **A.** UMSCC22A Tet3G reporter cells stably expressing firefly luciferase cloned into pLVX-TRE3G-mCherry were seeded into 6 well plates and luciferase activity measure in a plate reader 36 hours after induction with increasing concentrations of DOX. A dose of ~400 ng/ml resulted in luciferase activity that was 80% of the *dose response* plateau, but not outside linear response of the plate reader **B**. Standard curve relating relative *in vivo* luciferase luminescence to DOX concentration given to mice by oral gavage for 4 days, demonstrating that 1 mg DOX yielded activity that was 80% of the in *vivo* plateau.

Supplementary Figure 14

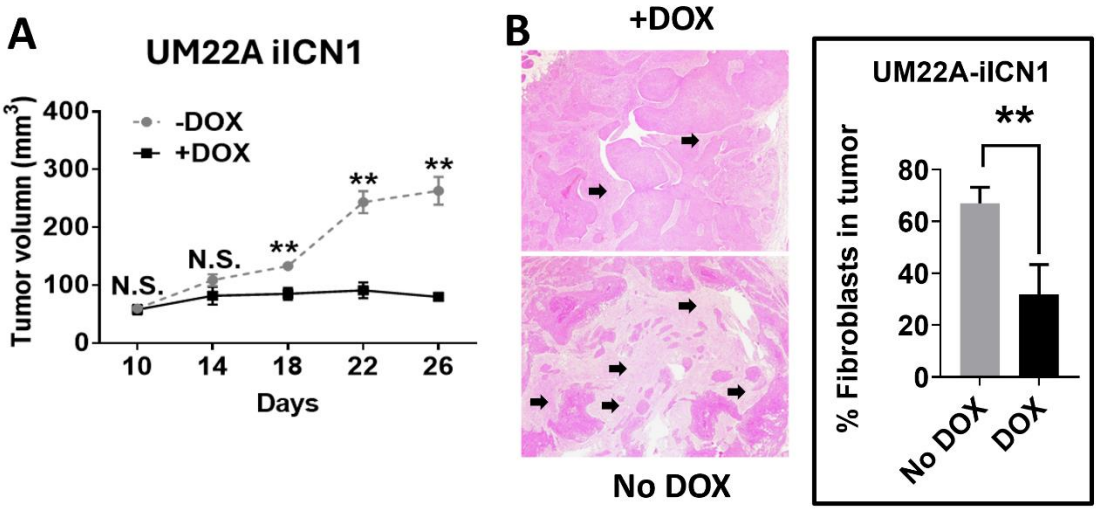

Supplementary Figure 14. **Activation of NOTCH1 signaling in *NOTCH1* mutant tumors profoundly inhibits *vivo* tumor growth and reduces the number of CAF cells. A.** UMSCC22A-iICN1 was inoculated into mouse flanks and mice were randomly assigned to receive either no DOX or daily DOX (1 mg) by oral gavage for two weeks. Tumor volumes were compared over time. **B**. H&E staining of a representative tumor that eventually formed in mice treated with DOX (top panel) and a tumor that formed in the absence of DOX (bottom panel). Arrows designate areas predominately populated by CAFs. The percentage of CAFS in tumors was significantly lower when ICN1 was induced with DOX. Differences in tumor volumes between treatment groups at each time point were evaluated by a two-sided student's t-test. ** $P < 0.01$.

Supplementary Figure 15

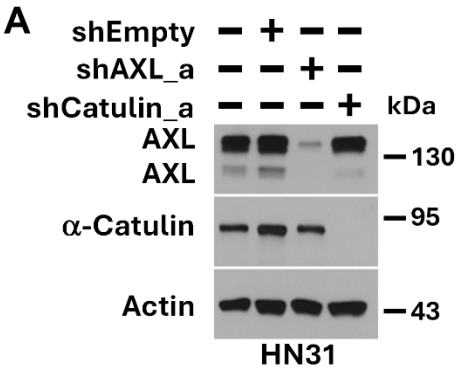

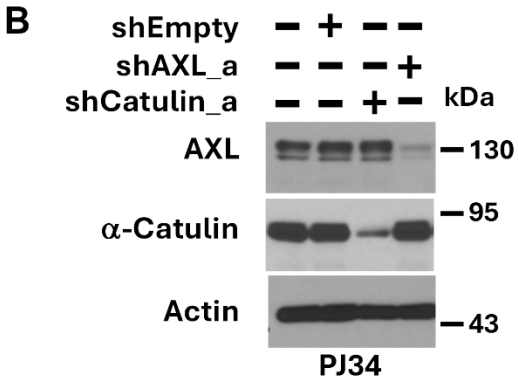

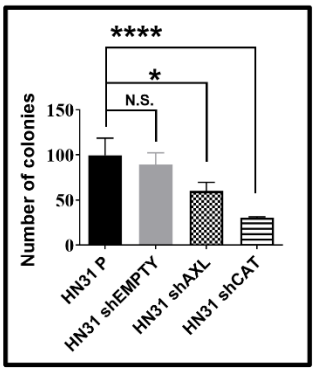

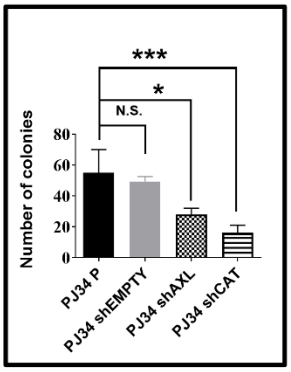

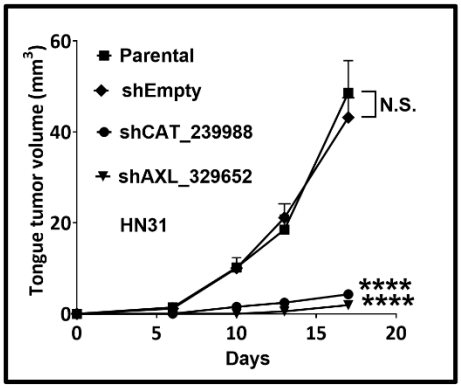

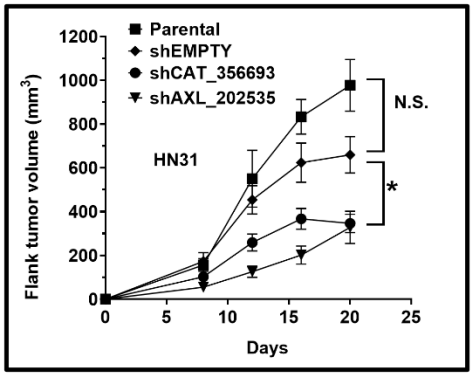

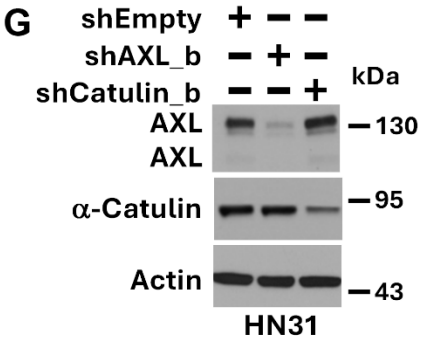

Supplementary Figure 15. Knockdown of *AXL* and α-CATULIN to mirror NOTCH1 signaling inhibits *in vitro* and *in vivo* tumor growth. A. Western blot confirmation of AXL and α-CATULIN protein inhibition following KD in *NOTCH1* mutant HN31 cells 96 h post-infection with shAXL_a (Cat # 329652) and shCatulin_a (Cat # 239988). **B.** Western blot confirmation of AXL and a-CATULIN protein inhibition following shRNA KD in NOTCH1 WT PJ34 cells 96 h post-infection with specific shRNA. **C.** KD of AXL (i.e., shAXL_a) and a-CATULIN (i.e., shCatulin_a) blocks *in vitro* colony formation in HN31. **D.** KD of AXL (shAXL_a) and a-CATULIN (shCatulin_a) blocks *in vitro* colony formation in PJ34. **E.** KD of AXL and a-CATULLIN profoundly inhibits HN31 *in vivo* tumor growth in an orthotopic tongue tumor model. **F.** KD of AXL and a-CATULLIN with alternate shRNA vectors targeting different regions inhibits HN31 *in vivo* tumor growth in a subcutaneous flank model. **G.** Western blot validation of target KD with alternate shCAT_356693 (shCatulin_b) and shAXL_202535 (shAXL_b) vectors used in the subcutaneous tumor experiment. Difference in colony formation or *in vivo* tumor volumes between treatments were analyzed by an ANOVA, followed by a post-hoc Tukey test to determine P-values for individual comparisons (C, D, E, F). *P < 0.05, ***P < 0.001, ****P < 0.0001

Supplementary Figure 16

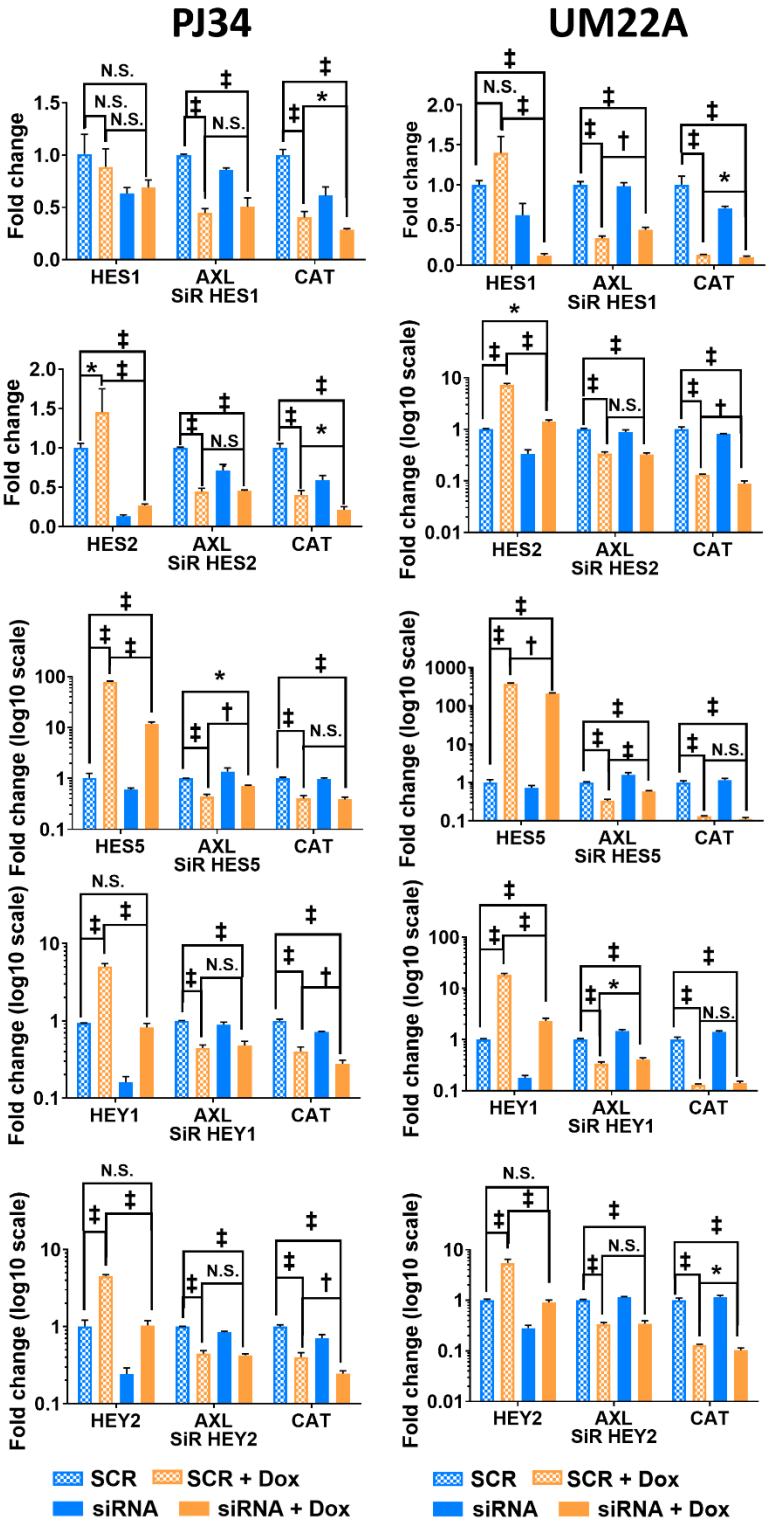

Supplementary Figure 16. Canonical HES/HEY family members are not key mediators of ICN1 induced reductions in *AXL* and a-*CATULIN* expression. PJ34-iICN1 (left) or UMSCC22A-iICN1 (right) were pretreated with siRNA (SIR) to HES1, HES2, HES5, HEY1, or HEY2 or control non-targeting siRNA (SCR) for 48 h before replating in the absence or presence of 300 ng/ml DOX for 24 h. Expression of the HES/HEY knockdown targets, AXL, and α-Catulin were quantitated by qPCR. Differences in RNA among treatments for each gene were evaluated with an ANOVA followed by a post-hoc Tukey test to determine P-values for individual comparisons. * $P < 0.05$, † $P < 0.001$, ‡ $P < 0.0001$.

Supplementary Figure 17

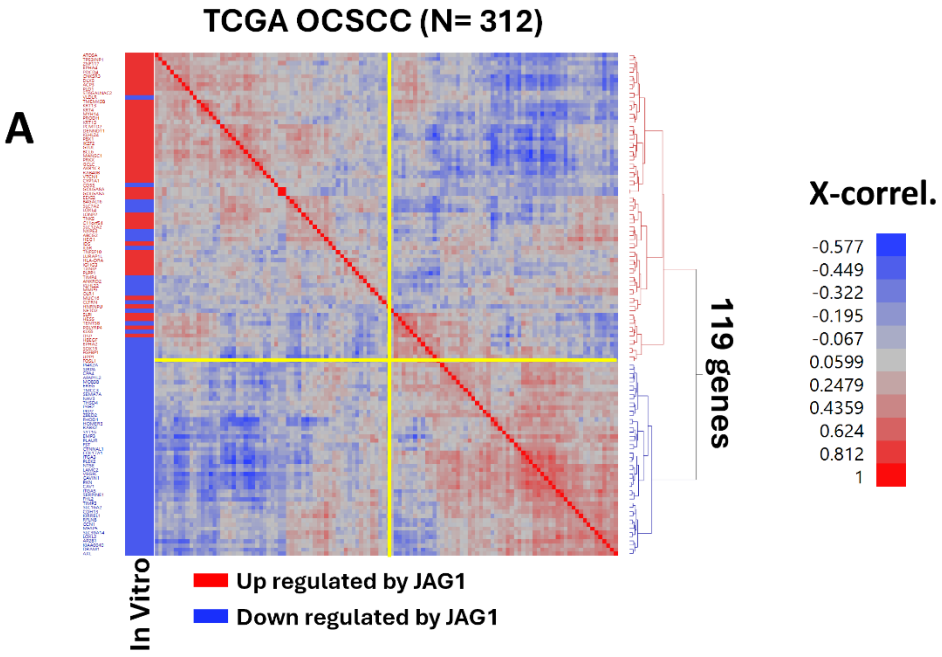

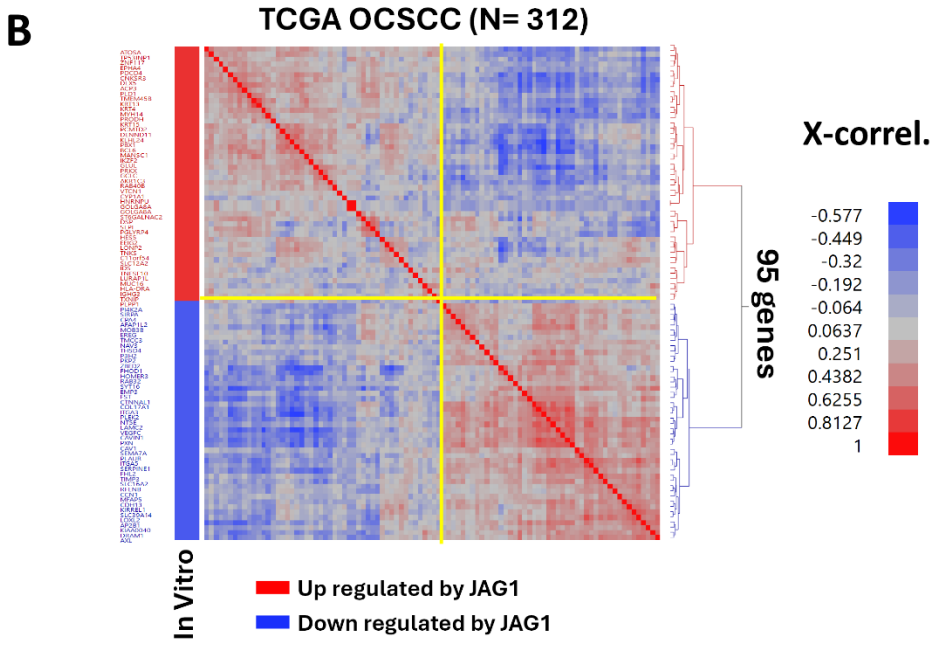

Supplementary Figure 17. Development of an *in vivo* NOTCH1 signaling gene expression signature. **A.** The TCGA OCSCC RNA-seq cohort was mined for cross-correlation of RNA expression using gene candidates from the list of 119 top genes regulated *in vitro* after JAG1 exposure. Hierarchical two-way clustering of cross-correlation coefficients identified two main gene clusters annotated by whether the genes were up-regulated (red box) or down regulated (blue box) after JAG1 exposure. **B.** Re-clustering TCGA OCSCC cross-correlation coefficients with the remaining 95 genes after removal of those with inconsistent *in vitro* and *in vivo* behavior.

Supplementary Figure 18

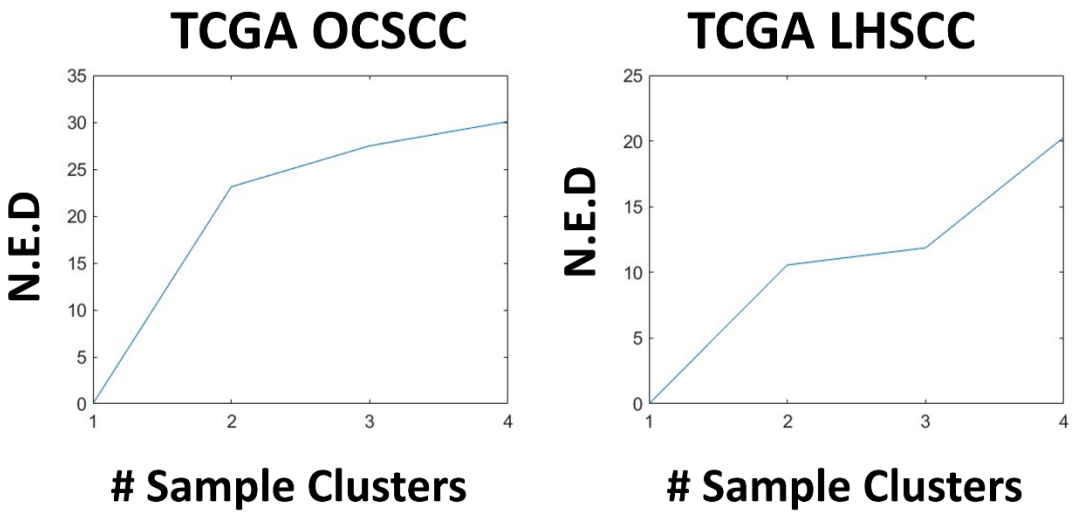

Supplementary Figure 18. Selection of optimal sample clusters numbers with the NOTCH1 gene signature. Consensus hierarchical clustering of TCGA OCSCC and LHSCC samples using the 95 gene NOTCH1 signature was performed and the similarity matrices achieved using increasing numbers of sample clusters (e.g. N=1 to 4) were compared to theoretical perfection matrices to select a local minimum for the normalized Euclidean distances (N.E.D.) to identify an optimal number of sample clusters, which happened to be N =2 clusters for each disease subsite.

Supplementary Figure 19

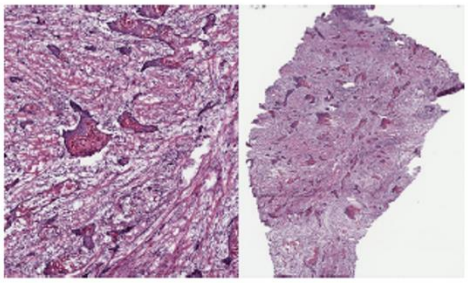

CN-6019 (ssGSEA 8862)-NOTCH off

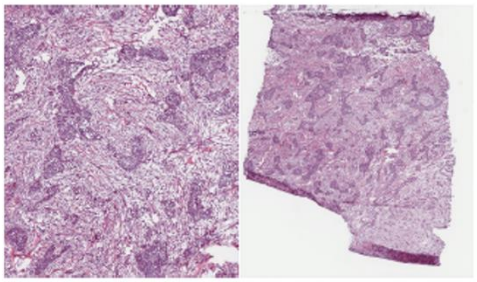

CQ-6019 (ssGSEA 8955)-NOTCH off

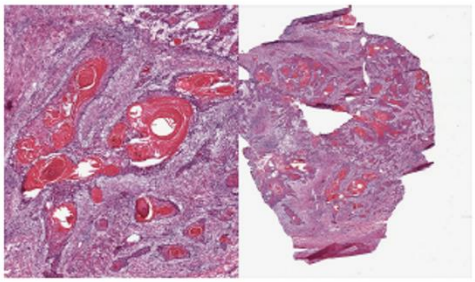

CN-4742 (ssGSEA 8389)-NOTCH off

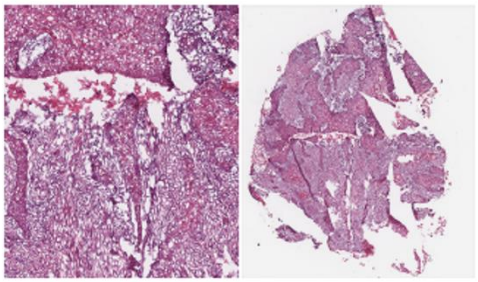

CV-7413 (ssGSEA 7935)-NOTCH off

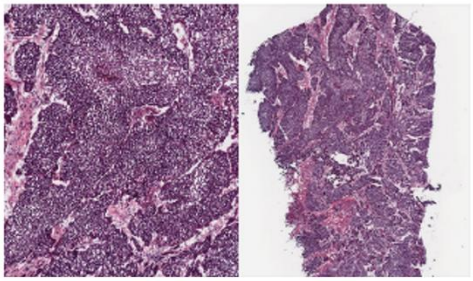

P3-A6T6 (ssGSEA 3662)-NOTCH on

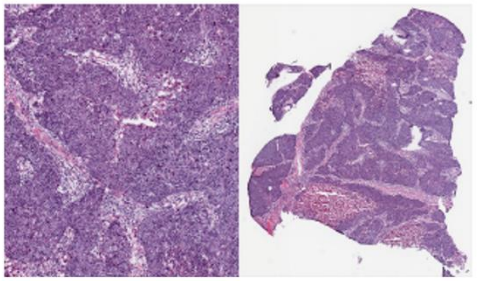

P3-A5QF (ssGSEA 4259)-NOTCH on

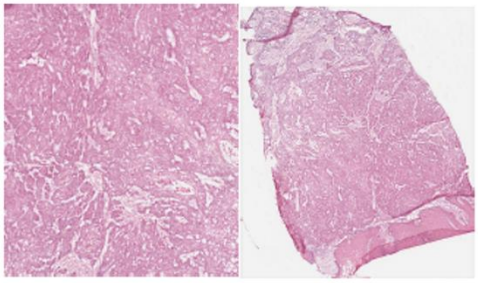

BB-4224 (ssGSEA 3955)-NOTCH on

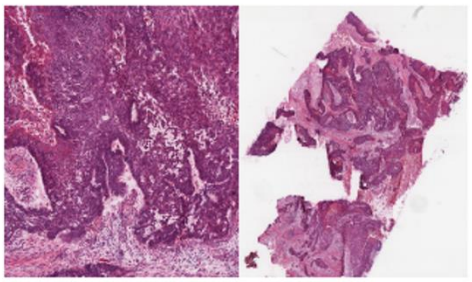

BB-8601 (ssGSEA 3752)-NOTCH on

Supplementary Figure 19. Visual confirmation that TCGA tumor samples identified with active NOTCH1 signaling contain fewer CAF. H&E images were downloaded from the TCGA data portal and the CAF ssGSEA scores appear in parenthesis alongside the sample TCGA identification numbers.

Supplementary Figure 20

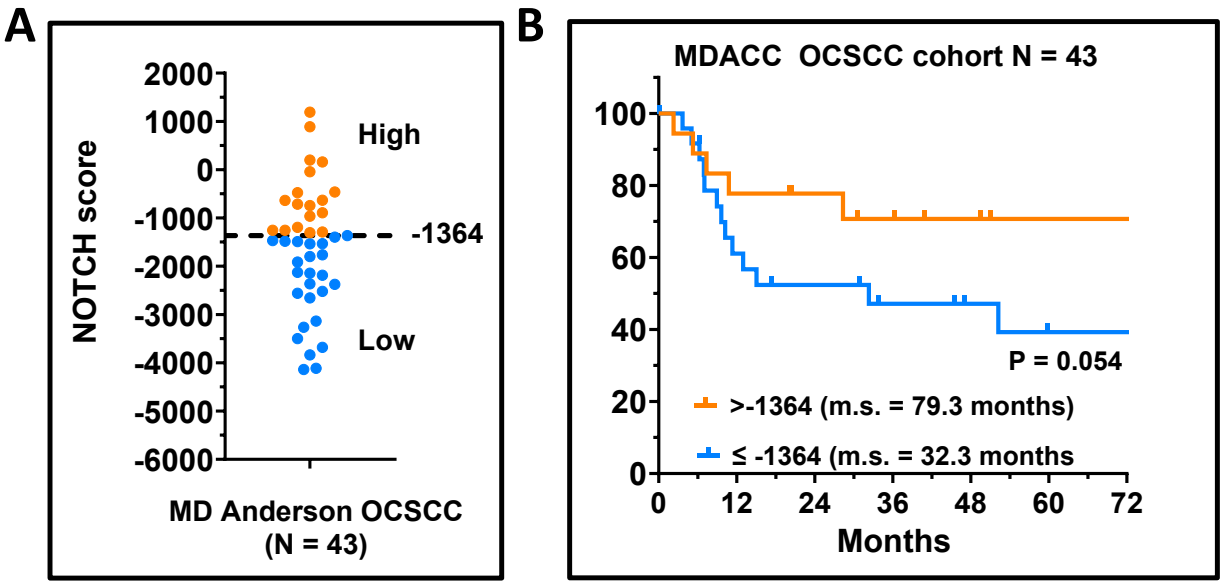

Number at risk (number censored)													
Time	0	12	24	36	48	60	72	84	96	108	120	132	143
NOTCH low	25 (0)	14 (2)	11 (3)	8 (5)	6 (7)	4 (8)	4 (8)	3 (8)	2 (8)	0 (8)	0 (8)	0 (8)	0 (8)
NOTCH high	18 (0)	14 (0)	11 (3)	9 (4)	7 (6)	5 (8)	5 (8)	3 (8)	3 (8)	3 (8)	2 (9)	1 (10)	1 (10)

Supplementary Figure 20. NOTCH activation is associated with better prognosis in an independent validation cohort. **A.** Distribution of NOTCH scores in the MD Anderson OCSCC cohort with the optimal cutpoint (-1364) shown as a horizontal dotted line. Tumor specimens above the cutoff (high) have orange symbols while those below the cutoff have blue symbols. **B**. Kaplan-Meir curve depicting overall survival and median survival (m.s.) of patients based on their tumors NOTCH score group from panel A. Differences in survival approached significance (P =0.054 by a log rank test). The at-risk table for the Kaplan-Meir data is shown at the bottom of the figure.

Supplementary Figure 21

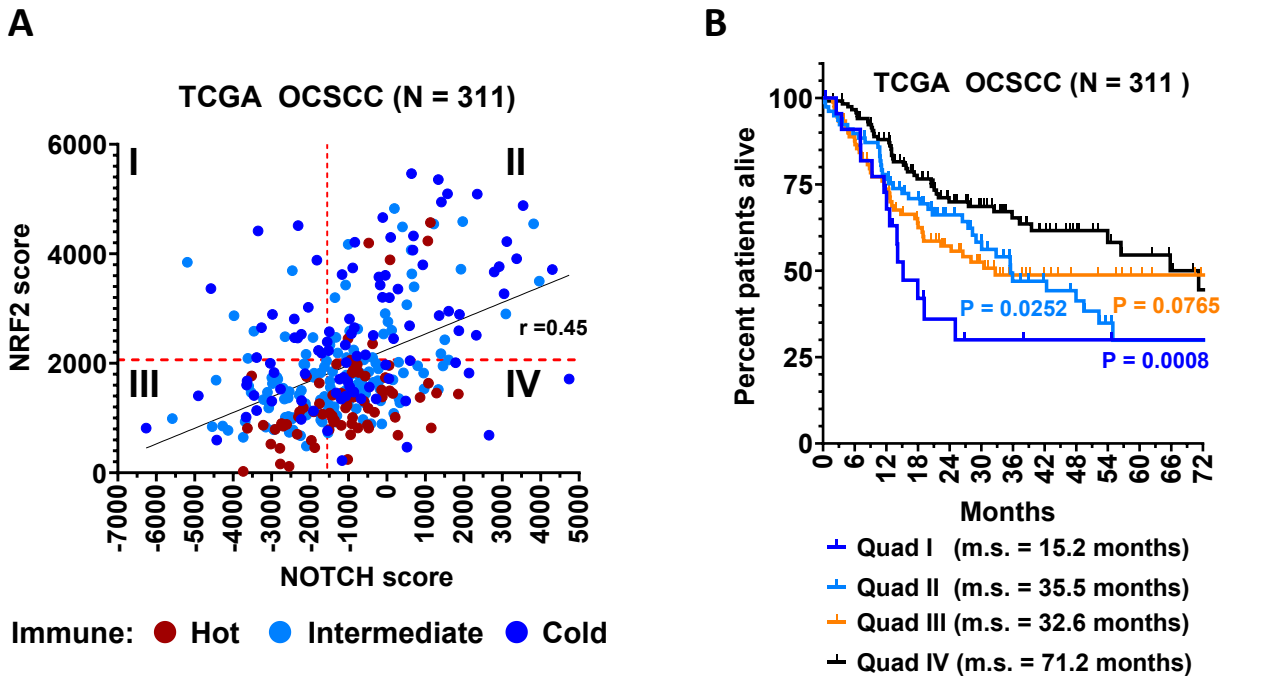

Number at risk (number censored)							
Time	0	12	24	36	48	60	72
Quad I	23 (0)	15 (2)	6 (4)	4 (5)	3 (6)	2 (7)	2 (7)
Quad II	78 (0)	58 (2)	35 (18)	20 (24)	14 (28)	6 (33)	6 (33)
Quad III	90 (0)	62 (5)	38 (16)	21 (28)	14 (35)	9 (40)	5 (44)
Quad IV	120 (0)	99 (7)	59 (29)	37 (48)	22 (61)	14 (67)	8 (71)

Supplementary Figure 21. NOTCH and NRF2 pathways define unique risk groups. A. Patient tumors from the TCGA OCSCC cohort (N = 311) were plotted in two dimensions based on their NOTCH and NRF2 scores determined from ssGSEA. Previous optimal cutpoint thresholds for NOTCH (-1554) and NRF2 (2063) are indicated with dotted red lines to divide tumors into four quadrants: I) low NOTCH/high NRF2; II) high NOTCH/high NRF2; III) low NOTCH/low NRF2; IV) high NOTCH/low NRF2. A linear regression (black line) demonstrates a positive correlation between NOTCH and NRF2 scores (Pearson correlation = 0.45, P <0.001). The immune cluster (hot, intermediate, cold) of each tumor sample from the prior analysis (Fig. 6) is annotated by colored symbols according to the legend. B. Kaplan-Meir survival plots of patients from the four risk quadrants defined in panel A demonstrate that patients whose tumors had low NOTCH but high NRF2 signaling (quadrant 1) had the worst median survival times. Difference in survival curves were analyzed with a log rank test comparing each risk group to quadrant IV which had the best median survival. An at-risk table indicating the number of patients still at risk or censored is depicted underneath.

Supplementary Figure 22

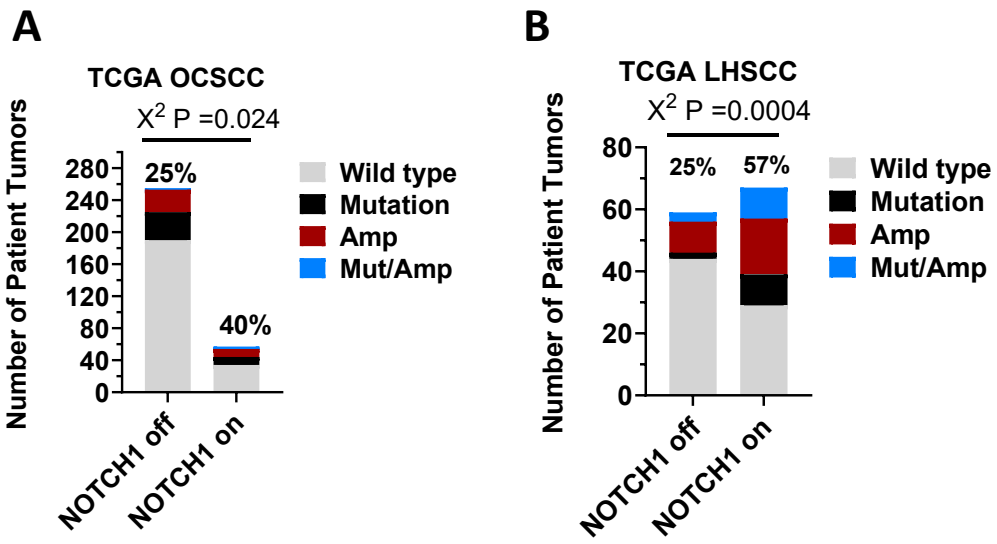

Supplementary Figure 22. Patients lacking NOTCH1 mutations are significantly enriched for genomic alterations in PIK3CA. The proportion of tumors with genomic alterations in PIK3CA (i.e., numbers above bar graphs), including mutations and/or high-level gene copy gains, is significantly higher (ChiSquare test) in in the group associated with NOTCH signaling identified through hierarchical clustering of TCGA OCSCC (A) or (B) LHSCC.

LIST OF ADDITIONAL FILES AND TABLE DESCRIPTIONS

NOTCH_suppelmentary methods.docx: Detailed methods of experimental procedures and statistical analyses.

NOTCH_Supplementary Tables S1 to S14.xlsx:

S1. NOTCH1 and NOTCH2 genotype of established HNSCC tumor cell lines used in the study and their expression of 157 different protein analytes measured by Reverse Phase Protein Arrays.

S2. Protein analytes correlating with cl-NOTCH1 levels across 53 different HNSCC cell lines either WT or mutant for NOTCH1.

S3. Genes downregulated by extended growth on the NOTCH1 ligand JAG1 identified as a main effect or individually for NOTCH1 WT cell lines PJ34 and/or 183.

S4. Genes upregulated by extended growth on the NOTCH1 ligand JAG1 identified as a main effect or individually for NOTCH1 WT cell lines PJ34 and/or 183.

S5. Gene ontology (GO) enrichment analysis of biological processes for the top 120 genes regulated by prolonged growth on the NOTCH1 ligand JAG1.

S6. Annotation of enriched GO pathways for top genes regulated by JAG1.

S7. Comparison of genes significantly altered after ICN1 induction by DOX in PJ34-iICN1 and after growth of parental PJ34 on JAG1 ligand, along with their fold changes.

S8. Genes significantly bound by activated NOTCH1 protein in Chip-seq experiments after induction of iICN1 by DOX in PJ34-iICN1 cells.

S9. List of genes from different sectors of the Venn diagram depicted in Fig. 3F, identifying overlap between genes downregulated by iICN1, growth on JAG1, or bound by ICN1 in chip-seq.

S10. List of genes from different sectors of the Venn diagram depicted in Fig. 3G, identifying overlap between genes upregulated by iICN1, growth on JAG1, or bound by ICN1 in chip-seq.

S11. Frequency of tumor formation from FaDu-iICN1 in presence or absence of DOX treatment and statistical analysis of estimated tumor initiating cell (CSC) frequencies.

S12. The final 95 gene NOTCH1 activation signature list along with their cross-correlation coefficients of expression from the TCGA OCSCC RNA-seq cohort.

S13. Consensus hierarchical clustering of TCGA OCSCC cohort based on 95 gene NOTCH1 activation signature, which predicts the NOTCH1 pathway status.

S14. Consensus hierarchical clustering of TCGA LHSCC cohort based on 95 gene NOTCH1 activation signature, which predicts the NOTCH1 pathway status.

NOTCH_Supplementary Table S15.xlsx:

S15. Significant genes differentially expressed between OCSCC tumors with NOTCH1 signaling active (consensus cluster 2) and inactive (consensus cluster 1).

NOTCH_Supplementary Table S16.xlsx:

S16. Significant genes differentially expressed between LHSCC tumors with NOTCH1 signaling active (consensus cluster 2) and inactive (consensus cluster 1).

NOTCH_Supplementary Table S17 to S21.xlsx:

S17. List of genes commonly upregulated in cells grown on JAG1, the NOTCH1 gene signature, and patient tumors with active NOTCH1 signaling in OCSCC and LHSCC TCGA cohorts.

S18. List of genes commonly downregulated in cells grown on JAG1, the NOTCH1 gene signature, and patient tumors with active NOTCH1 signaling in OCSCC and LHSCC TCGA cohorts.

S19. List of gene signatures defining cell types present in the tumor microenvironment.

S20. Comparison of ssGSEA scores for leukocyte subtypes, CAFS, and endothelial cells among TCGA OCSCC tumors with NOTCH1 signaling on and off.

S21. Comparison of ssGSEA scores for leukocyte subtypes, CAFS, and endothelial cells among TCGA LHSCC tumors with NOTCH1 signaling on and off.

S22. Cox proportional hazards analysis of survival as a function of NOTCH and NRF2 scores

S23 Logistic regression analysis of tumor immune phenotype as a function of NOTCH and NRF2 scores.

MC_Full_westerns_7_10_25.pdf: Contains full blot images for all western blot figures

SUPPLEMENTAL METHODS:

Notch activation

For NOTCH activation experiments, tissue culture wells were pre-coated overnight at room temperature (RT) with Protein G (Prospec, East Brunswick, NJ) at 50 ug/ml, washed twice in phosphate buffered saline (PBS), blocked in 1% BSA/PBS for 2 hours at RT, washed three times with PBS, coated with either human recombinant chimeric Jag1 fused to an FC fragment (R&D Systems, Minneapolis, MN) or control purified IgG FC protein (Jackson ImmunoResearch, West Grove, PA) at 2 ug/ml in 0.1% BSA/PBS for 3 hours RT, stored overnight at 4°C, and washed three times immediately before use.

Viral vectors, shRNA Vectors, and siRNA Reagents

A 7.3 kb cDNA encoding WT full length human NOTCH1 receptor (NFL1) with a Kozak sequence was provided by Origene (Rockville, MD) and digested with EcoR1/XhoI to subclone into an empty retroviral vector MigR1 (Addgene, Watertown, MA), where the multiple cloning site (MCS) that had been previously modified to contain MfeI (EcoR1 compatible) and Xho1 sites from 5' to 3'. Sanger sequencing confirmed that the entire NFL1 cDNA insert matched the reference sequence for full length human NOTCH1 (NM 017617) encoding 2555 amino acids. The MCS of MigR1 is upstream of an IRES-EGFP (enhanced green fluorescence protein) cassette so NFL1 cDNA is expressed from the same mRNA as EGFP, allowing purification of infected cells by flow cytometry. An ICN1 construct encoding human NOTCH1 Pro1770 to Lys2555 cloned into MigR1 was obtained from Dr. Patrick Zweidler-McKay (MD Anderson, Houston, TX). To express inducible activated cleaved NOTCH1 that could be recognized by cl-NOTCH1 antibodies we utilized RNA from *NOTCH1* WT FaDu to generate a cDNA fragment encoding Val1754 to Lys2555 which was amplified with primers containing a Kozak sequence and artificial ATG methionine start site. Amplified cl-NOTCH1 cDNA was then cloned into the tetracycline/doxycycline lentiviral plasmid pLVX-TRE3G-mCherry using an In-Fusion cloning kit (Takara). GIPZ shRNAs used for targeting AXL and a-CATULIN (CTNNAL1) were from Horizon and included, V2LHS_239988 (AXL, AACTTAGATGCTTAGGATC), V3LHS-329652 (AXL, TGAGGATGGAGTCGTCCTG), V2LHS-239988 (CTNNAL1, TATTTCCAGAGGTTCTGTC), and V3LHS_356693 (CTNNAL1, TGTTTTCTTGCTTTGAGCT). SMARTPool siRNA mixtures targeting either human HES1, HES2, HES5, HEY1, and HEY2 were purchased from Horizon. CRISPR-Cas9 NOTCH1 (sc-400167-KO-2), and NOTCH2 (sc-401323-KO-2) plasmids were obtained from Santa Cruz.

ICN1 Retroviral Construct Validation

The ICN1 fragment encoded by this vector (Pro1770 to Lys2555) is missing several N-terminal amino acids at the cleavage site and is therefore not recognized by antibodies specific for activated NOTCH1. Construct integrity was confirmed through DNA sequencing and detection of its protein product after infecting NOTCH1-null mutant UMSCC22A with an antibody that binds the C-terminus of NOTCH1 (Supplementary Fig. S6A).

Antibodies

Antibodies to cl-NOTCH1 (#4147), AXL (#8661), SOX2 (#23064) and LAMC2 (#53884) were purchased from Cell Signaling Technology (Danvers, MA). Antibodies to total NOTCH1 (Sc 6014), total NOTCH2 (sc 5545), α-Catulin (sc 390584) were from Santa Cruz Biotechnology (Santa Cruz, CA). The β-Actin antibody (A1978) was bought from Sigma (St Louis, MO), and anti-ITGA3 (#PA5-143239) was purchased from ThermoFisher (Waltham, MA).

Viral Mediated Ectopic Gene Expression and shRNA Knockdown (KD)

Retroviral and lentiviral particles were generated by transfecting expression plasmids into helper cell lines—HEK-293GP2 for retroviruses and HEK-293F17 for lentiviruses. For retroviral production, a mixture of MigR1, ICN1, or NFL1 (10.8 mg) with 1.2 mg of the packaging plasmid pCMV-VSV-G (Addgene) was transfected into a 10 cm dish of 6 million adherent HEK-293GP2 cells using GenJet Plus (SignaGen, Frederick, MD) under a modified protocol that minimized volumes during the initial 45 minutes at 37 °C in a tissue culture incubator. After this period, complete media was added for an additional 8 hours at 37 °C before the transfection reagents were washed out. The cells were then incubated at 33 °C to optimize viral production, and the virus-containing supernatants were harvested at 48 and 72 hours, centrifuged, and pooled. Lentiviral particles (e.g., shRNA or inducible expression plasmids) were produced similarly, using a mixture of 10 µg expression plasmid, 5 µg packaging plasmid pCMV-dr8.2 (Addgene), and 5 µg envelope plasmid pMD2.G (Addgene) to transfect HEK-293F17 cells with GenJet Plus. The cells were incubated at 37 °C, and virus was harvested from the supernatants at 48 and 72 hours.

Cells were infected with retroviral or lentiviral particles using a reverse spin inoculation protocol. Briefly, trypsinized tumor cells were counted and mixed with serial dilutions of viral supernatant, fresh media, and polybrene (final concentration of 8 µg/mL). One million cells were then seeded in 2 mL per well in 6-well plates. The plates were centrifuged at 12,000 × g for 1.5 hours at room temperature, then transferred to a 37 °C tissue culture incubator for 48 hours. Infected cells were subsequently purified by flow cytometry or, in some cases, selected using antibiotics. Cell lines expressing DOX-inducible lentiviral constructs were

generated by first infecting cells with pLVX-Tet3G (Takara, San Jose, CA) encoding the Tet-ON 3G regulator protein and selecting for G418 resistance to obtain Tet3G modified cells. Cells stably expressing Tet3G were then infected with human ICN1 that had been subcloned into pLVX-TRE3G-mCherry (iICN1) and selected for 1 week in puromycin. For some experiments, polyclonal puromycin selected cells were used while in other cases, cell sorting was used to generate and screen clones with minimal leakiness and maximal ICN1 induction.

Mouse Tumor models

Cell lines infected with equivalent titers of shRNA lentivirus (AXL, α-CATULIN, or empty vector) were sorted for GFP positivity by flow cytometry, allowed to recover for 2 days and then 50,000 cells (in 30 µl PBS) were injected into the anterior tongues of anesthetized mice using a 30-gauge needle. For flank models utilizing shRNA-infected tumors or iICN1-inducible cell lines (FaDu-iICN1 or UMSCC22A-iICN1), 3-4 million cells were injected subcutaneously into flanks of nude mice in 200 µl PBS. For some groups, mice were administered 1 mg doxycycline (DOX) dissolved in 200 µl water by oral gavage 5 days per week for 1 to 3 weeks.

Analysis of RNA expression

Total RNA was isolated from replicate samples of PJ34 or 184 cells grown for 5 days on plates coated with either JAG1 or control FC. The RNA isolated with Trizol was purified by ethanol precipitation and hybridized to Affymetrix HuGene 2.0 ST arrays by the MD Anderson Sequencing and Microarray Core Facility. Data was processed using aroma.affmetrix package in R to quantify the CEL files with Robust Multiarray Averages (RMA) , apply background correction, quantile normalization, and RMA Probe-level summarization. The processed data was log2 transformed before analysis of differentially expressed genes (DEGs) using a linear model fit with both treatment and cell line as fixed effects. Two-sided P values were modeled using a beta-uniform mixture model and combined with false discovery rate at 0.05 to determine P value cutoffs.

RNA-seq was used to identify genes differentially expressed after iICN1 expression in PJ34. Replicate cultures of either PJ34-Tet3G or PJ34-iICN1 cells were incubated in the presence or absence of 1000 ng/ml DOX for 36 h and total RNA isolated with a RNeasy Kit was sequenced by the MD Anderson Sequencing and Microarray Core Facility. Gene expression was normalized as counts per million and log2 transformed before identifying differentially expressed genes using the response screening module in JMP19 statistical software, which conducts individual two-tailed T-tests for every gene and applies a B-H correction (FDR = 0.1, significance cutoff) to calculate adjusted P values. To minimize the number of tests, poorly expressed

genes were filtered out before the analysis by removing any gene whose average for at least one treatment group failed to exceed a low expression threshold (e.g., log2 expression < 2). Data from control Tet3G cells were used to identify and exclude any genes regulated by DOX alone, in the absence of iICN1 expression.

Consensus Hierarchical Agglomerative Clustering

Z scores from select genes were employed in a two-way consensus hierarchical agglomerative clustering analysis using Ward's minimum variance method, implemented via a custom Matlab script (available at https://github.com/aif33/Hierarchical-two-way-agglomerative-consensus-clustering) that we previously described (30). This approach is based on a modification of the resampling method described earlier by Monti et al., wherein 80% of the samples are randomly selected without replacement in each iteration. For each resampled set, Ward's clustering partitions the samples into N clusters, with N varied over a user-specified range (e.g., 2, 3, 4, etc.), and the frequency with which any two samples co-occur in the same cluster is recorded in a similarity matrix. This matrix is then transformed by retaining the original similarity values for pairs that consistently cluster together and replacing the values for pairs that do not with one minus the similarity value, effectively representing the fraction of iterations in which the samples did not co-cluster. Ideally, this transformation would yield an identity matrix, with all off-diagonal values equal to one, indicating perfect separation. The deviation of the observed transformed matrix from this ideal is quantified by computing the Euclidean distance between the two matrices, which is then normalized by dividing by N to yield a normalized Euclidean distance (NED). The optimal number of clusters is determined by identifying a localized minimum on the NED versus cluster number plot, thereby balancing the tradeoff between increasing cluster granularity and the preservation of meaningful information. For graphical representation, the untransformed similarity matrix was subsequently used for Wards clustering (JMP13) in each dimension to generate dendrograms that robustly depict how samples or features cluster and should be ordered for a given choice of N clusters, which can then be overlayed aside the heatmap generated using the original Z scores. For two-way clustering one set of Z scores calculated from the same dimension (e.g. across samples for each gene) are independently subjected to consensus clustering to define the dendrograms and order for both features and samples, which are combined to generate a final heatmap.

Chip-seq

For Chip-seq experiments, PJ34-iICN1 cells were seeded into six T175 flasks at 6 million cells each and on the following day cells were treated with 1000 ng/ml doxycycline for 36 h to induce ICN1 expression before scraping and processing cells for Chip-seq according to our detailed published protocol (45). Briefly, the processed sample was divided into two equal parts. One part was incubated with a rabbit monoclonal antibody against cl-NOTCH1 (Cell Signaling, #4147) to immunoprecipitate ICN1 cross-linked to DNA,

while the other part was treated with purified Rabbit IgG as a negative control for background signal subtraction. Following washes and reverse crosslinking, DNA was eluted, purified, quantitated and used to generate libraries for next generation sequencing performed on a HiSeq 3000 instrument. Raw reads were aligned to hg19 using Bowtie, 30 million reads were randomly sub-sampled, and peaks called with the Model-based Analysis for Chip-seq tool in Python.